2014

Dynamic decay of motion of rocking concrete members

Dimitrios Kalliontzis
Iowa State University

Dynamic decay of motion of rocking concrete members

by

Dimitrios Kalliontzis

A thesis submitted to the graduate faculty

in partial fulfillment of the requirements for the degree of

MASTER OF SCIENCE

Major: Civil Engineering (Structural Engineering)

Program of Study Committee:
Sri Sritharan, Major Professor
Jeramy Ashlock
Simon Laflamme

Iowa State University
Ames, Iowa
2014

TABLE OF CONTENTS

NOMENCLATURE

A, A_g	Ground horizontal acceleration magnitude
a, a_{po}	Angular acceleration magnitude
b	Half-width of a rocking block
c	Linear damping coefficient
c_o	Rod wave velocity magnitude
$\frac{d}{dt}$	Differentiation with respect to time
E_{total}	Energy content of a free rocking system
e	Coefficient of restitution of a bouncing object
F	Force magnitude
$\boldsymbol{F}$, $\vec{F}$	Force vector
F_{el}	Prestressing force due to the elongation of the post-tensioned strand
F_h	Horizontal support force applied to a free rocking system
F_{PT}	Initial prestressing force
F_T	Total support force applied to a free rocking system – CHAPTER 3
F_T	Total prestressing force – CHAPTER 4
F_v	Vertical support force applied to a free rocking system
g	Acceleration due to gravity
h	Half-height of a rocking block
I_o	Rocking rotational moment of inertia

K	Kinetic Energy
k	stiffness
M	Total mass of a rocking block
m	Mass
p	Dynamic parameter of a free rocking block
p_c	Dynamic parameter in controlled rocking
p'	Dynamic parameter of the alternative free rocking system – phase 1
p_r'	Dynamic parameter of the alternative free rocking system – phase 2
R	Distance from the rocking edge to the center of mass
r	Coefficient of restitution (COR)
r'	Recovery parameter used in the MFRM – phase 2
r_{PT}	Reduction coefficient to accurately estimate the elongation of the post-tensioned strand
$S(\theta)$	Sign convention for rocking motion
s_1	Approximate slope in the $F_T - \dot{\theta}$ graph
s_2	Approximate slope in the $\Delta K - F_T$ graph
$\frac{T}{4}$	Natural quarter period of a free rocking block
U	Gravitational potential energy
v	Linear velocity magnitude
$\vec{v}$, $\boldsymbol{v}$	Linear velocity vector

v_o	Linear impact velocity
$\ddot{x}$	Linear acceleration magnitude
$\dot{x}$	Linear velocity magnitude
x	Linear displacement magnitude
x	Elongation of the post-tensioned strand – CHAPTER 4
x_o	Initial linear displacement magnitude
x_m	Linear displacement peak at the end of *m* cycles
α	Linear acceleration magnitude
$\vec{a}$	Linear acceleration vector
a	Aspect ratio of a rocking block
β	Inclination angle of the foundation surface – CHAPTER 3
β	Parameter used in the definition of MFRM – CHAPTER 3
β	Parameter used in the definition of SRM-CR – CHAPTER 4
ΔK	Amount of impact energy dissipation
ε	Coefficient of restitution of a bouncing object
Θ	Angular displacement magnitude
θ	Angular displacement magnitude
θ_o	Initial angular displacement magnitude
θ_n	Angular displacement amplitude at the end of *n* cycles
$\dot{\theta}$	Angular velocity magnitude
$\dot{\theta}_o$	Initial angular velocity magnitude
$\ddot{\theta}$	Angular acceleration magnitude

μ	Static friction coefficient
ξ	Equivalent viscous damping ratio
φ_o	Initial angular displacement amplitude
Ω	Frequency of the sinusoidal excitation
ω_p	Frequency of ground excitation

ACKNOWLEDGEMENTS

First and foremost, I would like to thank the National Science Foundation and the Precast/Prestressed Concrete Institute for their financial support.

I would like to sincerely thank my supervisor Wilson Engineering Professor Sri Sritharan for his help and guidance throughout this study. Dr. Sri, your encouragement and continuous assistance added an extra incentive for me to do my best. It was my honor to have you as my supervisor.

I would like to thank my parents, Theodoros Kalliontzis and Kalliopi Ouzouni, for the support and understanding they showed even by being far away. They always supported my choices and showed remarkable patience during my graduate studies.

A special thank goes to Hussam Saleem for your friendship throughout my graduate studies and your help during my first steps in the realm of academic research.

Finally, I would like to thank Maryam Nazari for her help and collaboration during this research project.

ABSTRACT

This study was conducted as part of a research project aiming at understanding the dynamics of precast rocking concrete members. The characteristics and energy dissipation associated with the dynamic response of these systems were investigated.

The simple rocking model broadly used by the previous and current research society and a finite element modeling approach developed herein were used as guidelines and reference modeling methods to assess experimental free rocking responses and produce methodologies to more accurately estimate the actual rocking decay of motion. Two discrete energy dissipation mechanisms were identified, namely, instantaneous dissipation due to the impact phenomenon and continuous dissipation. It was found that the instantaneous dissipation formula used in the simple rocking model serves as a lower-bound limit for the amount of energy dissipation per impact. The rocking coefficient of restitution can be alternatively expressed through its relationship with the impact velocity, base force and rocking body inertia. Finally, the continuous dissipation mechanism was modeled by using a velocity-dependent term in the original simple rocking model for accurately estimating the real-time displacement responses.

As far as controlled rocking is concerned, it was shown that its decay of motion is mainly dependent on the instantaneous dissipation mechanism, while the coefficient of restitution by the simple rocking model significantly overestimates decay of controlled rocking motion. To provide a safe upper bound limit for coefficient of restitution associated with controlled rocking systems, a simplified method which makes use of the original simple rocking model was proposed.

CHAPTER 1: INTRODUCTION

1.1 Overview

Free-standing precast concrete members supplemented with a post-tensioning mechanism are expected to enter rocking motion when subjected to an earthquake load. Accordingly, their bottom edge uplifts and rocking motion takes place with respect to one of the bottom corners. After reaching its peak lateral displacement, a rocking member re-centers due to the applied restoring force by the post-tensioned steel. Impacts with its foundation and rocking motion continues with respect to the opposite bottom corner. During dynamic motion, damage in a rocking precast member is restricted to its bottom edge, while by properly attaching angles-channels at its bottom corners, damage is further minimized. In addition, rocking precast members are characterized by some energy dissipation, anecdotally attributed to a radiation damping mechanism associated with the rocking impact phenomenon. As a method to account for the rocking energy dissipation has not yet been proposed, supplemental elements able to dissipate the seismic energy have been implemented to improve the seismic performance of these systems. These elements include various types of steel shear connectors which have been introduced in order to create a system of two or more horizontally connected rocking walls.

The use of prestressing for providing self-centering capacity to a rocking precast concrete wall operating as seismic-resisting system has been experimentally investigated by the PREcast Seismic Structural Systems (PRESSS) Research Program (Priestley et al. 1999). A rocking precast concrete wall system was successfully tested as part of a 5-story precast concrete building to more than 100% of the Design Basis Earthquake (Zone 4). This outcome of the PRESSS Research Program has given an insight into the capabilities of a rocking

precast system which (1) is very easy to construct; (2) is versatile; (3) provides reliable performance while ensures minimal damage throughout an earthquake event; and (4) provides a desirable re-centering capacity to the structure.

Figure 1-1. Post-testing observation on the rocking wall used in the 5-story Precast Concrete Building of the PRESSS Research program (Source: Precast Concrete Walls for Seismic-Resistant Design_from PRESSS Research to PreWEC webinar)

Following the PRESSS Research Program, various types of rocking precast concrete walls have been introduced by researchers, trying to either improve or offer alternative solutions of precast concrete wall systems (e.g. Aaleti and Sritharan 2007; Nicknam and Filiartault 2012). While a variety of these systems have been proposed in literature, their behavior has been experimentally investigated based on quasi-static or pseudo-dynamic

testing, which cannot provide an understanding on their dynamic behavior associated with the aforementioned energy dissipation due to rocking.

1.2 Free Rocking

Rocking has been viewed as a dynamic mode of motion which benefits the response of structural systems able to uplift from their underlying soil surface while subjected to an earthquake excitation. Accordingly, rocking provides a base-isolation feature to these structures as it allows the development of a gap at their interface with the soil and consequently prevents the formation of a plastic hinge which is commonly seen in conventional lateral force resisting systems.

Free rocking motion is the rocking motion of a structural member without the use of a supplemental self-centering mechanism, e.g. provided by an unbonded post-tensioned strand. Assuming the occurrence of free rocking motion, structural engineers were able to explain the survival of seemingly unstable structures under severe earthquake motions that occurred in the past. Based on this understanding, the structural engineering society was motivated to investigate the structural advantages and potential dangers associated with free rocking motion of structures. Prominent steps were made by Housner (1963) towards this direction with the proposal of a comprehensive formulation which analytically described free rocking rigid body behavior under free vibration and ground excitation. In all cases, Housner attributed the decay of motion of a free rocking rigid body to an instantaneous energy dissipation mechanism, which occurs during the impact of the rocking body with its underlying rigid ground surface.

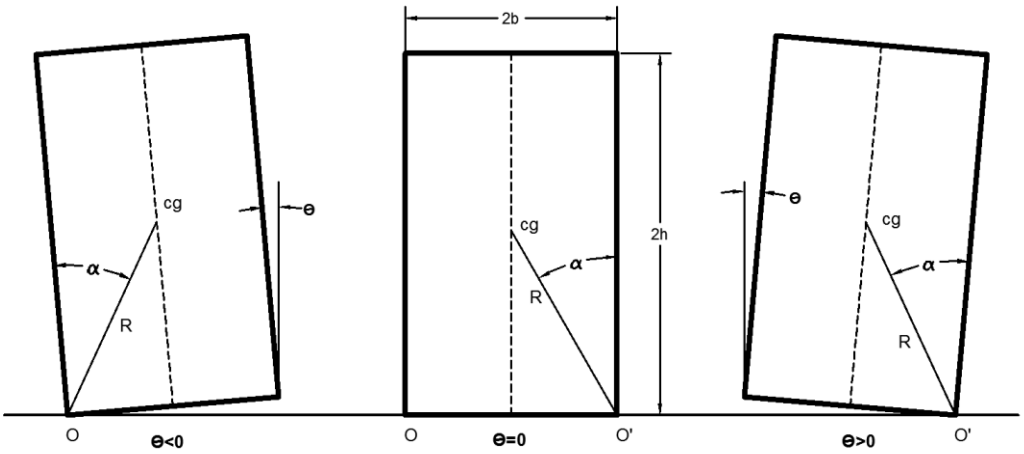

Figure 1-2. A rigid free rocking block as described by Housner (1963)

Housner's work has been routinely used as a reference point by the latter researchers to analytically study free rocking behavior and has also been the driving force for the development of novel approaches aiming at further exploring and explaining this phenomenon. In the post-Housner's model era, researchers supplemented the original model proposed by Housner with other types of motion besides rocking, in order to develop a more comprehensive model of the free rigid-body motion and examine alternative features of this motion which may also contribute to its structural isolation from a base excitation (e.g. relative horizontal motion due to low friction forces along the contact interface, existence of a flight mode in the response due to the vertical earthquake acceleration component). Alternative modelling approaches of free rocking motion have also enriched the knowledge on this topic by suggesting a flexible rocking system, in which the rocking body is able to deflect during its motion, and its rocking interface is modeled via a series of spring-dashpot mechanisms imposed along the total contact length, as shown in Figure 1-3.

Accordingly, effects such as the stiffness of the rocking body, its viscous damping properties and flexibility, and viscous behavior of the rocking interface were analytically

studied for their influence in the body's free rocking motion under free vibration and earthquake motion. It was shown that damping due to free rocking plays a critical role in a structural system's free rocking response under earthquake load, where its peak displacement decreases with increase in damping.

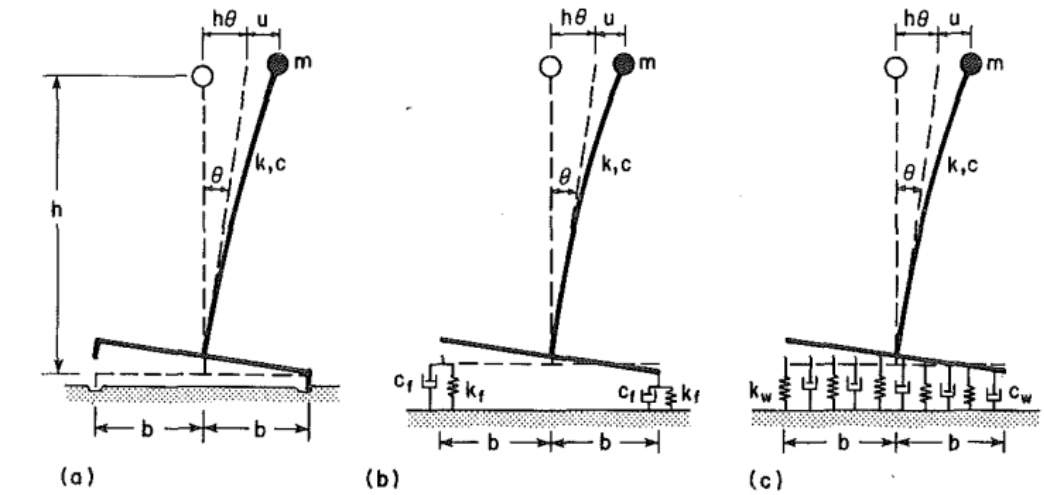

Figure 1-3. Three approaches proposed by Chopra and Yim (1985) for modeling free rocking of a structural system subjected to foundation uplift.

Furthermore, stability of a body free to rock under an earthquake excitation has been thoroughly investigated by various researchers (e.g. Fielder et al. 1997; Makris and Zhang 2001) in order to determine the potential of an overturning which is inherently associated with free rocking motion. It was shown that rocking instability cannot be directly associated with the stronger earthquake excitations. In contrast, it was analytically and numerically indicated as a complex aspect of free rocking which can be dependent on more than one variables, i.e. size, geometry and damping characteristics of the rocking body, and ground acceleration and frequency. Figure 1-4 presents typical stability analyses results of a free rocking rigid block under base excitation, showing there is no direct relationship between the

overturning possibility and the peak ground acceleration. For example, a free rocking block may survive a ground excitation of certain horizontal acceleration amplitude, while failing by overturning under a ground excitation of the same frequency and lower horizontal acceleration amplitude.

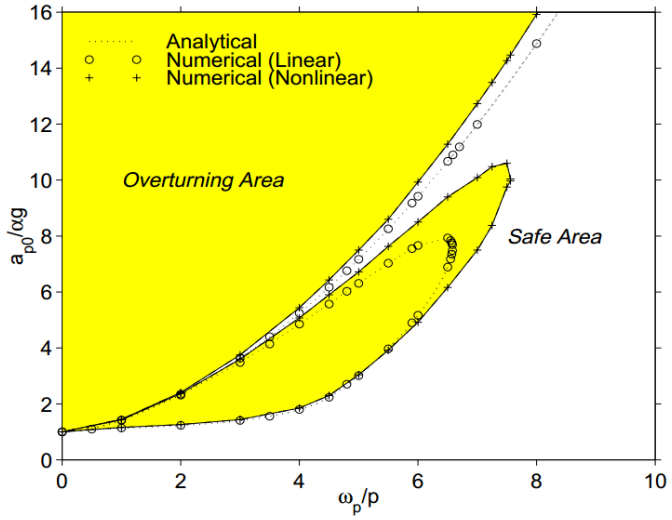

Figure 1-4. Typical prediction of an overturning spectra of a rigid block subjected to free rocking under horizontal ground excitation (Makris and Zhang 2001).

Free rocking motion was also considered as a beneficial feature of free-standing ancient structures contributing to their stability under seismic load. Using existing knowledge on free rocking motion, several researchers have theoretically investigated seismic behavior of typical ancient structural configurations (Fig. 1-5 and 1-6).

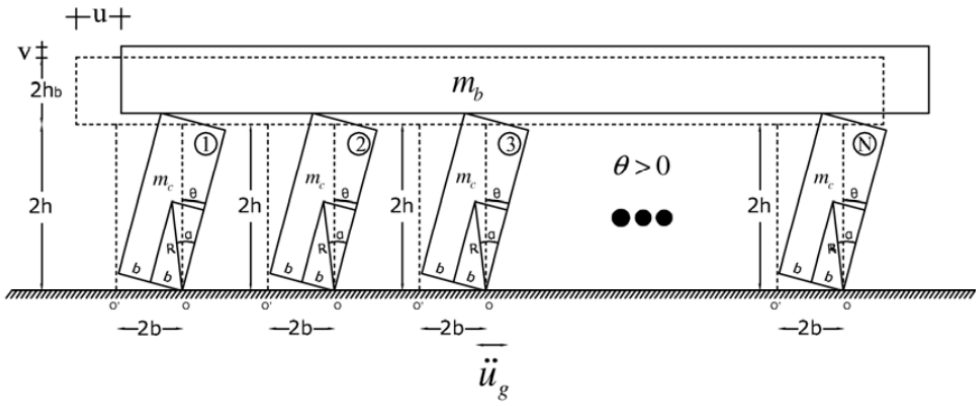

Figure 1-5. Structural configuration representing a typical free-standing ancient structure studied by Makris and Vassiliou (2013) for its seismic response and stability. It was analytically shown that a heavier rigid beam leads to a more stable structure.

Figure 1-6. Specimens representing ancient free-standing monolithic columns subjected to ground motion during experimental and analytical studies conducted by Manos et al. (2013) in an effort to establish suitable numerical methods for estimating earthquake response of these simple ancient structural systems.

1.3 Controlled Rocking

The use of an unbonded post-tensioning system in free rocking members, leading to a behavior designated as controlled rocking, has created a new type of a rocking system which is enhanced with a self-centering capability. Consequently, it is able to better resist overturning which was initially seen as the problematic aspect of free rocking motion under earthquake excitation.

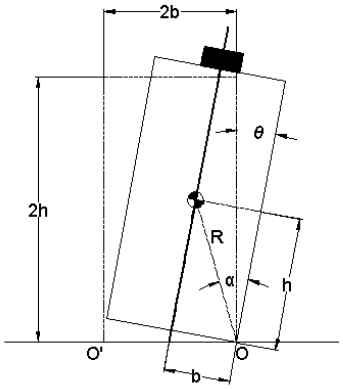

Figure 1-7. A controlled rocking block

The concept of self-centering rocking structural systems has been envisaged as a promising technology which can introduce a new design approach in the territory of seismic force-resisting systems which ensures minimal damage for a structural system under earthquake load. Accordingly, evolutionary structural models operating as seismic-resisting systems incorporated a controlled rocking mechanism in order to ensure a functional structural configuration in the post-earthquake phase and the desirable re-centering action during and after a seismic event. Typical examples of these systems are presented in Figures 1-8 and 1-9.

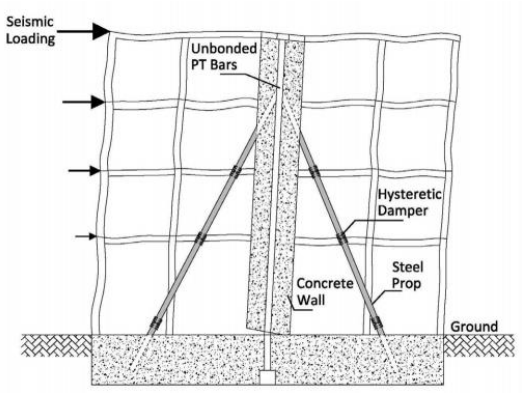

Figure 1-8. Propped Rocking Wall (Nicknam and Filiatrault 2012)

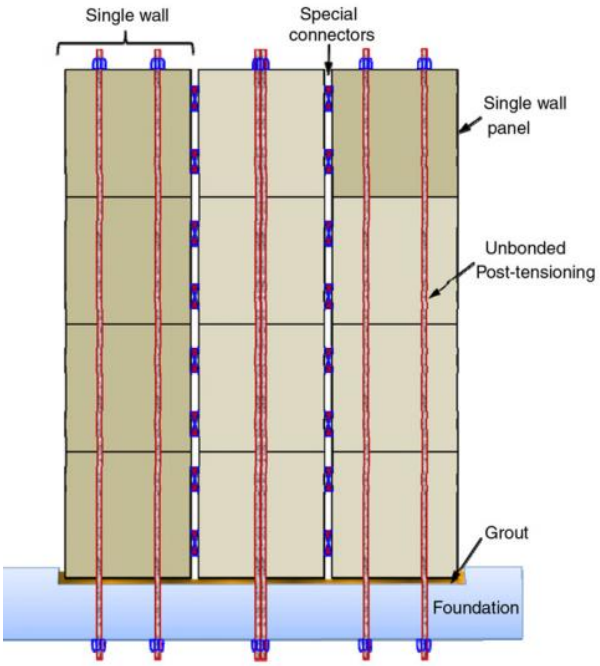

Figure 1-9. A jointed wall system (Aaleti and Sritharan 2009)

While researchers have been able to successfully implement controlled rocking in precast concrete seismic resistance systems and validate their performance through pseudo-dynamic testing, a fundamental understanding of controlled rocking dynamic behavior, which is strongly dependent on the mechanisms of dynamic energy dissipation, has not yet been achieved.

Given that simple controlled rocking systems, as shown in Figure 1-6, do not provide a reliable hysteretic energy dissipation mechanism, their dynamic decay of motion cannot be captured through quasi-static test schemes. More appropriately, dynamic testing is necessary to determine the inherent ability of these systems to dissipate energy during their rocking motion. Several researchers, who conducted dynamic tests on controlled rocking members, provided general conclusions on their decay of motion, however, without systematically proposing specific solutions suitable for modeling and design use.

1.4 Scope of Research

This research study focused primarily on understanding dynamic decay of controlled rocking precast concrete members. In order to reach the goal of this research study, it was necessary to initially investigate the fundamentals of free rocking behavior of concrete members through experimental and analytical work. A critical step of this investigation was to examine the applicability of the original simple rocking model proposed by Housner to these systems and conclude in modeling improvements to better characterize and quantify the energy dissipation mechanisms associated with free rocking motion.

The knowledge acquired from this initial phase was used as a reference point to investigate controlled rocking. Accordingly, this research work aimed at (a) determining the differences between free and controlled rocking motion of precast concrete members; (b) introducing a finite element modeling technique applicable to both free and controlled rocking; and (c) proposing a modeling approach to conservatively estimate energy dissipation in controlled rocking with a potential of future use in practice. This work was carried out with a goal of adding to the existing knowledge on free and controlled rocking systems and designing of cost-effective controlled rocking systems which make use of a minimum additional hysteretic energy dissipation.

1.5 Thesis Layout

A comprehensive literature review on rocking behavior is developed in Chapter 2. This Chapter covers published work on impact problems which present similar energy dissipation trends with rocking behavior. The literature review proceeds with the published studies on

free rocking motion of a block under free vibration and ground excitations. Finally, an overview of the current knowledge on controlled rocking systems is presented.

Chapter 3 presents a study on free rocking precast concrete members. This work summarizes the experimental results of the free vibration tests conducted on three discrete rocking concrete members which were subjected to various levels of initial lateral displacement. These tests took place in the structural laboratory at Iowa State University. The experimental results were supported and analyzed by using finite element modeling and employing Housner's simple rocking model. An alternative approach for estimating impact energy dissipation was introduced, while a method to model an identified continuous dissipation mechanism participating in free rocking was also investigated.

Chapter 4 presents the second phase of the experimental study which focused on free vibration responses of controlled rocking precast concrete members. The experimental results of free vibration tests conducted on two discrete rocking concrete members, which were subjected to various levels of initial prestressing force and lateral displacement, are summarized in this Chapter. These tests took place in the structural laboratory at Iowa State University. The experimental results were supported and analyzed by using finite element modeling and employing Housner's modeling approach modified to account for the controlled rocking effect. A simplified approach for providing a safe estimation of dynamic energy dissipation in controlled rocking is presented.

Chapter 5 summarizes the conclusions from this work and provides recommendations for future research.

Finally, the APPENDIX presents a finite element approach for modeling rocking behavior which has been employed throughout this study for comparison with the experimental free and controlled rocking responses.

A paper format follows.

1.6 References

Aaleti, S., Sritharan, S., 2007. A precast wall with end columns (PreWEC) for seismic application, *Proc. 8th Pacific Conf. Earthquake Eng.*

Aaleti, S., and Sritharan, S., 2009. A simplified analysis method for characterizing unbonded post-tensioned precast wall systems, *Engineering Structures*, **31**(12), 2966-2975.

Aaleti, S., and Sritharan, S., 2011. Performance Verification of the PreWEC Concept and Development of Seismic Design Guidelines, ISU-CCEE Report Submitted to the Precast/Prestressed Concrete Institute.

Aslam, M., Godden, W.G., and Scalise, D. T., 1980. Earthquake rocking response of rigid bodies, *Journal of the Structural Division*, **106**(2), 377-392.

Chopra, A., and Yim, S., 1985. Simplified earthquake analysis of structures with foundation uplift, *J. Struct. Eng.*, ASCE, **111**(4), 906-930.

Housner, G. W., 1963. The behavior of inverted pendulum structures during earthquakes, *Bull. Seismol. Soc. Am*, **53**(2), 403-417.

Makris, N., and Vassiliou, M., F., 2013. Rocking response and stability analysis of an array of free-standing columns capped with a free-standing rigid beam, *4th ECCOMAS Them. Conf. on COMPDYN*.

Makris, N., and Zhang, J., 2001. Rocking response of free-standing blocks under cycloidal pulses, *J. Eng. Mech.*, ASCE, **127**(5), 473-483.

Manos, G., Petalas, A., Demosthenous, M., 2013. Numerical and experimental study of the rocking response of unanchored body to horizontal base excitation, *4th ECCOMAS Them. Conf. on COMPDYN*.

Priestley, M., J., N., 1996. The PRESSS Program – Current status and proposed plans for phase III, *PCI J.*, **41**(2), 22-40.

Priestley, M., J., N., Sritharan, S., Conley, J., R., Pampanin, S., 1999. Preliminary results and conclusions from the PRESSS five-story precast concrete test building, *PCI J.*, **44**(6), 42-67.

Nakaki, S. D., Stanton, J. F., Sritharan, S., 1999. An overview of the PRESSS five-story precast test building, *PCI Journal*, **44**(2), 26-39.

Nicknam, A., and Filiatrault, A., 2012. Seismic design of propped rocking wall systems, *15 WCEE*, Lisboa.

CHAPTER 2: LITERATURE REVIEW

A literature review is presented herein aiming at providing a comprehensive understanding of the main features of free and controlled rocking behavior and their mechanics. As rocking appears to be very similar to other physical phenomena (e.g. the bouncing ball impact problem), it may be suitable to first discuss the physics behind simple impact problems, encountered even in daily life, and are intuitively relevant to the more complicated rocking mechanics. Next, the review focuses on the behavior of rigid and flexible blocks subjected to both free and controlled rocking motion.

2.1 Impact Mechanics

Consider what happens when a bowling ball hits a pin. The ball exerts a force on the pins, which gain velocity very rapidly. The impact between the bodies takes place in a very short and negligible time interval. According to Newton's third law, the pins exert an equal and opposite force on the ball. However, the ball is much more massive than the pins, therefore it decelerates much less than the pins accelerate. Also, the force acting on the pins varies with time, as well as their acceleration, a behavior which makes an intuitively simple phenomenon more complicated. On the other hand, if one is able to measure the kinetic energy of the ball just before the impact and the kinetic energy of the total system (ball and pins) just after the impact, it will be concluded that the second is less than the first. This signifies that the impact induced some energy loss to the dynamic system.

In order to tackle the aforementioned problem, it is important to introduce the concepts of momentum and conservation of momentum. The momentum is associated with the mass and the velocity of a body. The momentum leads to the conservation law, that of

conservation of momentum. This law is very useful when it comes to a collision of two bodies, or collision of a rocking body with its foundation.

Let us consider an isolated system of two particles with masses m_1 and m_2 and velocities $\boldsymbol{v_1}$ and $\boldsymbol{v_2}$ respectively, which collide at an instant of time. Thus, they form a Newton's third law action-reaction pair, so that $\boldsymbol{F_{12}=-F_{21}}$. This condition can be expressed, as follows,

$$\vec{F}_{12} + \vec{F}_{21} = 0 \tag{2-1}$$

Using Newton's second law, Eq. 2-1 can be further analyzed,

$$m_1\vec{a_1} + m_2\vec{a_2} = 0 \tag{2-2}$$

Using the definition of acceleration, we can write,

$$\frac{d}{dt}(m_1\vec{v_1} + m_2\vec{v_2}) = 0 \tag{2-3}$$

The sum $m_1\vec{v}_1 + m_2\vec{v}_2$ of Eq. 2-3 must be constant. The quantity $m\boldsymbol{v}$ of a body, which is called the momentum of the body, is a very important parameter, in that the sum of these quantities for an isolated system (i.e. two particles) is conserved. This statement is known as the *conservation of linear momentum*.

Besides the impact of two particles, researchers have thoroughly studied another impact phenomenon referred to as "the bouncing ball problem"; a small body colliding with the plane surface of a massive floor-base. Hertz (1882) was the first to develop a mathematical theory on the collision of elastic solids. In the aftermath, much research has been done aiming at developing efficient modeling techniques, able to precisely describe this behavior. A simple way to approach this problem is to model the bouncing ball as a single

spring-dashpot model (Nagurka and Huang 2004) and use the simple dynamic equation of motion, as shown below.

$$m\ddot{x} + c\dot{x} + kx = 0 \tag{2-4}$$

where the damping term, *c*, becomes zero when the ball is not in contact with the floor.

Provided that an appropriate selection of damping coefficient is made, the energy loss of the system is expressed through the coefficient of restitution (COR), defined as the ratio of the ball velocity just after the impact to the ball velocity just before the impact. The COR value is controlled by the selection of the damping coefficient. The user of this method should be very careful on selecting the stiffness of the ball, as well.

In parallel with the theoretical investigation, significant experimental work was conducted on the bouncing ball problem and the associated COR. Experimental results showed that COR tends to remain constant with minor fluctuations in time, as presented in Figure 2-1. However, it tends to decrease when the oscillation comes closer to its end-last cycles (Falcon et al. 1998).

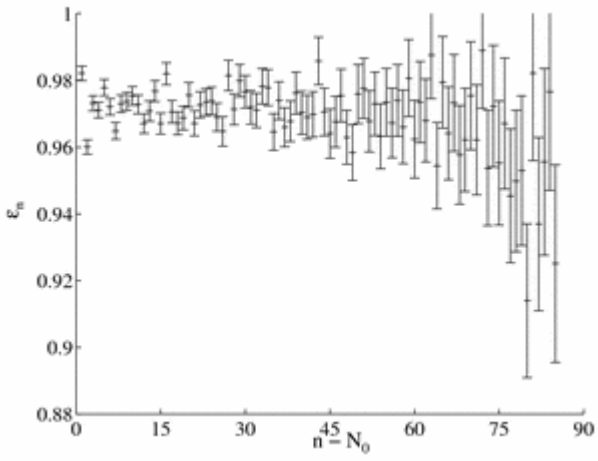

Figure 2-1. Evolution of the COR (ε_n) as a function of number of cycles (n – No) for a tungsten carbide bead dropped from a height *ho=2 mm* (Falcon et al. 1998)

In the comparison of COR with the impact approaching velocity presented in Figure 2-2, it is shown that COR fluctuates around a mean number for the most part and tends to decrease after 75-80 bounces when the impact approaching velocity becomes very small. This signifies that the amount of energy dissipation of the bouncing object is proportional to the impact approaching velocity for higher velocity values, while the impact mechanism may change characteristics for smaller velocities; despite the fact that COR seems to remain approximately constant for the most part. A trial to mathematically reproduce the displacement response using the simplification of a mean COR may not fit the experimental displacement time history due to the small fluctuations of COR, which will gradually induce a phase angle between the two responses as COR per impact would be slightly different.

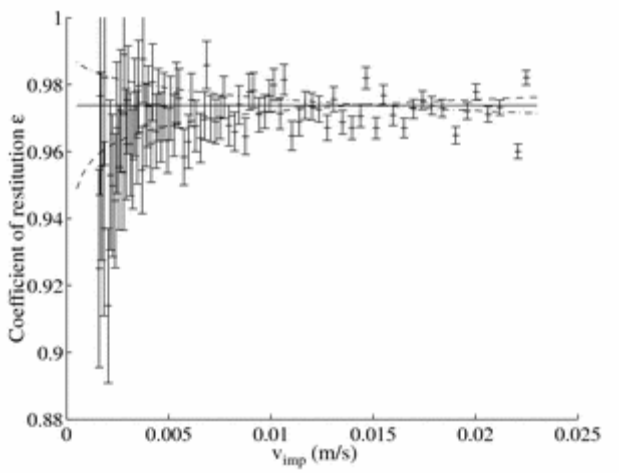

Figure 2-2. COR as a function of object velocity exactly before the impact, as presented by Falcon et al. 1998

Another interesting observation made by Falcon et al. was on the relationship between the velocity just after the impact and the duration of a dynamic cycle (Fig. 2-3). This

researcher observed a nonlinear relationship between the two variables concluding that the velocity after an impact dictates the period of an oscillation.

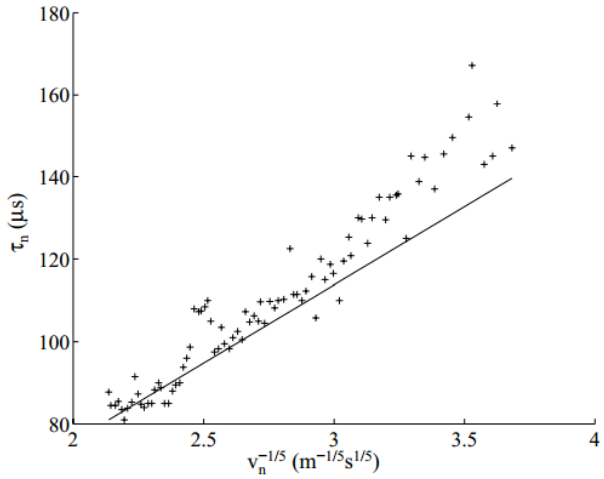

Figure 2-3. Duration of the *n*th bounce as a function of the $v_n^{-1/5}$ (Falcon et al. 1998)

In order to achieve a better understanding on the COR and its behavior in the window of small velocities, several researchers have experimentally researched the behavior of parameters theoretically shown to have a strong impact on the response of a bouncing object. In contrast to what was originally believed, these studies concluded that COR does not always have a relatively constant value, as under certain conditions it can experience a remarkably different behavior (Tillett 1954; Koller and Kolsky 1987; Zener 1941). For example, according to theoretical investigations, COR may be independent of the finite extent of the target, if the floor-base is thicker than a few diameters of the impacting object. If this condition is not satisfied, COR will decrease when the impact approaching velocity increases. To show the influence that the floor thickness has on the COR associated with the impact of the object, Tillett plotted the experimentally determined COR values with respect

to the number reflections taking place during the impact, as shown in Figure 2-4. The number of reflections refers to the number of times that a longitudinal elastic wave could be reflected from the top and bottom of the base during the impact time. As shown in Figure 2-4, Tillett concluded a decrease in the thickness of the floor (more wave reflections) leads to decrease in COR. COR is slightly below unity for very thick floors, where there is not sufficient time for even one reflection to occur; however, there can still be some energy dissipated due to the elastic wave radiated inside the floor.

Furthermore, Tillett observed a significant dependence of COR on temperature that is COR decreases with increase in temperature (Fig. 2-5). The relationship between contact area versus maximum vertical displacement reached by the ball and contact force has also been investigated both analytically and experimentally resulting in a linear pattern where increase in the contact area leads to increase in the contact force and displacement (Jamari and Schipper 2006; Brake 2012).

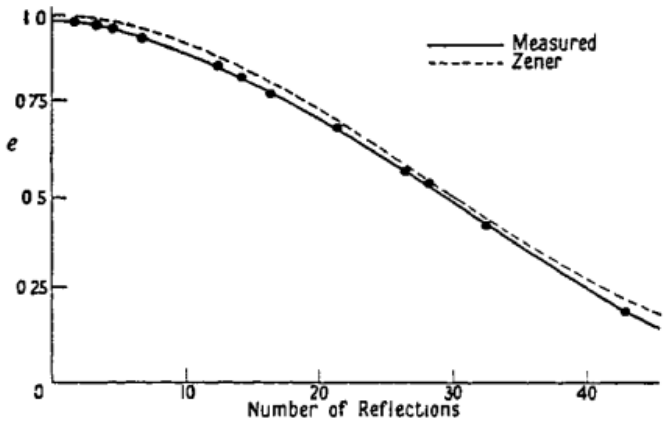

Figure 2-4. The variation of the COR of glass plates with the thickness of the specimen; variable *e* stands for COR (Tillett 1954)

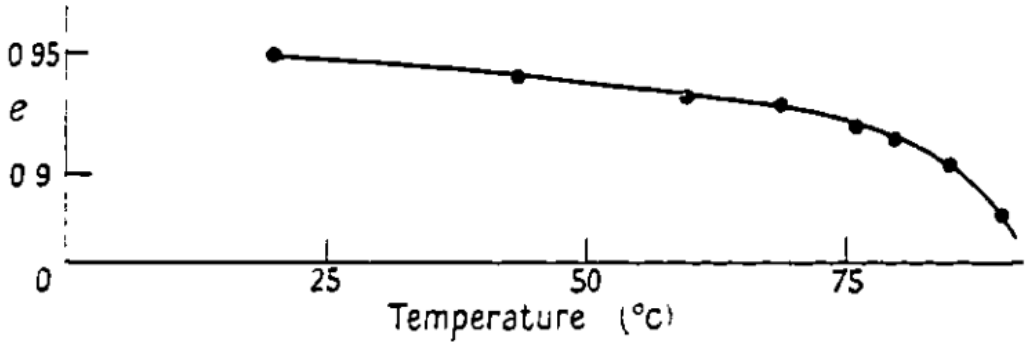

Figure 2-5. The variation of the COR of Perplex with temperature (Tillett 1954)

Regarding the behavior of COR for small velocities, researchers investigated the energy dissipation mechanisms involved in the impact interaction taking place in this region. Falcon et al. claimed that COR experiences a significant drop mainly due to increased energy dissipation in the form of elastic waves, flexural vibrations of the floor and viscoelastic behavior of the object and the target. It was also speculated that the gravity effect can become more influential during the last bounces and it may lead to decrease in COR (Fig. 2-2). Arguing their side, Falcon et al. explained the significant influence of gravitational forces is attributed to an increase in the contact time during the last cycles, and, in other words, the work produced by gravitational forces plays a more critical role in impact energy dissipation.

Experimental and analytical work has also revealed an influence of the materials which come into contact on COR (Tabor 1948; Hardy et al. 1971; Lee et al. 1972; Reed 1985; Brake 2012). After an experimental investigation, Reed observed that when a steel sphere collides with glass, COR decreases with increase in impact velocity. Hunter (1957) mentioned that there is always a finite amount of energy loss taking place during an elastic impact between a body and a massive target and it is in the form of wave propagation, no matter what material is used and what other mechanisms would participate in the total energy

dissipation. Therefore, the propagation of elastic waves determines a maximum possible value of COR. The energy dissipation due to wave propagation was found to be dependent on the relationship between the duration of an impact and the time needed for an elastic wave to travel through the colliding bodies. Love (1944) supported that there will be no energy loss during an impact between two perfectly elastic bodies if the time duration of the impact is very long in comparison with the time taken for an elastic wave to traverse either body. Consequently, it follows in the case of a ball impacting on a floor of infinite thickness, that there will be a finite amount of energy dissipation in the ball attributed to the energy carried by the elastic waves lost inside the floor.

At this point, it would be appropriate to also revisit Goldsmith's approach regarding energy dissipation during an impact (Goldsmith 1960). Goldsmith suggested "The predictions of the stereo mechanical theory will be seriously in error when a significant percentage of the total energy is converted into vibrations. In general, this effect will be small when the period of action of the applied force, in other words, the duration of contact, is large compared to the period of the lowest natural frequency of either body. In this event, several reflections of the wave will have occurred during the contact period, and the bodies may be considered to be in a state of quasi-equilibrium." Furthermore, Goldsmith defined the ratio of vibrational to total energy or the impact as:

$$ratio\ of\ vibrational\ to\ total\ energy\ of\ the\ impact = \frac{\frac{1}{50}v_o}{c_o} \tag{2-5}$$

Where $c_o = \sqrt{E/\rho}$ is the material-dependent rod longitudinal wave velocity and v_o the impact velocity.

Later, Finite Element Methods (FEM) for simulating the bouncing ball problem were developed for comparison with mathematical as well as experimental results, and for a

deeper understanding of the impact mechanisms (Zhang and Vu-Quoc 2002; Seifried et al. 2005). These simulations provided more information regarding the plastic deformation inside the colliding bodies, force versus displacement relationship etc. It was, also observed that the discretization patterns, contact algorithms and solution methods can significantly influence the theoretical response of the oscillating objects.

2.2 Free Rocking of Rigid Blocks

Free rocking modeling techniques available in the literature and their efficiency to predict experimental results are discussed herein.

2.2.1 Housner's simple rocking model

During severe earthquakes of the past, appearing unstable structures and objects, such as water towers not firmly connected to the ground, free-standing equipment and ancient monuments were capable of withstanding strong ground excitations. Their survival was anecdotally attributed to their free rocking motion, which had been seen as a potential seismic isolation mechanism. This on-site behavior of these free-to-rock structural and non-structural systems triggered Housner (1963) to investigate free rocking motion of rigid bodies under free vibration and various types of ground motion.

Housner developed a mathematical model of a rigid block rocking on its foundation, designated as the simple rocking model (SRM). This model was based on several assumptions: (a) both the free rocking block and the base are rigid; (b) there is no sliding between the block and the base; (c) no bouncing of the block occurs; (d) energy dissipation takes place instantaneously during the impact and is expressed through a coefficient of

restitution (COR) which is dependent on the geometric properties of the block; (e) the impact takes place at the corners of the bottom edge of the block; and (f) the block oscillates in a two-dimensional fashion. According to Figure 2-7, a free rocking block rocks about the two points of rotation, O and O'.

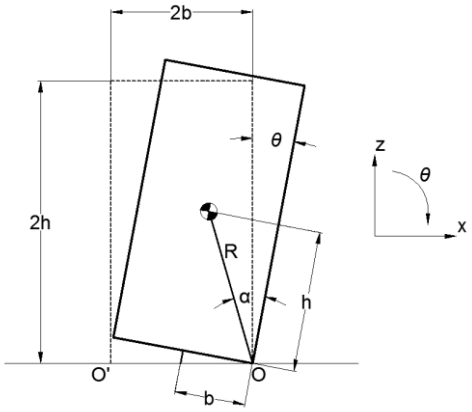

Figure 2-7. A free rocking block as described by Housner (1963)

The equation of motion for a free vibration excitation, with respect to the point of rotation (O or O').can be expressed in a compact form as,

$$I_o\ddot{\theta} + S(\theta)MgR\sin(a - |\theta|) = 0 \tag{2-6}$$

where

$$I_o = \frac{4}{3}MR^2 \tag{2-7}$$

Where I_o is the rotational moment of inertia of the rocking block with respect to the rotation center (i.e. O or O'), M is the total mass of the block and R is the distance from the rotation center to the center of mass of the block.

$S(\theta)$ is defined as:

$$S(\theta) = \begin{cases} 1, for\ \theta > 0 \\ -1, for\ \theta < 0 \end{cases} \quad (2\text{-}8)$$

For the case of a slender block, where the aspect ratio noted as a is less than 20^o, the sine function of a can be approximated to the angle a (Housner 1963). Therefore, Eq. 2-6 can be linearized and written as,

$$I_o\ddot{\theta} + S(\theta)MgR(a - |\theta|) = 0 \quad (2\text{-}9)$$

In order to solve Eq. 2-9 the initial conditions should be applied. For the first case where $\theta(0) = \theta_o$ and $\dot{\theta}(0) = 0$, the solution for $\theta(t)$ gives:

$$\theta(t) = a - (a - \theta_o)\cosh pt \quad (2\text{-}10)$$

Where the constant p (*dynamic parameter*):

$$p = \sqrt{\frac{MgR}{I_o}} \quad (2\text{-}11)$$

Eq. 2-10 describes the motion which starts from the release of the free-standing block at t=0 and from a position with $\theta(0) = \theta_o$ and zero initial velocity. The block will reach the condition $\theta(t) = 0$ at time $t = \frac{T}{4}$:

$$\frac{T}{4} = \frac{1}{p}\cosh^{-1}\left(\frac{1}{1 - \theta_o / a}\right) \quad (2\text{-}12)$$

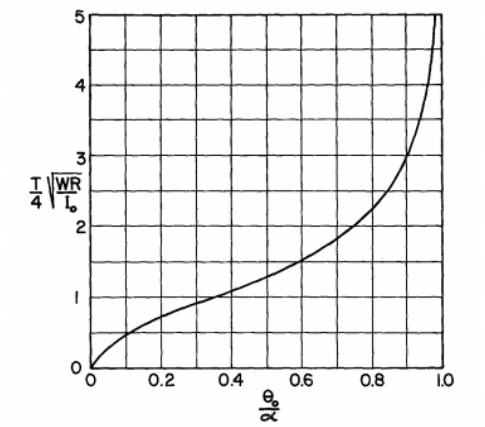

Figure 2-8. Period T of block rocking with amplitude θ_o (Housner 1963)

After the impact with the base, the block continues to rock with respect to the point O', Housner's model assumes that some energy of the free rocking system is dissipated during an impact. Accordingly, impact mechanics is used to examine the impact energy dissipation. Equating the moment of momentum just before the impact to the moment of momentum just after the impact about the point of rotation after the impact:

$$I_o\dot{\theta}_1 - 2MRb\dot{\theta}_1 \sin a = I_o\dot{\theta}_2 \tag{2-13}$$

In Housner's model impact energy dissipation is expressed through COR defined as the square ratio of the velocities before and after the impact:

$$r = (\frac{1}{2} I_o\dot{\theta}_2^2) / (\frac{1}{2} I_0\dot{\theta}_1^2) = (\frac{\dot{\theta}_2}{\dot{\theta}_1})^2 \tag{2-14}$$

From Eq. 2-13 and 2-14, COR is finally calculated as:

$$r = [1 - \frac{MR^2}{I_o}(1 - \cos(2a))]^2 \tag{2-15}$$

COR of Eq. 2-15 expresses the energy dissipation of a free rocking block during its impact with the base, given rocking motion continues smoothly after the impact with respect

to the opposite rotation center, i.e. point O'. Equation (2-15) assumes that COR depends only on the aspect ratio of the rigid block; it consequently follows that the geometric characteristics of the block dictate the energy loss per impact.

Finally, Housner's study included a stability study. The overturning phenomenon associated with free rocking was discussed and significant conclusions were made regarding the geometric properties of the block and characteristics of a ground motion which influence rigid block stability. This discussion is further developed later in Section 2.2.4.

2.2.2 Other rigid body models and validation of SRM

In the aftermath of Housner's model, researchers experimentally investigated the validity of the rigid block – rigid base theory and moreover, they proposed other methods to model free rocking motion. It was shown that the actual COR exhibits large scatter during free rocking motion, while COR proposed by SRM (1) provides an approximately average estimation of the experimentally determined COR values.

A novel approach to the rigid body-rigid base modeling was proposed by Prieto and Lourenco (2005) who replaced the COR with an energy dissipation effect due to impulsive impact forces. This way, Prieto and Lourenco were able to bridge the equation of free rocking motion introduced by Housner with the impact action for which a Dirac-delta force was implemented. The simulation results of this analytical model were in good agreement with SRM (Figure 2-9).

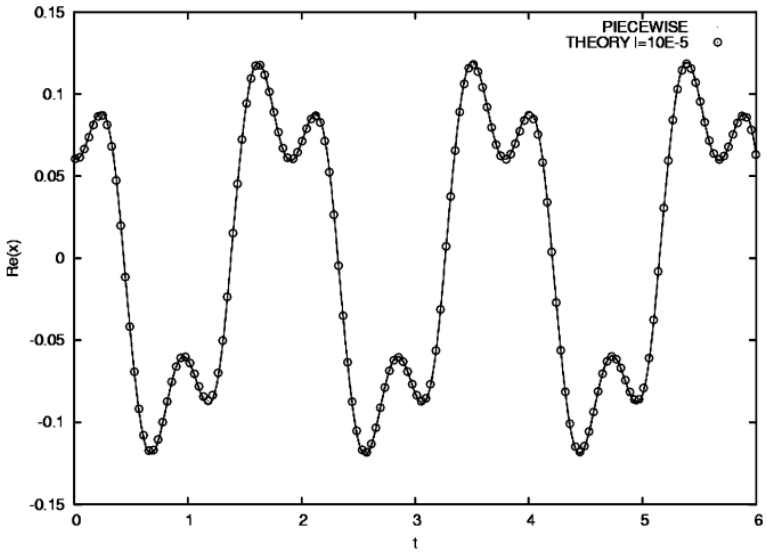

Figure 2-9. Comparison between SRM and complex formulation proposed by Prieto and Lourenco; Where $\mathrm{Re}(x) = \chi\cos(\psi)$, $x = \frac{\theta}{\alpha}$, l was a parameter of the complex formulation and ψ the horizontal excitation frequency

Lipscombe and Pellegrino (1993) conducted experimental work to investigate the accuracy of SRM in predicting the free rocking motion of steel block units of various aspect ratios. These blocks were tested in free rocking under free vibration with initial top lateral drifts close to the overturning limit ($\theta_o \le \alpha$). Lipscombe and Pellegrino noticed a significant discrepancy of SRM's COR with respect to the experimentally measured values. In particular, this deviation was increasing with decrease in the block's slenderness (Lipscombe 1990). Generally, it was shown that experimental COR values for a block with a certain aspect ratio correspond always to SRM's COR value of a slenderer block. Lipscombe and Pellegrino also observed that the specimen with $\frac{h}{b} = 1$ did not behave according to SRM's fundamental assumption of no bouncing, as it was shown that bouncing was dictating its response. In order to better estimate the behavior of a square block, these researchers

incorporated other mathematical theories into the original SRM to account for bouncing motion. Furthermore, Lipscombe and Pellegrino introduced a division of COR into a tangential and a normal component and drew on the classical bouncing ball theory to investigate the validity of the original rigid body assumption. It was mentioned the free rocking body is considered as rigid provided that "the duration of a collision is sufficiently long to allow several reflections of the waves associated with the impact".

Later, the behavior of free rocking blocks was thoroughly investigated by Ma (2009). Ma examined the efficiency of Housner's model to predict the dynamic motion of a free rocking concrete block. A significant scatter in the experimental COR was observed, while SRM's COR was shown to be close to the average of the experimentally measured COR values. Furthermore, Ma studied the relationship between the amount of energy dissipated during a rocking impact with respect to the impact approaching velocity and impact force. This researcher was not able to associate the impact force with impact energy dissipation. However, a clear relationship between energy dissipation and the approaching velocity was discerned.

2.2.3 Dynamics of rigid blocks

Researchers have also examined motions of a rigid body besides rocking such as shear sliding (Younis and Tadjbakhsh 1984) and shear sliding with rocking motion taking place simultaneously. In fact, sliding motion could be used as a form of base isolation from ground horizontal excitations, which can secure the stability of a structural system. A small coefficient of friction (i.e. $\mu \leq 0.1$) would provide an efficient isolation from horizontal ground motions, however, a value a bit greater would produce a response which may

combine rocking with sliding leading to a more complicated structural response. Sinopoli (1987) suggested a relationship for the minimum coefficient of friction needed to ensure a free rocking motion without participation of sliding motion. Sinopoli and Sepe (1993), also, presented the conditions required for a rigid block to pass from a resting condition into a combined sliding-free rocking motion.

In order to enrich the understanding on rigid body motion, other researchers analytically studied other modes of dynamic motion under horizontal and vertical ground excitations, besides rocking and sliding, which should be included into the original SRM. Mochizuki and Kobayashi (1976) proposed four modes of rigid body motion: (a) slip; (b) rock; (c) rock-slip; and (d) jump. Shenton (1996) stated rigid body motion can be described by five modes: (a) rest, (b) slide, (c) rock, (d) slide-rock and (e) free flight, as shown in Figure 2-10. With Stenton's work, it was shown that sliding and rocking do not always occur separately but there is a dynamic mode in which these two motions are taking place simultaneously. The proposed condition that suggests the occurrence of this mode depends on (a) the coefficient of friction of the rigid block-rigid base interface; (b) the geometric properties of the block; and (c) the acceleration of the base. Furthermore, Shenton suggested "analyses of pure-rocking response, in which the available static friction is just greater than the width-to-height ratio of the body, are most likely in error (i.e., could not be physically realized)." Ishiyama (1982) classified the dynamic motions into six types namely (a) rest; (b) slide; (c) rock; (d) slide rock; (e) translation jump; and (f) rock jump (Fig. 2-11).

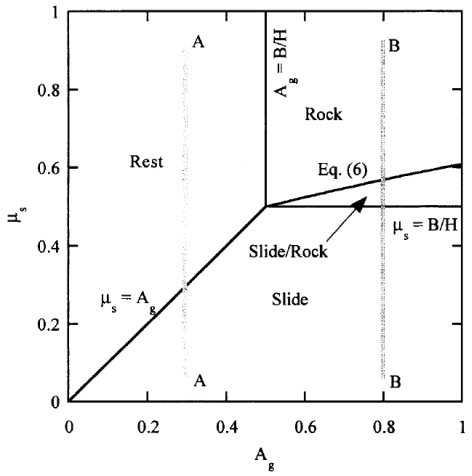

Figure 2-10. Boundaries of Rest, Slide, Rock and Slide-Rock Modes for *h/b*=2; where A_g is the peak ground acceleration and μ coefficient of static friction of the rocking interface (Shenton 1996)

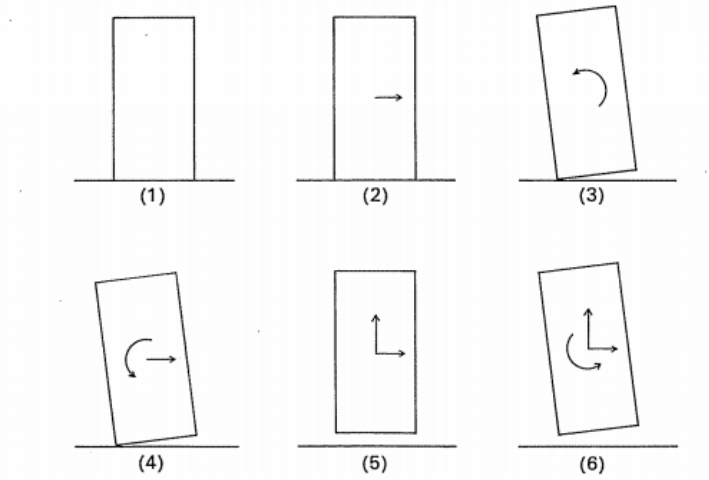

Figure 2-11. The six types of rigid body motion under vertical and horizontal ground excitation, as defined by Ishiyama (1982): (1) rest, (2) slide, (3) rock, (4) slide and rock, (5) translation jump and (6) rock jump.

Ishiyama developed equations of motion to describe the above modes of dynamic rigid body motion, appropriately defined the limits to induce transition from one motion to another and incorporated the idea of a tangential COR into these equations (i.e. COR was divided into a normal and a tangential component with respect to the ground plane). A

computer program was employed to numerically investigate Ishiyama's analytical model. It was shown a coefficient of static friction greater than the ratio $\frac{b}{h}$ is needed to ensure pure free rocking motion, while the tangential and normal COR values corresponding to an impact after translation jump significantly affect the subsequent motions.

Scalia and Sumbatyan (1996) conducted a qualitative study on rigid body slide-rock motion. It was shown that when the body motion is in the slide-rock mode, a coefficient of friction significantly less than unity makes separation impossible. It was also observed that a jump mode of motion is possible only for a coefficient of friction close to unity.

Pompei et al. (1998) adopted an analytical approach in order to define the boundaries of stick-slip transition during rigid body motion. The (a) geometric properties of the body; (b) coefficient of friction; and (c) ground acceleration were considered as the critical parameters for this transition.

2.2.4 Free rocking response and stability under ground excitation

Looking back, stability and rocking of rigid bodies have been used as the criteria to assess the severity of earthquake motions when the earthquake engineering community was not equipped with seismographs for an accurate record of seismic activities (Omori 1899; Omori 1900; Ikegami and Kishinouye 1949; and Ikegami and Kishinouye 1950). The peak acceleration of an earthquake would be measured by observing the ability of rigid bodies, such as tombstones, to remain standing when subjected to ground motion (Milne 1885; Milne and Omori 1893; Kirkpatrick 1927; Brune 1992; Brune 1994; and Brune 1996). Motivated by previous studies on evaluation of seismic intensity using rocking bodies, Shi et al. (1996) examined the stability of precariously balanced symmetric and asymmetric rigid bodies.

Even though this qualitative technique gained a lot of popularity in the past, recent studies concluded monitoring tombstones response for understanding an earthquake event may be an inappropriate and misguided approach (Apostolou 2007).

In the modern earthquake engineering society, free rocking response of rigid bodies and their possibility for overturning under seismic activity is of critical importance when seismic safety of free-standing bodies is concerned. Overturning of house furniture could be a result of medium or strong earthquake motions (Chiriatti and Cimellaro 2012). Also, overturning of equipment, not firmly anchored on their base such as those located in nuclear facilities, would cause significant damages, loss of function and delays in the working process. To prevent this, it is necessary to conduct appropriate safety checks to secure their stability (Moran 1995; Morrow and Uldrich 1995; and Schau and Johannes 2013).

Free rocking of rigid blocks under earthquake excitation can also take place in larger or smaller scale structural systems characterized by a loose bond with the ground. When structural systems are supported by shallow foundations, which may be unable to create a strong bond between the structure and the soil, ground motions may cause uplift of the shallow foundation resulting in the free rocking motion of the whole system. This behavior can either contribute to its survival through the avoidance of the strong ground forces or lead to its overturning.

Accordingly, it can be understood that a rocking structural response under ground motion is fundamentally different from the behavior of a structural system firmly attached on the soil. When a relatively rigid structure is subjected to free rocking, the conventional way of estimating its seismic response using the ideas of structural flexibility, ductility, viscous

damping and hysteretic response do not apply any more (Petrini et al. 2008; Hall 2006; Priestley and Grant 2005; and Otani 1981).

The parameters which influence free rocking response under earthquake motion have been extensively studied by researchers in the past. Aslam et al. (1980) investigated both analytically and experimentally the earthquake response of radiation shielding systems through free vibration and horizontal ground excitation tests. Energy dissipation, assumed to take place only during the impact, was analytically modeled using COR proposed by Housner (1963). The free vibration tests were used to determine the experimental COR value associated with these free rocking systems. When the earthquake tests were executed, Aslam et al. (1980) observed rocking response of free blocks under ground motion can be very sensitive to changes in COR, aspect ratio and size of the rocking block. These results were in general agreement with trends captured by these researchers' analytical study. It was concluded the possibility of overturning decreases with decrease in COR, slenderness ratio $(\frac{h}{b})$ and increases with decrease in the size of the block.

Yim et al. (1980) confirmed that the free rocking response of rigid blocks under earthquake excitation is sensitive to their aspect ratios and sizes. Interestingly, these researchers concluded there is no straightforward relationship between the geometric properties of a block (i.e. its size and aspect ratio), its stability characteristics and the intensity of the earthquake excitation. In contrast to what would be expected, it was shown that a block which overturns when subjected to a certain seismic excitation, may avoid overturning if a more intense earthquake motion is applied. Since a deterministic approach was deemed insufficient to provide a relationship able to directly associate the geometric properties of a block with its stability and applied ground motion characteristics, Yim et al.

(1980) employed a probabilistic approach to produce systematic trends regarding free rocking survival-overturning boundaries. According to their findings, overturning danger (1) increases with increase in the slenderness ratio ($\frac{h}{b}$); (2) decreases with increase in the size of the block; and (3) increases with increase in intensity of the horizontal base excitation.

Spanos and Koh (1984) investigated the free rocking response of rigid bodies under horizontal harmonic excitations and introduced criteria which classify the stability regions (stable rocking system versus failure due to overturning). The proposed classification was developed with respect to the horizontal base excitation amplitude and frequency. Figure 2-12 presents a typical classification into overturning and stable regions. Note that "A steady-state mode is called the (*m*, *n*) mode, where *m*, *n* are positive integers, if it has a minimum interval of repetition which is equal to *n* periods of the excitation and if during that interval it changes sign with positive slope *m* times".

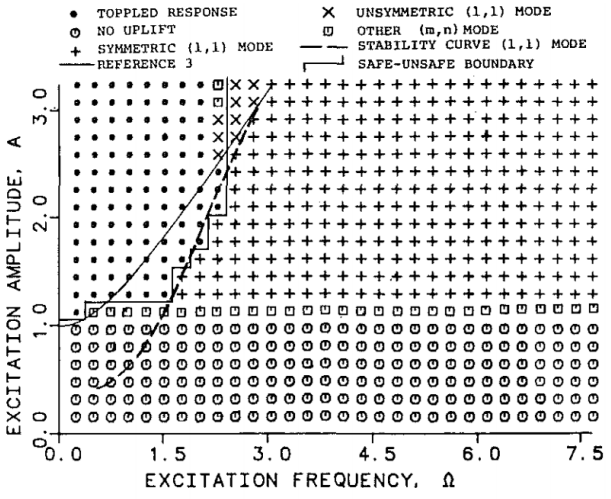

Figure 2-12. Typical classification of rigid body motion response under horizontal harmonic excitation into unsafe-overturning and safe regions, as presented by Spanos and Koh (1984); REFERENCE 3 refers to predictions made by Housner (1963)

Ogawa (1980) analytically developed the conditions necessary to induce a steady state harmonic free rocking response under horizontal sinusoidal excitation. Accordingly, Ogawa established a relationship which associates the harmonic response amplitude with the horizontal ground excitation amplitude and frequency. Steady state response of rigid blocks was also studied by Tso and Wong (1989) who established the conditions necessary to induce a symmetric steady state response. These conditions were dependent on the horizontal base excitation amplitude and frequency. It was shown that an in-phase with respect to horizontal base excitation response is unstable; it always leads to overturning. On the other hand, only out-of-phase responses can be stable. Tso and Wong also observed that an increase in the dynamic parameter p of the block leads to a larger amplitude in its out-of-phase steady state response. Wong and Tso (1989) conducted an experimental study on steady state response of rigid blocks in order to supplement and validate their analytical study. Experimental tests under harmonic excitations were in good agreement with their theoretical estimations regarding the free rocking displacement amplitude versus excitation frequency relationship.

Fielder at al. (1997) examined the free rocking response of symmetric and asymmetric rocking blocks subjected to base excitations. In asymmetric blocks the center of mass is located closer to one of the rotation centers and the response is associated with two different moments of inertia and COR values, with respect to the rotation center. Fielder et al. studied the effect of two parameters influencing rocking block stability: the excitation (a) amplitude; and (b) frequency.

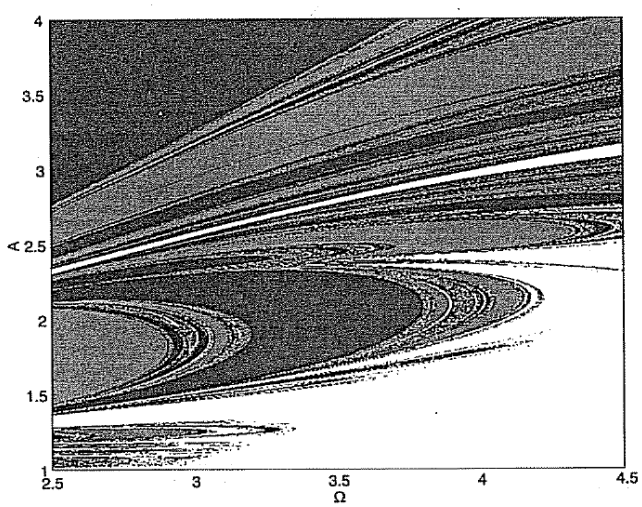

Figure 2-13. Overturning dependence on the forcing parameters for the symmetric block based on numerical simulation with COR=0.95. The direction of overturning: dark-gray – overturning to the left with negative angular displacement; light gray – overturning to the right with positive angular displacement. *A* is the nondimensional amplitude of the horizontal acceleration and Ω is the excitation frequency (Fielder 1997)

Overturning criteria due to horizontal base excitation were thoroughly investigated by Makris and Roussos (2000). These researchers showed that when a free rocking block is subjected to a half-sine pulse, overturning can take place only during the free vibration phase. This finding contradicted the assumption that failure may occur only during the application of a ground excitation originally made by Housner, who also determined the minimum ground excitation amplitude necessary to tip over the rocking block. Furthermore, Makris and Roussos studied the response of a free-standing rigid block under near-source base excitations simulated as trigonometric pulses. It was confirmed that stability of the block is dictated by its aspect ratio and size, and the exciting pulse acceleration and frequency induced by the base.

Later, Zhang and Makris (2001) studied and classified the overturning modes of a free rocking block subjected to a pulse-type horizontal base excitation, as follows: "(a) by

exhibiting one impact; and (b) without exhibiting any impact." Respectively, Zhang and Makris determined (1) a 'safe'; (2) an 'overturning with impact'; and (3) an 'overturning without impact' regions which all were presented on an 'overturning acceleration spectrum'. Hao et al. (2011) conducted computer simulations to determine overturning criteria of a free rocking block leading to conclusions which were in full agreement with the overturning acceleration spectrum originally proposed by Zhang and Makris.

Further understanding on stability of free rocking blocks was achieved by studying the horizontal ground excitation characteristics able to amplify their angular displacement, eventually leading to their overturning. Housner suggested that "the behavior of the rocking block could be quite variable in that relatively small ground motion may fortuitously build up the amplitude at the beginning of the ground motion and lead to overturning the block" (Housner 1963). More recently, amplification of free rocking was thoroughly investigated by DeJong (2012) in order to determine sinusoidal and earthquake ground motion characteristics necessary for amplifying the response of a rigid block, and consequently reaching a "resonance" condition. In contrast to structural systems which have a strong bond with their base, free rocking resonance, defined as the gradual amplification of the rocking displacement amplitude, cannot occur when a harmonic excitation is applied, as rocking of a rigid block is not characterized by a constant natural period; its natural period is an angular displacement and velocity dependent variable. DeJong employed the free rocking energy balance to understand the ground excitation mechanism able to continuously increase the energy content in a free rocking block until failure occurs. According to DeJong's findings, the sinusoidal horizontal ground motions able to cause resonance (1) are always directed opposite to the block's linear horizontal velocity; and (2) their period increases gradually.

Finally, DeJong followed a probabilistic approach to study free rocking overturning under different synthetic horizontal seismic motions. It was observed that the failure probability is sensitive to the period, duration and intensity of the ground excitation.

While most of the free rocking stability studies assumed a horizontal ground excitation, during a real-life earthquake event ground motion may also include a vertical acceleration component. To investigate its effect on free rocking, several researchers simulated the response of a rigid block under an earthquake excitation taking place in both a vertical and horizontal manner.

Taniguchi (2002) developed equations of free rocking motion for a rigid block subjected to horizontal and vertical ground motion. This study stressed the importance of accounting for the vertical excitation component in estimating seismic response of free-standing rigid blocks. According to Taniguchi, when a combination of vertical and horizontal motions are applied to the underlying base, flight of the block (designated as the mode of rigid body motion in which there is no contact between the block and its base) may become part of its response. Hao, also, discussed about the flight mode induced due to vertical ground motion. Hao's analytical study concluded this mode is possible when vertical acceleration of the ground (1) becomes larger than the acceleration due to gravity, g; and (2) points downward. It was suggested that this mode can be beneficial for the free rocking stability as the rocking block may avoid a window of the horizontal excitation time history while being in the flight mode.

2.2.5 Rocking block connected with secondary structural elements

Water towers, radiation shields and ancient monuments are examples of free-standing systems where a relatively rigid structure is combined with one or more secondary elements attached on its top face (e.g. Fig. 2-14). Free rocking motion of these systems was researched and presented in the rocking literature.

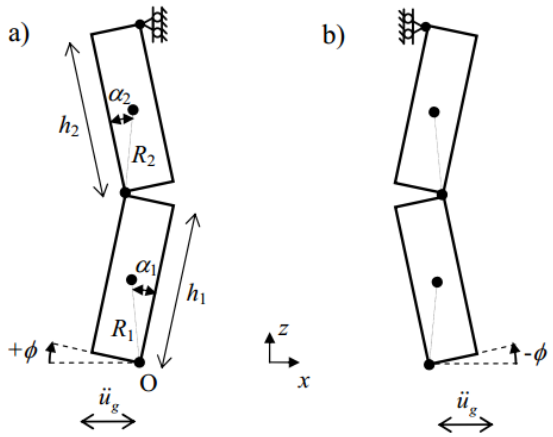

Figure 2-14. Example of a free rocking block with a secondary block on its top; idealization used by DeJong and Dimitrakopoulos (2013) to analytically investigated free rocking response of masonry walls.

The increased mass effect and relative oscillation of the secondary structure were theoretically shown to be critical for a free rocking response. Particularly, they may influence the stability criteria associated with rocking motion of the overall structure (Kovaleva 2010).

Masonry arches subjected to rocking may be also modelled as rigid blocks with one or more secondary elements attached on the primary block. De Lorenzis et al. (2007) analytically examined the behavior of these systems under horizontal base pulses. De Lorenzis et al. (2007) aimed at a better understanding of the excitation characteristics associated with failure of masonry arches. DeJong and Dimitrakopoulos (2013) discussed

free rocking behavior of masonry walls. It was assumed that masonry walls can be divided into a series of rigid blocks which are standing without any bond between each other.

Motivated by the seismic stability displayed by ancient monuments, Makris and Vassiliou (2013) studied free rocking response of ancient columns with a rigid beam sitting on their top. Makris and Vassiliou noticed that this behavior is similar to the response of a single rigid block, however, the existence of a secondary body at the top of the block can influence the stability of the whole system; the heavier the rigid beam is, the more stable the rocking system becomes.

2.2.6 Chaotic free rocking behavior

Research studies aiming at analytically estimating the response of experimental free rocking units subjected to either free vibration or base excitations concluded with questions about why actual free rocking motion may not always be easy to accurately predict. Findings in the current literature suggest that while the quarter period of free rocking is, in general, successfully predicted by different mathematical models, the complex impact phenomenon adds an uncertainty issue in the analytical estimation and experimental repeatability of virtually identical experimental procedures.

Wong and Tso (1989) concluded some of their experimental results cannot be explained with routinely employed analytical approaches. Using a mapping technique, Hogan (1989) was able to explain uncertainty in free rocking motion by introducing another domain of free rocking motion designated as chaos. Yim and Lin (1991) defined the chaotic free rocking response, “Its response behavior is characterized by a random-like unpredictable aspect as well as a certain order in the motion, although the excitation is straightly

deterministic and periodic". This unpredictability was attributed to the extreme sensitivity of rocking to initial and impact conditions. Lin and Yim (1996) employed horizontal periodic excitations with random noise to analytically study the chaotic response of free rocking blocks. Lin and Yim investigated the relationship between chaos and overturning showing that when noise was accompanied with periodic excitation to form the ground motion, possibility of failure increases. Later, Jeong et al. (2003) examined free rocking response of both (a) an undamped; and (b) a damped rocking system – (a) no energy dissipation; and (b) accounting for energy dissipation due the impact, respectively – with respect to the chaotic response. Response of an undamped free rocking block included quasi-static and chaotic motions, which were strongly dependent on the properties of the horizontal ground motion and the geometric characteristics of the block. On the other hand, a damped free rocking block was shown to respond into periodic motions dependent on its damping properties expressed through COR.

2.3 Flexible Free Rocking Systems

The assumption of a rigid free rocking system was questioned by researchers, who introduced alternative modeling techniques to account for the flexibility of (a) the free rocking system; and (b) the underlying base. This way, researchers aimed at explaining the effect of soil flexibility on free rocking response, while arguing that a slender rocking structure would exhibit self-deflection which should be taken into account in the modeling process.

In one of the proposed structure-soil idealizations (Chopra and Yim 1985), the free rocking structure was simulated as a SDOF with its mass concentrated at the top, while the

foundation-soil interface was assumed to be rigid. In the second idealization, the SDOF system was interacting with the soil via two spring-dashpot mechanisms located at the corners of the bottom edge of the structure. A third approach suggested a Winkler type soil surface constructed using a continuous distribution of spring-dashpot elements along the rocking base. Psycharis and Jennings (1983) also developed two models which considered a flexible structure-base contact interface. The first model used two concentrated springs at the corners, while the second one followed the Winkler foundation concept. An extensive study on structures free to rock on flexible foundations was conducted by Palmeri and Makris (2008). The importance of considering a flexible rocking interface was examined by these researchers who concluded "the smaller the angle of slenderness, the less sensitive the response to the flexibility of the foundation";

Other approaches on flexible modeling of free rocking motion included other modes of motions besides rocking, similarly to modeling of rigid body motion introduced by Ishiyama (1982). Andreaus and Casini (1998) assumed a set of two horizontal and two vertical springs located at the two bottom corners of the free rocking block, as shown in Figure 2-15. These spring mechanisms were operating as the contact points between the block and its base. Energy dissipation due to interaction at the normal direction, associated with the vertical springs, was accompanied with energy dissipation due to friction, associated with the horizontal springs.

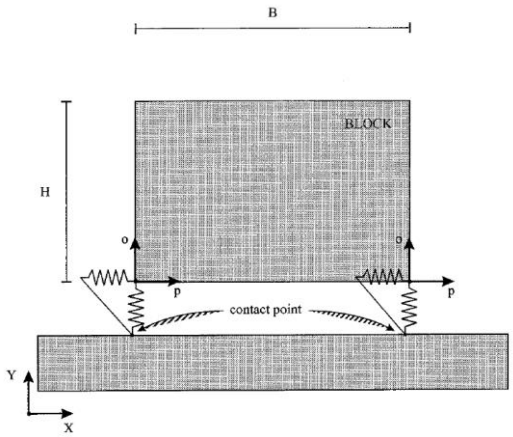

Figure 2-15. Rocking Model developed by Andreaus and Casini (1998)

Later, Chatzis and Smyth (2012) proposed two spring models considering the effects of sliding, uplift, contact interface flexibility, and geometric nonlinearities. The response of these models was shown to be very sensitive to selection of damping and spring stiffness parameters of the spring-dashpot mechanisms. The first model consisted of two spring-dashpot mechanisms located at the bottom corners and the second one was a free rocking model with a Winkler foundation. Both models were analytically examined for free vibration and horizontal base excitations. Effects of stiffness and damping parameters in the free rocking response were analytically investigated and stability analysis was conducted to determine the boundaries between overturning and safety domains.

Vassiliou et al. (2013) developed a spring model which considered both a flexible free rocking body and a flexible contact interface consisted of spring-dashpot mechanisms. Vassiliou et al. concluded influence of the flexibility properties of a rocking body increases with increase in its size.

Truniger (2013) also conducted an experimental study on flexible free rocking systems. This study was conducted on a column unit with an extra mass attached at its top, as shown in Figure 2-16.

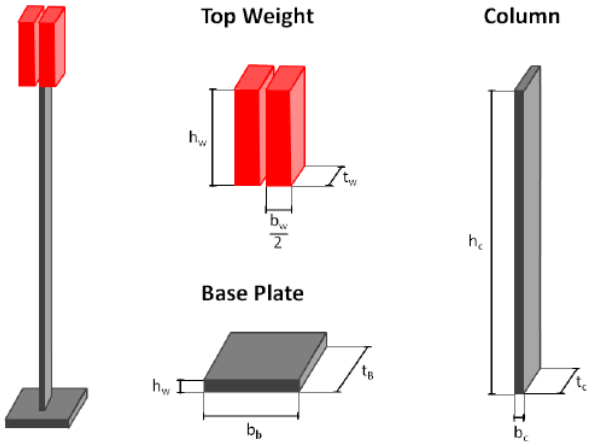

Figure 2-16. Column Specimen with the supplemental mass and the rocking base plate (Truniger 2013)

Truniger observed that smooth free rocking response was combined with frequency vibrations resulting from relative elastic oscillations of the upper part of the free rocking unit.

2.4 Controlled Rocking of Rigid Blocks

The introduction of unbonded post-tensioned in rocking structures provided a self-centering capacity to these systems, added to the original re-centering ability resulting from their self-weight. The new systems, designated as controlled rocking systems, are characterized by different "natural" properties (i.e. dynamic parameter, quarter period) which, as would be expected, are significantly affected by the prestressing force applied by the post-tensioned steel.

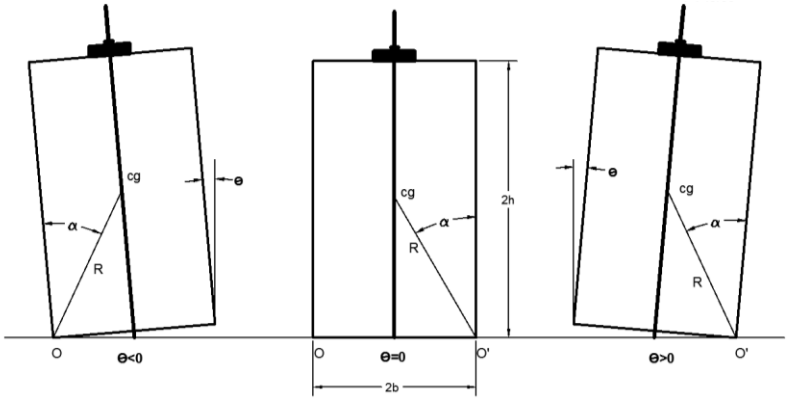

Figure 2-17. A block subjected to controlled rocking

Comparison of the stability characteristics of free and controlled rocking was conducted by Dimentberg et al. (1993) who studied rocking response of both unanchored and anchored blocks. Using a probabilistic method, Dimentberg et al. (1993) found that a block subjected to controlled rocking is generally more stable than a free rocking block. A comparison of the stability features of unanchored and anchored blocks was also conducted by Makris and Zhang (2001). These researchers followed a deterministic approach to mathematically define the instability domains of an anchored block subjected to horizontal pulse ground excitation. Two instability domains were observed and classified as follows: (a) overturning without any impact; and (b) overturning with one impact. In contrast to the conclusions made by Dimentberg et al., Makris and Zhang observed that there is a frequency domain, in which free rocking blocks can be more stable than controlled rocking blocks (Fig. 2-18). It was specifically stated that "The stronger the restrainer, the smaller is the acceleration amplitude needed to overturn an anchored block, whereas a free-standing block can withstand the higher acceleration amplitude".

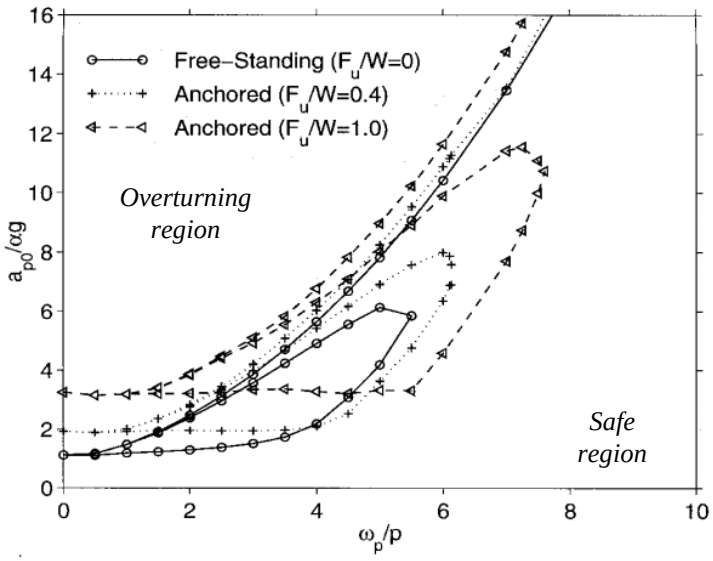

Figure 2-18. Typical overturning acceleration spectra, as presented by Makris and Zhang (2001). F_u is the ultimate strength of the anchored steel and W the weight of the controlled rocking block

2.5 Finite Element Analysis of Rocking Motion

Finite Element Analysis (FEA) has been used to assess rocking response of both free and controlled rocking blocks. Various modeling approaches have been introduced with different degrees of success.

Ardila-Giraldo et al. (2013) developed a two-dimensional FE free rocking model for simulating platform-container systems under earthquake excitation. This rocking model used a fine uniform mesh, where Rayleigh damping was used to simulate rocking energy dissipation. The two-dimensional model used four-node plane elements and the contact algorithm employed the augmented Lagrangian method.

In order to investigate the dynamic response of ancient structural systems located in Greece and Italy, Manos et al. (2013) developed FE free rocking models of scaled ancient

columns. The models were subjected to free vibration, sinusoidal and earthquake motion simulations. These analyses results were in good agreement with experimental results.

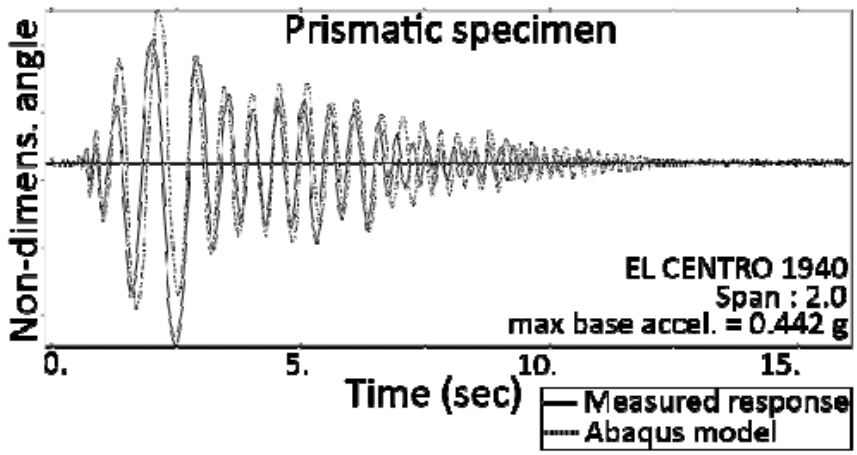

Figure 2-19. Typical comparison between experimental and FEA results, as presented by Manos et a. (2013); Prismatic specimen subjected to earthquake excitation

The earthquake response of tall concrete walls with free rocking foundation systems was simulated by Lemieux and Koboevic (2013). Inelastic material properties were used for the wall to capture its inelastic behavior and non-linear material behavior was used to simulate soil behavior. The Winkler foundation was used to simulate the structure-foundation interface. It was analytically shown that by allowing tall concrete walls to rock, a significant reduction in the seismic force demand is achieved in comparison with conventional reinforced concrete structures.

Belleri et al. (2013) conducted dynamic FEA of a controlled rocking wall using different FE techniques. First, a three-dimensional rocking wall model, using brick elements, was developed. Fine mesh was used for the bottom corners of the wall, while the contact surface interaction was modeled with a tangential and a normal direction component. The

tangential interaction used the "rough" algorithm and the normal interaction used the "hard contact" algorithm (Abaqus Analysis User's Guide, Abaqus 6.13). Second, one-dimensional models with spring and fiber elements were also proposed. It was shown one-dimensional models are able to estimate the global behavior of a controlled rocking wall, while two- and three-dimensional FE modeling is necessary for adequately estimating local behavior of the wall (i.e. neutral axis variation and compressive strains at the bottom rocking edge).

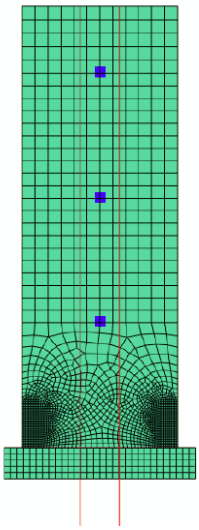

Figure 2-20. Finite Element Model of a rocking wall proposed by Belleri et al. Finer mesh was used only for the bottom corners. The violet points represent imposed point masses and the red lines represent the post-tensioned tendons (Belleri et al. 2013)

2.6 Dynamic Decay of Structures

Damping is defined as the energy-absorbing mechanism causing decrease in the amplitude of an oscillation or vibration. In structural engineering, damping ratio, ζ constitutes a simplified approach to express the inherent ability of a structure to dissipate the seismic energy. The magnitude of damping ratio plays a critical role in the structural response and amplification of motion under an earthquake excitation. For instance, as the frequency of the

excitation is centered on the natural frequency of the structure, the resulting condition, designated as resonance, tends to increase the displacement amplitude of the structure. If this happens, the system can suffer severe damages. Estimating the inherent damping of a structure can help to avoid resonance, accurately predict the decay of motion and the displacement time history.

Furthermore, when tall multistory buildings are concerned, damping becomes very critical, due to the increased flexibility these systems exhibit. Many high-rise structures appear to oscillate with excessive lateral drifts, despite the fact that they have been designed to avoid such displacements. Even though these oscillations might not induce structural damages, safety and serviceability requirements can be violated. Therefore, accurate estimation of damping ratio is deemed critical for the prognosis and prevention of this behavior. However, understanding of damping in structural systems has been one of the most difficult topics in structural dynamics.

Unlike other properties of a structure, like mass and stiffness, damping is dependent on various physical mechanisms that convert strain and kinetic energy into heat. Material damping and interfacial damping are the two governing damping mechanisms.

Material damping refers to microscopic phenomena that occur between the different particles of the structure. It's a complex molecular interaction due to relative displacements of the particles being in vicinity which dissipates mechanical energy. Secondly, when the material elastic limits are exceeded, the structure starts to behave in an inelastic manner and develops a hysteresis loop due to the resulting residual strain. This behavior due to the inelastic action can also be classified as a material damping mechanism.

Interfacial damping takes place due to frictional phenomena. This mechanism can be activated in different ways, e.g. at the interface of the connection between structural and nonstructural components. In cast-in-place concrete structures, energy dissipation due to interfacial damping occurs at the closing and opening of micro cracks. In steel structures, connections tend to develop high friction rates leading to important contribution of interfacial damping in the total energy dissipation.

Another damping mechanism, less important in conventional structural systems, is radiation damping. Radiation damping is a concern in soil-foundation and rocking structure-foundation interaction problems, dynamic analysis of soil and impact phenomena. Radiation damping refers to the energy dissipation induced due to geometric diffusion of waves propagating inside a solid.

2.6.1 Role of damping in precast controlled rocking members

In precast controlled rocking systems, there is no continuity in the longitudinal reinforcing steel and concrete material between the rocking structure and the underlying foundation, and therefore tension in concrete is avoided. Under an earthquake load, a rocking structure is expected to form a gap between its bottom edge and the foundation surface, avoid major damages due to plastic hinge action and transmit the seismic energy to the foundation through the impact mechanism.

During an ideal impact of a rocking block with its base, some kinetic energy is converted into elastic strain energy and then it is reconverted into kinetic energy when the block's bottom edge takes off. However, during this cycle there is some energy loss induced

by damping mechanisms associated with the impact. According to the available literature, the governing impact dissipation mechanism is radiation damping.

As was previously discussed in Sections 2.2.1 and 2.2.2, researchers adopted the concept of COR to simulate and measure rocking decay of motion. However, the limitations of this approach and the evidence of its inefficiency to accurately predict a controlled rocking motion motivated researchers to further investigate energy dissipation in controlled rocking structures.

Cheng (2007) conducted a series of free vibration tests on controlled rocking blocks with various slenderness characteristics and interface materials between the rocking system and its foundation. Cheng noticed that blocks of a larger aspect ratio tend to dissipation a measurable amount energy through sliding and that the use of different interface materials can significantly affect energy dissipation during rocking motion. In this study, damping was evaluated by correlating COR with an equivalent viscous damping ratio, referred to as radiation damping ratio. Interface material effects were also investigated by ElGawady et al. (2011) who conducted a series of tests using concrete, steel, timber and rubber materials at the contact interface. Blocks of various aspect ratios were subjected to free rocking under free vibration to assess the influence of each interface material on their dynamic energy dissipation characteristics. The use of a rubber layer at the contact interface was found to significantly increase the amount of energy dissipation per cycle. It is also shown that by using a rubber interface, a more continuous energy dissipation takes place during rocking motion.

Later, O'Hagan et al. (2013) showed that energy dissipation due to controlled rocking cannot be exclusively described by COR and a combination of different damping

mechanisms is necessary to accurately model decay of controlled rocking motion under free vibration. Suggested damping components by O'Hagan et al. included COR, equivalent viscous damping (EVD) and a coulomb friction damping (CFD), while the combinations of (1) COR – CFD; and (2) EVD – CFD were suggested as the most appropriate (Fig. 2-21 and 2-22).

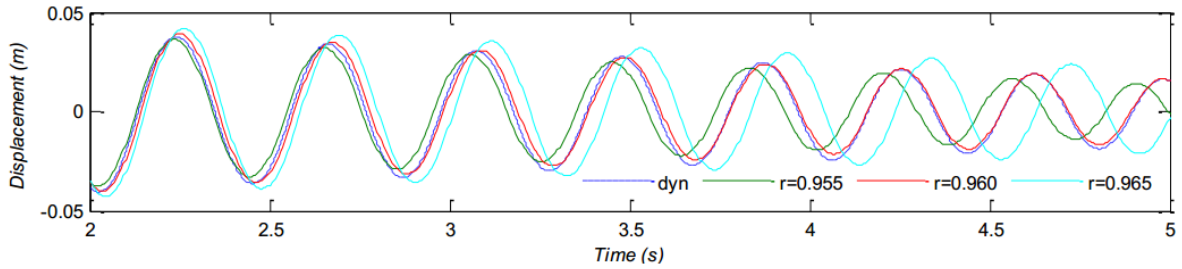

Figure 2-21. Comparison of the experimental (designated as dyn) and analytically estimated linear displacement time histories; r is the COR used in the analytical rocking model combined with a constant CFD force equal to 0.5 kN (O'Hagan et al. 2013)

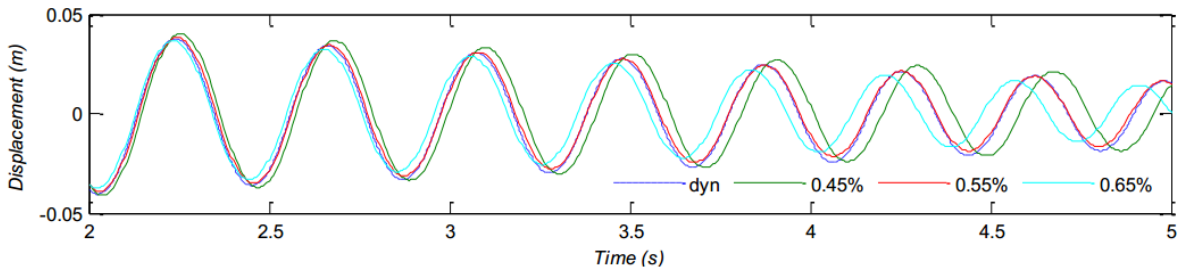

Figure 2-22. Comparison of the experimental (designated as dyn) and analytically estimated linear displacement time histories; different damping ratio values (i.e. 0.45%; 0.55%; 0.65%) were used in the analytical rocking model combined with a constant CFD force equal to 0.5 kN (O'Hagan et al. 2013)

2.7 Rocking in Design Practice

This section briefly discusses some of the knowledge provided by the published literature on design of seismic-resisting structural systems, which are subjected to free or controlled rocking motion.

2.7.1 Free rocking in design practice

A firmly bonded structure – foundation and foundation-soil condition is routinely assumed for designing seismic-resisting structural systems. However, under an earthquake excitation, structural systems not firmly attached to the ground can enter into a free rocking motion, resulting in a structural behavior initially not accounted in the design procedures. The possibility of a structure to enter rocking motion motivated Priestley et al. (1978) to propose a design approach which takes into account the effect of rocking in the structural response. Following SRM's definition for COR, Priestley et al. (1978) introduced an equivalent viscous damping model assuming free rocking energy dissipation due to impact.

$$\xi = \frac{1}{2\pi m} \ln\left(\frac{x_o}{x_m}\right) \tag{2-16}$$

Considering that every half a period a free rocking system is subjected to one impact, COR, *r*, is correlated with the equivalent viscous damping, as follows,

$$\xi = \frac{1}{\pi n} \ln\left(\frac{\theta_o}{\theta_n}\right) \tag{2-17}$$

where,

$$m = \frac{n}{2} \tag{2-18}$$

and

$$\theta_n = 1 - \sqrt{1 - r^n (1 - (1 - \theta_o)^2)} \quad (2\text{-}19)$$

This way, a structure which enters into a free rocking motion can be simulated as a SDOF system which dissipates energy continuously according to a constant damping ratio (ξ). Priestley et al. (1978) proposed the design of response spectra in order to estimate the displacement response of structural systems subjected to free rocking.

Makris and Konstantinidis (2003) called into question the approach followed by Priestley et al., arguing that it is an "oversimplified methodology" which was based on the assumption that "it is possible to represent a rocking block as a single-degree-of-freedom oscillator with constant damping, whose period depends on the amplitude of rocking." Conversely, Makris and Konstantinidis suggested that a free rocking system should not be modelled as a SDOF system, since its force-displacement response, damping mechanism and natural period are fundamentally different from the respective properties of a SDOF.

2.7.2 Controlled rocking in design practice

Despite their fundamentally different behavior from conventional structural systems, rocking motion has been realized as a beneficial feature, as it implicitly provides a means of base-isolation and minimizes structural damage. This advantage triggered the structural engineering society to use this concept for designing controlled rocking precast concrete seismic-resisting systems. Mander and Cheng (1997) used the concept of controlled rocking to develop their "damage avoidance design". It was stated a controlled rocking structural system is able to maintain serviceability after an earthquake event with reparable damage (Mander et al. 1998).

Design guidelines for a rocking precast concrete wall system was introduced by Nakaki et al. (1999). Two or more walls can be connected using special connectors designed to enhance hysteretic energy dissipation under seismic activity. Ajrab et al. (2004) proposed a lateral resisting frame consisted of rocking walls and a system of tendons. Damping of the system was provided by the impact mechanisms, supplementary damping devices, material damping and hysteretic response of the frame. Ajrab et al. (2004) concluded a lateral resistance system which adopts rocking behavior can be a reliable alternative solution in seismic regions.

In order to supplement design of rocking precast concrete seismic-resisting systems, Sriram and Sritharan (2009) proposed a simplified design method to estimate the neutral axis depth of the rocking base with respect to angular displacement. A simplified approach was also employed for accurately estimating the confined concrete strain close to the bottom layer of the rocking wall.

The current Rocking Concrete Shear Wall Design Requirements proposed by the American Concrete Institute (ACI ITG-5.2-09) specifies the design procedures for unbonded post-tensioned single or jointed rocking shear walls. Energy dissipation relies on supplementary damping mechanisms, such as coupling devices, unbonded vertical reinforcement.

2.8 Summary and Conclusions

A summary of the research work on free and controlled rocking was presented in this Chapter. In the primary rocking studies, researchers investigated and introduced analytical techniques for modeling free rocking motion, triggered by the idea that free rocking could be

the key mechanism for the survival of seemingly unstable structures during earthquake events of the past. From a different standpoint, other researchers suggested overturning of free-standing objects as an index for estimating the intensity of earthquake motions.

Latter research studies focused on incorporating the idea of free rocking into realistic design procedures. Accordingly, the overturning danger was systematically investigated to determine the risk behind allowing free rocking motion in structural systems. In addition, modeling techniques were introduced for developing earthquake response spectra of free rocking motion. Included in these modeling techniques were suggestions for estimating energy decay due to free rocking motion, with the most popular approach assuming an impact dissipation mechanism expressed through COR (Housner 1963). While this approach has been experimentally shown to provide inaccurate results in a series of cases, researchers showed limited interest for conducting systematic studies on better understanding decay of free rocking motion. In contrast, most of the analytical and experimental studies considered the use of an average COR as an adequate approach for characterizing decay of free rocking motion, despite the large scatter in the COR values exhibited during experimental free rocking tests.

The introduction of a post-tensioning mechanism in the primary free rocking systems revolutionized the science of seismic engineering. These new systems, designated as controlled rocking systems, were mainly investigated for their stability characteristics and seismic-resisting capacities. Unfortunately, researchers have showed limited interest on systematically studying decay of controlled rocking and, moreover, comparing it with decay of free rocking. In contrast, analytical work on controlled rocking has directly assumed SRM's COR as a valid approach for controlled rocking without any justification, while

experimental studies helped to understand only general trends of the energy dissipation due to controlled rocking, however, without proposing methods for modeling its behavior.

From the design standpoint, controlled rocking systems have been used as the main feature of innovative seismic-resisting configurations which are designed to operate with minimal damage concentrated at the bottom edge of the rocking structure. According to design recommendations, the most part of the seismic energy is directed to supplementary hysteretic damping mechanisms (e.g. special connectors). Dynamic energy dissipation due to rocking motion is not accounted.

This study aimed at researching the characteristics of energy dissipation in free and controlled rocking, which are considered as the missing component for a comprehensive understanding on rocking behavior. It is expected that the outcome of this study would provide an insight on this aspect of rocking to researchers interested in the rocking problem with the ultimate goal of (1) improving accuracy in estimating free and controlled rocking motion due to earthquake load; and (2) incorporating energy dissipation due to controlled rocking into the design procedures in order to improve cost-effectiveness of rocking precast concrete members.

2.9 References

Aaleti, S., and Sritharan, S., 2009. A simplified analysis method for characterizing unbonded post-tensioned precast wall systems, *Engineering Structures*, **31**(12), 2966-2975

Abaqus analysis user's guide version 6.13. *Dassault Systemes Simulia Corp.*

ACI ITG-5.2-09, Requirements for design of a special unbonded post-tensioned precast shear wall satisfying ACI ITG-5.1 and Commentary.

Ajrab, J., J., Pekcan, G., Mander, J., B., 2004. Rocking wall – frame sturctures with supplemental tendon systems, *J. Struct. Eng*., **130**(6), 895-903.

Andreaus, U., and Casini, P., 1999. On the rocking-uplifting motion of a rigid block in free and forced motion: Influence of sliding and bouncing, *Acta Mechanica*, **138**(3-4), 219-241.

Apostolou, M., Gazetas, G., Garini, E., 2007. Seismic response of slender rigid structures with foundation uplifting, *Soil D. Earthquake Eng*., **27**, 642-654.

Ardila-Giraldo, O., 2013. Contact interface modeling in the dynamic response of rigid blocks subjected to base excitation, *4th ECCOMAS Them. Conf. on COMPDYN*.

Aslam, M., Godden, W.G., and Scalise, D. T., 1980. Earthquake rocking response of rigid bodies, *Journal of the Structural Division*, **106**(2), 377-392.

Belleri, A., Torquati, M., Riva, P., 2013. Finite element modeling of 'Rocking walls', *4th ECCOMAS Them. Conf. on COMPDYN*.

Brake, M., R., 2012. An analytical elastic-perfectly plastic contact model, *International J. Solids and Structures*, **49**(22), 3129-3141.

Brune, J., N., 1992. Distribution of precariously balanced rocks in Nevada and California: correlation with probability maps for strong ground motion, *Bull. Seismol. Soc. Am.*, **73**(43), 351.

Brune, J., N., 1994. Constraints on ground motion from great earthquakes provided by groups of precarious rocks, *Seism. Res. Lett*., **65**(1), 64.

Brune, J., N., 1996. Precariously balanced rocks and ground-motion maps for Southern California, *Bull. Seismol. Soc. Am.*, **86**(1), 43-54.

Chatzis, M., and Smyth, A., 2012. Robust Modeling of the Rocking Problem, *J. Eng. Mech.*, ASCE, **138**(3), 247-262.

Cheng, C., T., 2007. Energy dissipation in rocking bridge piers under free vibration tests, *Earthquake Eng. Struct. Dyn*., **36**(4), 503-518.

Chiriatti, M., Cimellaro, G., P., 2012. Overturning ratio under one sine pulse, *15 WCEE LISBOA.*

Chopra, A., and Yim, S., 1985. Simplified earthquake analysis of structures with foundation uplift, *J. Struct. Eng.*, ASCE, **111**(4), 906-930.

DeJong, M. J., 2012. Amplification of rocking due to horizontal ground motion, *Earthquake Spectra* **28**(4), 1405-1421.

DeJong, M., J., and Dimitrakopoulos, E., G., 2013. Towards a unified description of rocking structures, *4th ECCOMAS Them. Conf. on COMPDYN*.

De Lorenzis, L., DeJong, M., J., Ochsendorf, J., 2007. Failure of masonry arches under impulse base motion, *Earthquake Eng. Struct. Dyn.*, **36**(14), 2119-2136.

Dimentberg, M., F., Lin, Y., K., Zhang, R., 1993. Toppling of computer-type equipment under base excitation, *J. Eng. Mech.*, ASCE, **119**(1), 145-160.

ElGawady, M. A., Ma, Q., Butterworth, J. W., and Ingham, J., 2011. Effects of interface material on the performance of free rocking blocks, *Earthquake Eng. Struct. Dyn.*, **40**(4), 375-392.

Falcon, E., Laroche, C., Fauve, S., Coste, C., 1998. Behavior of one inelastic ball bouncing repeatedly off the ground, *The European Phys. J. B*, **3**(1), 45-57.

Fielder, W., T., Virgin, L., N., Plaut, R., H., 1997. Experiments and simulation of overturning of an asymmetric rocking block on an oscillating foundation, *Eur. J. Mech, A/Solids*, **16**(5), 905-923.

Goldsmith, W., 1960. Impact, Edward Arnold Ltd, London.

Hao, H., and Zhou, Y., 2011. Rigid structure response analysis to seismic and blast induced ground motions, *Procedia Engineering*, **14**, 946-955.

Hall, J., F., 2006. Problems encountered from the use (or misuse) of Rayleigh damping, Earthquake Eng. Struct. Dyn., **35**(5), 525-545.

Hardy, C., Baronet, C., N., Tordion, G., V., 1971. The elasto-plastic indentation of a half-space by a rigid sphere, *International J. Num. Methods in Eng.*, **3**(4), 451-462.

Hertz, H., 1882. On the contact of elastic solids, *J. fur die Reine und Andgewandte Mathematik*, **92**, 156-171.

Housner, G., 1963. The behavior of inverted pendulum structures during earthquake excitations, *Bull. Seismol. Soc. Am.*, **53**(2), 403-417.

Hunter, S., C., 1957. Energy absorbed by elastic waves during impact, *J. of the Mech. and Phys. of Solids*, **5**(3), 162-171.

Ishiyama, Y., 1982. Motions of rigid bodies and criteria for overturning by earthquake excitations, *Earthquake Eng. Struct. Dyn*, **10**(5), 635-650.

Ikegami, R., Kishinouye, F., 1949. A study on the overturning of rectangular columns in the case of the Nankai earthquake, Un. *Tokyo Earthquake Res. Inst. Bull*., **25**(4), 49-55.

Ikegami, R., Kishinouye, F., 1950. The acceleration of earthquake motion deduced from overturning of the gravestones in case of the Imaichi earthquake, *Tokyo Earthquake Res. Inst. Bull*, **28**(2), 121-128.

Jamari, J., Schipper, D., J., 2006a. An elastic-plastic contact model of ellipsoid bodies, *Tribology Letters*, **21**(3), 262-271.

Jamari, J., Schipper, D., J., 2006b. Experimental investigation of fully plastic contact of a sphere against a hard flat, *ASME J. Tribology*, **128**(2), 230-235.

Jeong, M., Suzuki, K., Yim, C., S., 2003. Chaotic rocking behavior of freestanding objects with sliding motion, J. Sound Vibration, **262**(5), 1091-1112.

Kirkpatrick, P., 1927. Seismic measurements by the overthrow of columns, *Bull. Seism. Soc. Am.*, **17**(2), 95-109.

Koller, M., G., and Kolsky, H., 1987. Waves produced by the elastic impact of spheres on thick plates, *International J. Solids and Structures*, **23**(10), 1387-1400.

Kovaleva, A., 2010. The Melnikov criterion of instability for random rocking dynamics of a rigid block with an attached secondary structure, *Nonlinear Analysis: Real World Appl.*, **11**(1), 472-479.

Lee, C., H., Masaki, S., Kobayashi, S., 1972. Analysis of ball indentation, *International J. Mech. Sciences*, **14**(7), 417-426.

Lemieux, M., A., and Koboevic, S., 2013. Rocking response of taller reinforced concrete walls, *4th ECCOMAS Them. Conf. on COMPDYN*.

Lin, H., and Yim, C., S., 1996. Nonlinear rocking motions. I: Chaos under noisy periodic excitations, *J. Eng. Mech.*, ASCE, **122**(8), 719-727.

Lipscombe, P., 1990. Dynamics of rigid block structures, *PhD Thesis, University of Cambridge, Cambridge, England.*

Lipscombe, P., and Pellegrino, S., 1993. Free rocking of prismatic blocks, *J. Eng. Mech.*, ASCE, **119**(7), 1387-1410.

Love, A., E., H., 1927. A treatise on the mathematical theory of elasticity, Cambridge University Press.

Ma, Q., 2009. The mechanics of rocking structures subjected to ground motion, *PhD Thesis, Department of CEE, The University of Auckland, New Zealand.*

Makris, N., and Vassiliou, M., F., 2013. Rocking response and stability analysis of an array of free-standing columns capped with a free-standing rigid beam, *4th ECCOMAS Them. Conf. on COMPDYN.*

Makris, N., and Konstantinidis, D., 2002. The rocking spectrum and the limitations of design guidelines, *15th ASCE Eng. Mech. Conference June 2-5, Columbia University, New York, NY.*

Makris, N., and Konstantinidis, D., 2003. The rocking spectrum and the limitations of practical design methodologies, *Earthquake Eng. Struct. Dyn.*, **32**(2), 265-289.

Makris, N., and Roussos, Y., S., 2000. Rocking response of rigid blocks under near-source ground motions, *Geotechnique*, **50**(3), 243-262.

Makris, N., and Zhang, J., 2001. Rocking response of free-standing blocks under cycloidal pulses, *J. Eng. Mech.*, ASCE, **127**(5), 473-483.

Makris, N., and Zhang, J., 2001. Rocking response of anchored blocks under pulse-type motions, *J. Eng. Mech.*, ASCE, **127**(5), 484-493.

Mander, J., B., and Cheng, C., T., 1997. Seismic resistance of bridge piers based on damage avoidance design, *Tech. Rep. NCEER-97-0014, National Center for Earthquake Eng. Res., Buffalo, N. Y.*

Mander, J., B., Contreras, R., Garcia, R., 1998. Rocking columns: An effective means of seismically isolating a bridge, *Tech. Rep. MCEER-98-0001, Proc., U.S.-Italy Workshop on Seismic Protective Systems for Bridges, Columbia Un. New York*, 335-348.

Manos, G., Petalas, A., Demosthenous, M., 2013. Numerical and experimental study of the rocking response of unanchored body to horizontal base excitation, *4th ECCOMAS Them. Conf. on COMPDYN.*

Milne, J., 1885. Seismic experiments, *Trans. Seism. Soc. Japan*, **8**, 1-82.

Milne, J., and Omori, F., 1893. On the overturning and fracturing of brick and columns by horizontal applied motion, *Seism. J. Japan*, **1**, 59-86.

Moran, T., J., 1995. Uplift and rocking of a deformable body subject to base excitation, *Proc. Symp. Nat. Hazard Phen. Mit., ASME/JSME Joint Pressure Vessel and Piping Conf., Honolulu, Hawaii.*

Morrow, W., M., and Uldrich, E., D., 1995. Proposed criteria for the stability in earthquakes of nuclear-material shipping casks, *DOE Nat. Harards Mit. Symp., Denver, CO.*

Mochizuki, T., and Kobayashi, K., 1976. A study on acceleration of earthquake motion deduced from the movement of column – an analysis on the movement of column, *Trans. Architectural Inst. Japan*, 248, 63-70.

Nagurka, M., and Huang, S., 2004. A mass-spring-damper model of a bouncing ball, *American Control Conference, 2004*, **1.**

Nakaki, S. D., Stanton, J. F., Sritharan, S., 1999. An overview of the PRESSS five-story precast test building, *PCI Journal*, **44**(2), 26-39.

Ogawa, N., A study on overturning vibration of rigid structure, *Proc. 7th world conf. earthquake eng.*, Instanbul, Turkey, **7**, 205.

O'Hagan, J., Twigden, K., Ma, Q., 2013. Sensitivity of post-tensioned concrete wall response to modeling of damping, *New Zealand Society for Earthquake Engineering Conference.*

Omori, F., 1899. Horizontal pendulums for the mechanical registration of seismic and other earthquake movements, *J. College Science, Imperial Un. Tokyo, Japan*, **11**(3), 121-145.

Omori, F., 1900. Seismic experiments on the fracturing and overturning of columns, *Publ. Earthquake Inv. Committee in foreign lang.*, **4**(2), 69-141.

Otani, S., 1981. Hysteretic models of reinforced concrete for earthquake response analysis, *The Faculty of Engineering Un. Tokyo*, **XXXVI**(2), 24.

Palmeri, A., and Makris, N., 2008. Response analysis of rigid structures rocking on viscoelastic foundation, *Earthquake Eng. and Struct. Dyn.*, **37**(7), 1039-1063.

Petrini, L., Maggi, C., Priestley, M., J., Calvi, G., M., 2008. Experimental verification of viscous damping modeling for inelastic time history analyzes, *J. Earthquake Eng.*, **12**(1), 125-145.

Pompei, A., Scalia, A., Sumbatyan, M., A., 1998. Dynamics of rigid blocks due to horizontal ground motion, *J. Eng. Mech.*, ASCE, **124**(7), 713-717.

Priestley, M. J. N., Evison, R. J., and Carr, A. J., 1978. Seismic response of structures free to rock on their foundations, *Bulletin of the New Zealand National Society for Earthquake Eng.*, **11**(3), 141-150.

Priestley, M., J., N., 1996. The PRESSS Program – Current status and proposed plans for phase III, *PCI Journal*, **41**(2), 22-40.

Priestley, M., J., N., Sritharan, S., Conley, J., R., Pampanin, S., 1999. Preliminary results and conclusions from the PRESSS five-story precast concrete test building, *PCI J.*, **44**(6), 42-67.

Priestley, M., J., N., and Grant, D., N., 2005. Viscous damping in seismic design and analysis, *J. Earthquake Eng*., **9**(SP2), 229-255.

Prieto, F., and Lourenco, P., 2005. On the rocking behavior of rigid objects, *Mechanica*, **40**(2), 121-133.

Psycharis, I., and Jennings, P., 1983. Rocking of slender rigid bodies allowed to uplift, *Earthquake Eng. Struct. Dyn.*, **11**(1), 57-76.

Reed, J., 1985. Energy loss due to elastic wave propagation during an elastic impact, J. Phys. D., **18**, 2329-2337.

Seifried, R., Schiehlen, W., Eberhard, P., 2005. Numerical and experimental evaluation of the coefficient of restitution for repeated impacts, *International J. Impact Eng.*, **32**(1-4), 508-524.

Scalia, A., and Sumbatyan, M., A., 1996. Slide rotation of rigid bodies subjected to a horizontal ground motion, *Earthquake Eng. Struct. Dyn*., **25**(10), 1139-1149.

Schau, H., and Johannes, M., 2013. Rocking and sliding of unanchored bodies subjected to seismic load according to conventional and nuclear rules, *4th ECCOMAS Them. Conf. on COMPDYN*.

Shenton, H., 1996. Criteria for initiation of slide, rock, and slide-rock rigid-body modes, *J. Eng. Mech.*, ASCE, **122**(7), 690-693.

Shi, B., Anooshehpoor, A., Zeng, Y., Brune, J., N., 1996. Rocking and overturning of precariously balanced rocks by earthquakes, *Bull. Seismol. Soc. Am*, **86**(5), 1364-1371.

Sinopoli, A., 1987. Dynamics and impact in a system with unilateral constraints the relevance of dry friction, *Meccanica*, **22**(4), 210-215.

Sinopoli, A., 1991. Dynamic analysis of a stone column excited by a sine wave ground motion, *Appl. Mech. Rev*., **44**(11), 246-255.

Sinopoli, A., and Sepe, V., 1993. Coupled motion in the dynamic analysis of a three block structure, *Appl. Mech. Rev*., **46**(11), 185-197.

Spanos, P., D., and Koh, A., S., 1984. Rocking of rigid blocks due to harmonic shaking, *J. Eng. Mech.*, ASCE, **106**(2), 377-392.

Tabor, D., 1948. A simple theory of static and dynamic hardness, *Proceedings of the Royal Society of London, Series A*, **192**, 247-274.

Taniguchi, T., 2002. Non-linear response analyses of rectangular rigid bodies subjected to horizontal and vertical ground motion, *Earthquake Eng. Struct. Dyn.*, **31**(8), 1481-1500.

Tillett, J., P., A., 1954. A study of the impact on spheres of plates, *Proceedings of the Phys. Society, Section B.*

Truniger, R., 2013. Experimental investigation of rocking of elastic columns, Projektarbeit Master, *ETH Zurich – Institure of Structural Engineering*.

Tso, W. K., and Wong, C. M., 1989. Steady state rocking response of rigid blocks, Part 1: Analysis, *Earthquake Eng. Struct. Dyn*., **18**(1), 89-106.

Vassiliou M., F., Mackie, K., R., Stojadinovic, B., 2013. Rocking response of slender, flexible columns under pulse excitation, *4th ECCOMAS Them. Conf. on COMPDYN*.

Wong, C. M., and Tso, W. K., 1989. Steady state rocking response of rigid blocks, Part 2: Experiment, *Earthquake Eng. Struct. Dyn*., **18**(1), 107-120.

Yim, C., S., Chopra, A. K., and Penzien, J., 1980. Rocking response of rigid blocks to earthquakes, *Earthquake Eng. Struct. Dyn*., **8**(6), 565-587.

Yim, C., S., and Lin, H., 1991a. Nonlinear impact and chaotic response of slender rocking objects, *J. Eng. Mech.*, ASCE, **117**(9), 2079-2100.

Yim, C., S., and Lin, H., 1991b. Chaotic behavior and stability of free-standing offshore equipment, *Oc. Eng*., **18**(3), 225-250.

Younis, C., J., and Tadjbakhsh, G., 1984, Response of sliding rigid structures to base excitation, *J. of Eng. Mech*., ASCE, **110**(3), 417-432.

Zener, C., 1941. Phys. Rev., 59, 669.

Zhang, J., Makris, N., 2001. Rocking response of free-standing blocks under cycloidal pulses, *J. Eng. Mech*., ASCE, **127**(5), 2001.

Zhang, X., and Vu-Quoc, L., 2002. Modeling the dependence of the coefficient of restitution on the impact velocity in elasto-plastic collisions, *Impact Eng.*, **27**(3), 317-341.

CHAPTER 3: CHARACTERIZING DYNAMIC DECAY OF FREE ROCKING CONCRETE MEMBERS

A reduced version to be submitted to Earthquake Spectra

Dimitrios KALLIONTZIS and Sri SRITHARAN

3.1 Abstract

Free rocking is likely the primary dynamic mode of vibration during an earthquake response of structural members that are not firmly connected to their foundation. Understanding and accurately modeling free rocking motion of these members is a critical step in evaluating their seismic performance. The dynamic response of these members has been routinely characterized using a geometry dependent coefficient of restitution, which has been shown to be inadequate for accurately addressing the decaying dynamic response of a free rocking member. This investigation, which utilized both experimental testing and finite element analyses, concludes that free rocking members experience a combination of a continuous and an impact energy dissipation mechanism. Accounting for both mechanisms is necessary to produce accurate response of free rocking motion of structural members.

3.2 Introduction

Free rocking is defined as the rocking motion of a free-standing object which has no connection with the underlying base. This behavior was analytically examined by Housner (1963), who introduced a pair of equations to describe the motion of a free rocking block on its foundation. The simple rocking model (SRM) proposed by Housner (1963) assumes that

decay of motion for rigid blocks is solely dependent on an impact mechanism which can be described by a geometry dependent coefficient of restitution (COR). Essential assumptions of the SRM also included: block and foundation are rigid; no sliding occurs between the block and the foundation; no bouncing of the block takes place during free rocking motion; and the block oscillates in a two-dimensional fashion. Proposed equation of free rocking motion was described by Equation 3-1, as shown below.

$$I_o\ddot{\theta} + MgR\sin(\mathrm{S}(\theta)\alpha - \theta) = 0 \tag{3-1}$$

From Figure 3-1, which describes the above-referenced rigid block motion, R is the distance between gravity (designated as C.G.) and rotation center O or O'and α is the aspect ratio of the block. Also, M is the total mass of the block, I_o is the moment of inertia with respect to the rotation center and $S(\theta)$ expresses the sign convention (see Figure 3-1) used to define the positive and negative direction for the angular displacement, θ.

$$S(\theta) = \begin{cases} 1, for\ \theta > 0 \\ -1, for\ \theta < 0 \end{cases} \tag{3-2}$$

For small angular displacements (i.e. $a \le 20^o$), Equation 1 was linearized as,

$$I_o\ddot{\theta} + MgR(\mathrm{S}(\theta)\alpha - \theta) = 0 \tag{3-3}$$

Per Housner (1963), energy dissipation during a free rocking motion takes place while the block impacts with its foundation. The COR, defined by Equation 3-4, describes the reduction of kinetic energy underwent in the block.

$$COR = \frac{\frac{1}{2} I_o \dot{\theta}_2^{\,2}}{\frac{1}{2} I_o \dot{\theta}_1^{\,2}} \tag{3-4}$$

where $\dot{\theta}_1$ and $\dot{\theta}_2$ are the angular velocities of the block before and after the impact, respectively.

By equating the moment of momentum before and after the impact about the rotation center after the impact (see Equation 3-5), a solution for COR was derived, as shown in Equation 3-6.

$$I_o\dot{\theta}_1 - 2MRb\dot{\theta}_1 \sin a = I_o\dot{\theta}_2 \tag{3-5}$$

$$COR = [1 - \frac{MR^2}{I_o}(1-\cos(2a))]^2 \tag{3-6}$$

By using Equation 3-6 and initial conditions for free vibration of $\theta(0) = \theta_0$ and $\dot{\theta}(0) = 0$, Housner suggested that angular displacement amplitude after the nth impact, θ_n, can be estimated as follows.

$$\theta_n = 1 - \sqrt{1 - COR^n(1-(1-\theta_o)^2)} \tag{3-7}$$

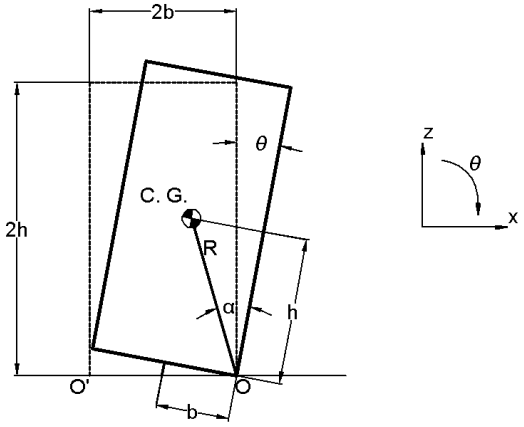

Figure 3-1. A free rocking block as described by Housner (1963)

Housner's approach for modelling decay of free rocking motion was evaluated on three free rocking concrete members in this study. The linearized equation of motion (Equation 3-5) was then modified to incorporate an experimentally and analytically identified continuous dissipation mechanism, which contributes to their response.

3.3 Background

Experimental studies before and after Housner (1963) have provided useful data which can be currently used for understanding the efficiency of SRM's COR model to estimate the response of free rocking members. From this viewpoint, the experimental studies by Muto et al. (1960), Priestley et al. (1978), Aslam et al. (1980), Fielder et al. (1997) and Pena et al. (2007) were informative for showing that SRM systematically predicts a consistently lower COR compared to the experimental values with only one exception, as reported by Aslam et al. These researchers did not further investigate their experimental findings on COR. Aslam et al. (1980) and Pena et al. (2007) showed that use of empirical COR values, different from SRM's suggestions, was necessary to achieve a good match with experimental responses. Similarly, Priestley et al. (1978) observed a significant difference between the COR by SRM and the value needed to accurately simulate the experimental response, while Fielder et al. (1997) simply stated that "modeling of energy dissipation is not a simple matter" and "the actual energy dissipation may have a continuous component" attributed to a viscous damping mechanism.

On the other hand, many theoretical studies (Spanos and Koh 1984; Tso and Wong 1989; Yim and Lin 1991; and Hogan 1994), which examined free rocking motion under horizontal base excitation, have employed a set of COR values in their analytical free rocking models, however, without supporting their hypotheses on these values with either theoretical or experimental findings. While these studies have enriched the knowledge on free rocking motion, the use of their conclusions in seismic applications would require that the selected COR is associated with some actual dynamic behavior.

A more systematic investigation on decay of free rocking motion was conducted by Lipscombe and Pellegrino (1993), who experimentally studied the response of four discrete steel blocks of square cross-sections and slenderness ratios (*h/b*) ranging from 1 to 8. It was showed that the actual COR can vary significantly throughout an experimental test run and accuracy of the SRM's COR increases with increase in the slenderness ratio. More recently, another experimental investigation into the ability of SRM to predict free rocking motion was presented by Ma (2009). To ensure a test set up which closely emulates Housner's free rocking block, Ma (2009) designed a free-standing and relatively rigid block able to enter planar rocking about its corners, while preventing bounce and slide motions. It was confirmed that experimental COR exhibits large scatter throughout an oscillation, nevertheless, averaging the experimental COR values yielded a mean value close to SRM's estimation. Interestingly, Ma (2009) showed that there is no correlation between impact energy dissipation and base force, concluding that for a rocking motion which is free from bouncing, "energy dissipation of a free rocking block arises from the requirement of conservation of angular momentum of the system", as shown by Housner (1963).

An alternative viewpoint on analysis of free rocking motion was introduced by Chopra and Yim (1985) who presented three methods for modelling rocking building systems, simulated as single degree of freedom (SDOF) systems. The soil-structure interface was modelled as (1) rigid, similar to SRM; (2) flexible with two vertical spring-dashpot elements at the rocking corners; and (3) flexible with the use of the Winkler foundation. Later, Andreaus and Casini (1998) came up with a free rocking model in which a rigid block was allowed to rock on a set of two horizontal and two vertical springs located at the bottom corners of the block. Chatzis and Smyth (2012) also used spring elements to formulate two

free rocking models which take into account the effects of sliding, uplift, base flexibility and geometric nonlinearities. Considering that these alternative analytical techniques were presented only on a theoretical basis, the combination of dashpot and impact mechanisms employed to simulate dynamic decay of motion lacked experimental evidence to ensure their validity for real structural applications.

3.4 Research Significance

Given the focus on understanding jointed precast construction and how free rocking will affect response of precast concrete members, this paper used prefabricated concrete columns to investigate decay of dynamic response of free rocking members and related energy dissipation characteristics. The objectives of this study are to: (1) demonstrate that Housner's model does not adequately capture the response of free rocking members; (2) present experimental and analytical evidence that a rocking member experiences two different energy dissipation mechanisms; and (3) provide a modified form of the Housner's model to accurately capture the dynamic decay of motion of free rocking structural members.

3.5 Experimental Investigation

3.5.1 Testing scheme

Experimental testing on three precast concrete rocking systems was conducted in the structural laboratory at Iowa State University. A reinforced concrete unit consisted of two parts: a column; and a mass were built for the experimental investigation. Figure 3-2 presents the three discrete geometric configurations created by relocating these parts. The column had a cross-section of 14x14 square inches, 66 inches height, 1220 lb weight and an aspect ratio

(h/b) of 33/7, and was firmly connected with the concrete mass which had dimensions of 12x50x50 (height x width x length) cubic inches and 2380 lb weight. As shown in Figure 3-2, the concrete mass was attached on two locations: at 17.5 inches under the top of the column (*Rocking System 1*); and at the top of the column (*Rocking System 2*). A strong connection was created between the concrete mass and the column by attaching two threaded bars at the bottom face of the mass and two longitudinal bars passing through the middle of the mass cross-section which were properly tighten on its exterior faces (Fig. 3-3). Two discrete free rocking systems were created from these assembling processes. Finally, a third rocking system was produced by detaching the concrete mass from the column (*Rocking System 3*).

The three systems were tested on a concrete foundation, which was firmly attached to the laboratory strong floor through four unbonded post-tensioned bars which connected the base with the top of the foundation.

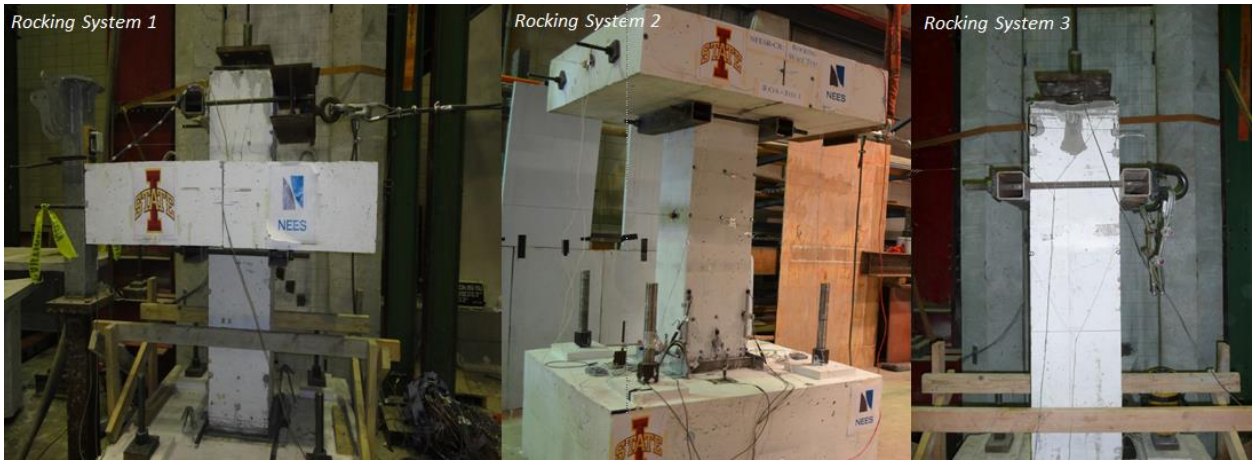

Figure 3-2. The three free rocking precast concrete units

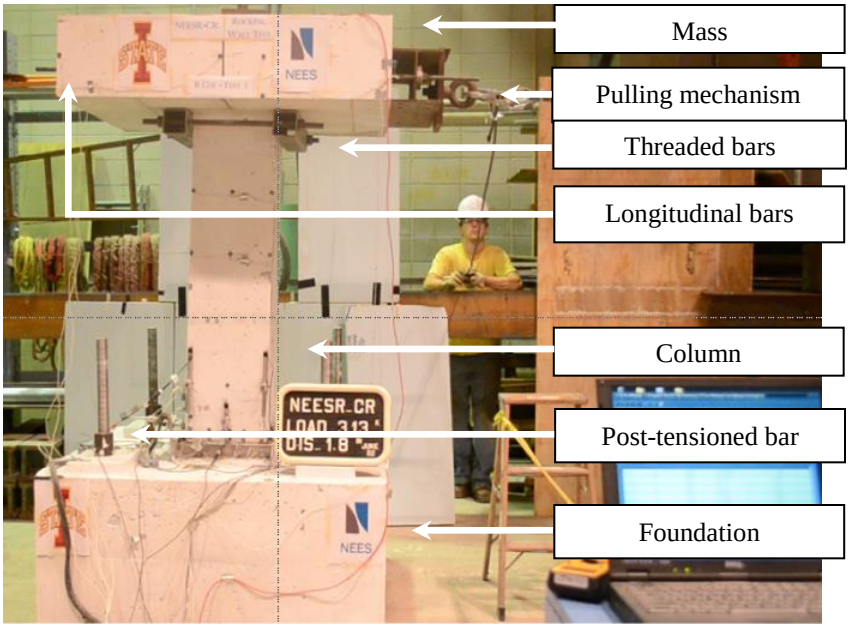

Figure 3-3. Experimental set-up for *Rocking System 2*

In order to secure full contact between the column and foundation; and help prevent shear sliding between the bottom edge of the rocking body and the foundation, a replaceable one inch thick nonshrink 6 ksi grout (PAGEL-USA. V1A/40) layer was cast at the interface between the foundation and concrete member. The grout was allowed to rise above the bottom of the column surface by one half of an inch around the perimeter of the column (Fig. 3-4). The grout pad was replaced after completion of testing in each of the free rocking systems as the column and mass blocks were reused.

Minimal damage for the bottom part of the column was ensured by using steel angles-channels with dimensions of 4 x 3 x 3/8 cubic inches which were firmly connected to the corners using steel studs. These steel elements prevented crushing of concrete in this region when an impact takes place and this is consistent with recent research and industry practice when jointed connections are used for precast construction in seismic regions.

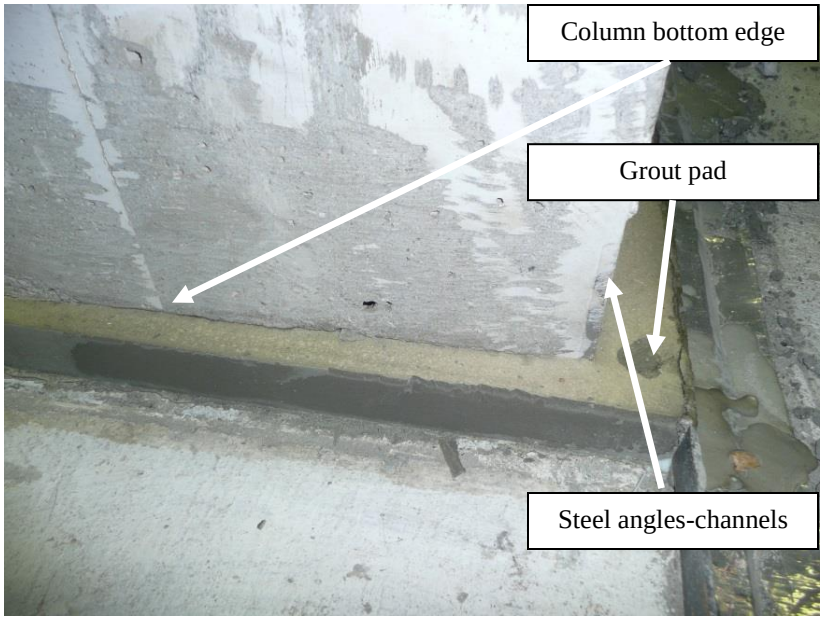

Figure 3-4. Grouting surrounds the bottom edge of the rocking column

3.5.2 Free vibration tests

The rocking systems were excited using four different levels of initial top lateral drift (ITLD): 0.5%, 1%, 2% and 3%. The free vibration test was repeated three times for each initial condition. The testing process was initiated with the 0.5% and proceeded with the higher ITLDs. The results for 1%, 2% and 3% ITLDs are presented herein, as the units exhibited comparable behavior for 0.5% and 1% ITLDs.

In order to excite the rocking units with the desired initial conditions, a pulling force was applied to an offset hook attached on their top by a hydraulic jack (power team 55 ton hydraulic 13 inch-double acting cylinder RD5513), which was located at the same height. The free vibration was initiated by pulling down a release rope connected with the offset hook.

3.5.3 Instrumentation

The instrumentation of the units used a series of light emitting diodes (LED) which were imposed on the bottom and; on the top of the specimens. String pots were also located at the half height and top of the rocking units in order to determine the desired ITLDs of the free vibration test.

For an effective operation for the monitoring process, which was required to adequately capture the rocking motion and impact interactions, a trial and error approach was followed to establish the optimum combination of sampling frequency and number of LED sensors used in a testing process, given that the first variable decreases with increase in the number of operating LED sensors. Accordingly, the experimental work was divided into two testing phases: 1) four LED sensors were imposed at the top of the specimen to capture the top displacement response; 2) 4 LEDs were attached along the bottom edge of the column to provide an understanding on the local behavior (Fig. 3-5).

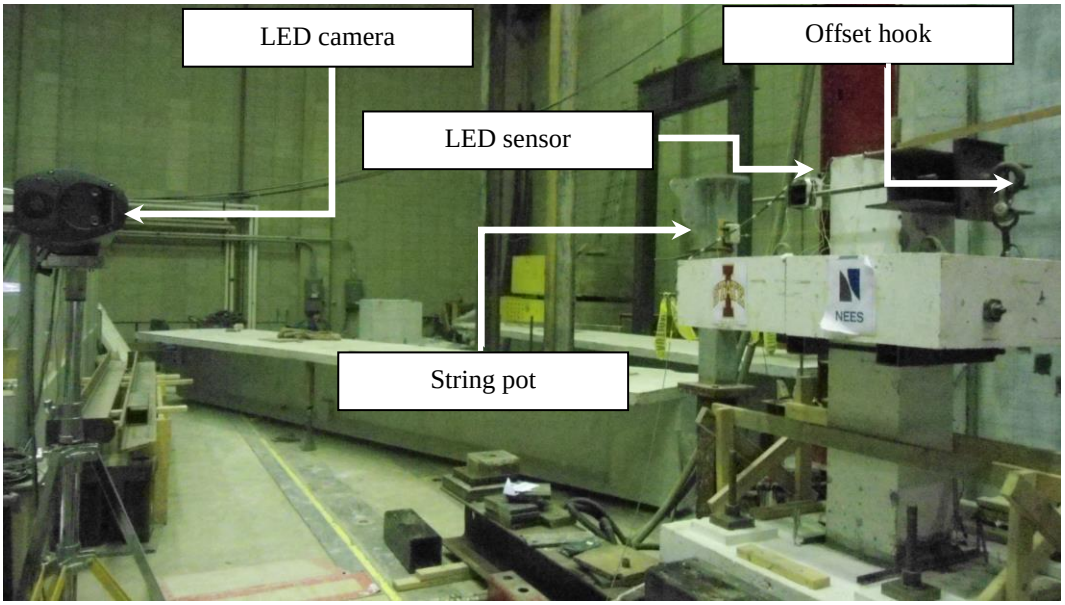

Figure 3-5. Experimental Set-up

A typical angular displacement response from an experimental test run is presented in Figure 3-7.

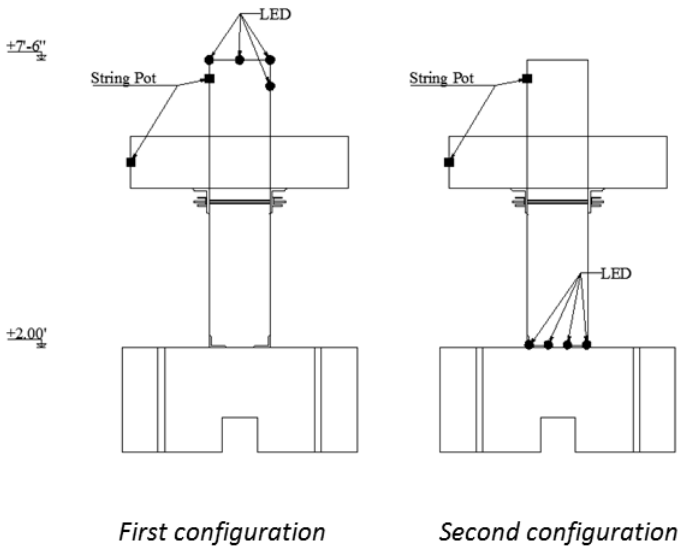

Figure 3-6. Typical instrumentation configurations

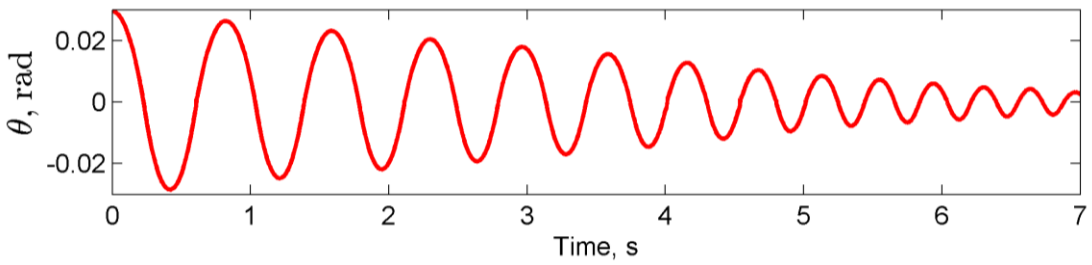

Figure 3-7. Typical experimental angular displacement response measured using an LED sensor of the first configuration

3.6 Finite Element Modeling

Three discrete FE models were developed to simulate free rocking response of the three concrete members (Fig. 3-8). These models were developed and executed following the modeling approach developed in APPENDIX for FE simulation of controlled rocking

systems. The original modeling technique was modified to capture free rocking motions by removing the post-tensioned mechanism and modeling the full dimensions of the concrete mass to ensure an accurate estimation of the inertia properties of the free rocking models. Decay of motion was simulated by using the Rayleigh damping model with the ALPHA and BETA values as was proposed by these researchers in their original model. Accordingly, a value of ALPHA=0.5 was used for the 2% and 3% and a value of ALPHA=0.9 was employed for the 1% ITLD FEAs.

The analysis was similarly divided into three sequential steps: the drift was imposed; horizontal motion was restricted for the rocking system to ensure its stability and sufficient decay of its kinetic energy before the beginning of a free rocking response under free vibration; free rocking motion takes place. Mass scaling with a 1E-6 seconds target time increment per 10 increments was used for all steps in order to reduce the solution time.

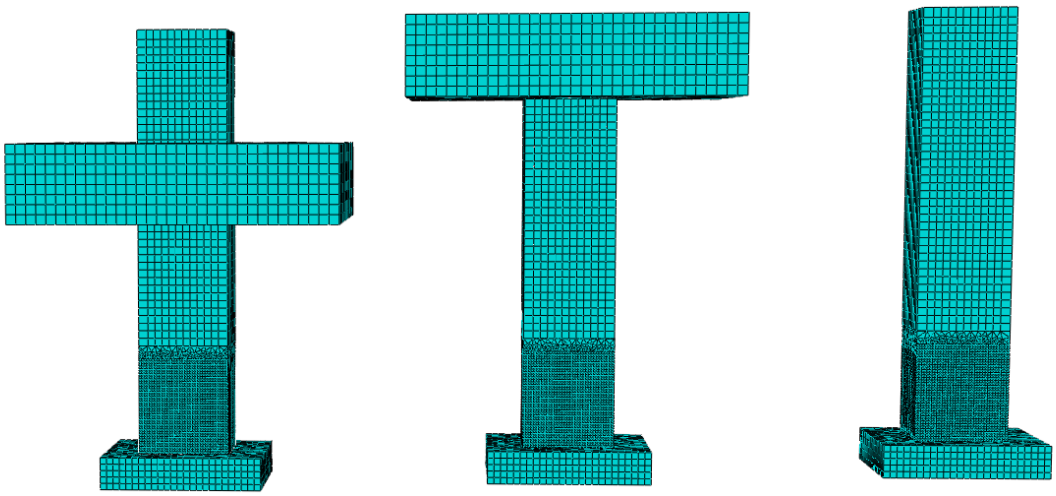

Figure 3-8. Free rocking FE models corresponding to the three free rocking precast concrete units used in the experimental work

3.7 Comparison of Results

3.7.1 Angular displacement responses

SRM and FEA were implements to assess the actual behavior of the three concrete members for 1%, 2% and 3% ITLD. As shown in Table 3-1, the geometric and mass properties of the three rocking systems were determined in order to evaluate their behavior based on the SRM.

Table 3-1. Geometric and mass properties of the three rocking systems. COR was estimated based on the SRM.

Rocking System	Total Mass, $k-s^2/in$	Moment of Inertia *Io*, $k-s^2-in$	R, *in*	Aspect ratio, α	Xcg, *in*	COR, *r*
1	0.0092	17.43	39.97	0.176	39.35	0.898
2	0.0092	28.49	51.53	0.136	51.05	0.937
3	0.0031	4.64	33.73	0.209	33	0.875

Investigation on decay of free rocking motion was initiated with the comparison of angular displacement responses as determined by SRM, FEA and experimental data from the first configuration (Figure 3-6). Figure 3-9 compares these responses for *Rocking Member 1*. SRM clearly predicted a faster decay in rocking motion, exhibited a reduced efficiency in capturing experimental time-histories with increase in ITLD. A significantly improved estimation was, in contrast, provided by the FE free rocking model for all initial conditions. Slight deviations were, however, induced with decrease in angular displacement amplitudes because of irregularly elongating natural periods in the experimental responses, which became more evident in free rocking with 1% and 2% ITLDs. This behavior is considered as a typical feature in precast rocking systems where imperfections induced in the construction

of the grout pad and localized deformation in its corners due to continuous impact actions can slightly affect free rocking motion.

Due to suchlike effects, an asymmetric motion was consistently experienced by *Rocking Members 2* and *3* which used a different grout pad from *Rocking Member 1*; their behavior was attributed to the inclined surface of the renewed grout, and is believed to have originated in the grout pouring process. The effect of this asymmetry is typically demonstrated in Figures 3-10 and 3-11 by plotting the absolute experimental angular displacement responses and "natural" quarter periods, respectively, for *Rocking Member 3*. As confirmed in Figure 3-11, asymmetric rocking motion may be analytically approximated by introducing an inclination parameter, β, in Equation 3-3 to produce the equation of motion of a modified SRM (Equation 3-8). Parameter β was approximately estimated with the use of experimental data in order to determine variations in the "natural" quarter period of *Rocking Member 3*. Motion of a rocking block on an inclined base is described in Figure 3-12.

$$I_o\ddot{\theta} + S(\theta)MgR(\alpha - |\theta| - \beta) = 0 \tag{3-8}$$

For $\theta(0) = \theta_o$ and $\dot{\theta}(0) = 0$, the solution for $\theta(t)$ gives,

$$\theta(t) = (a - \beta) - ((a - \beta) - \theta_o)\cosh pt \tag{3-9}$$

While the rocking quarter period is calculated as,

$$\frac{T}{4} = \frac{1}{p}\cosh^{-1}\left(\frac{1}{1 - \theta_o / (a - \beta)}\right) \tag{3-10}$$

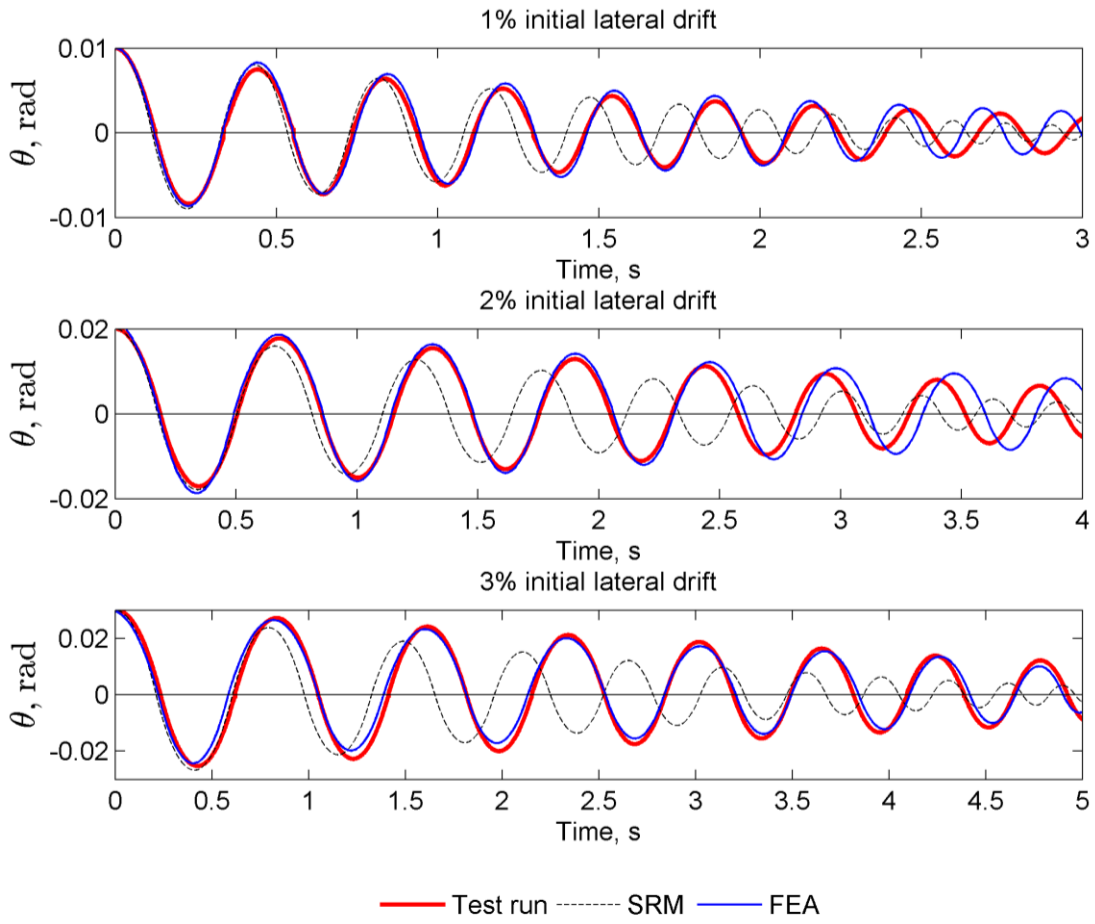

Figure 3-9. Angular displacement response of *Rocking System 1*

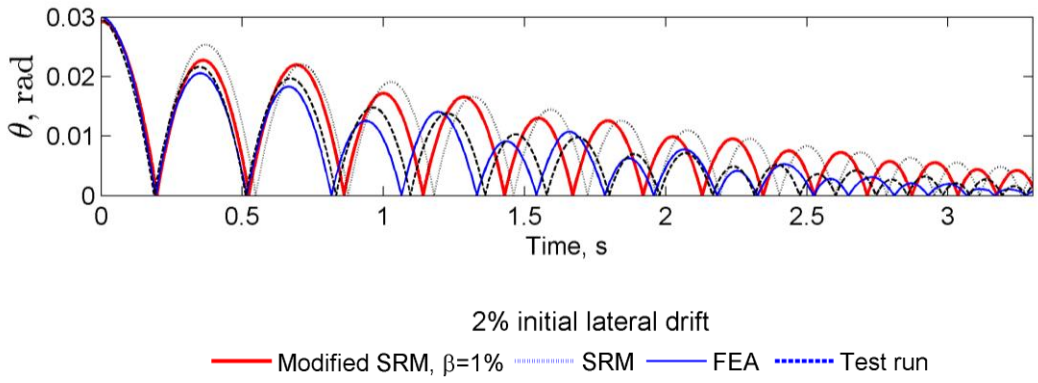

Figure 3-10. Typical absolute experimental angular displacement response of *Rocking System 3*

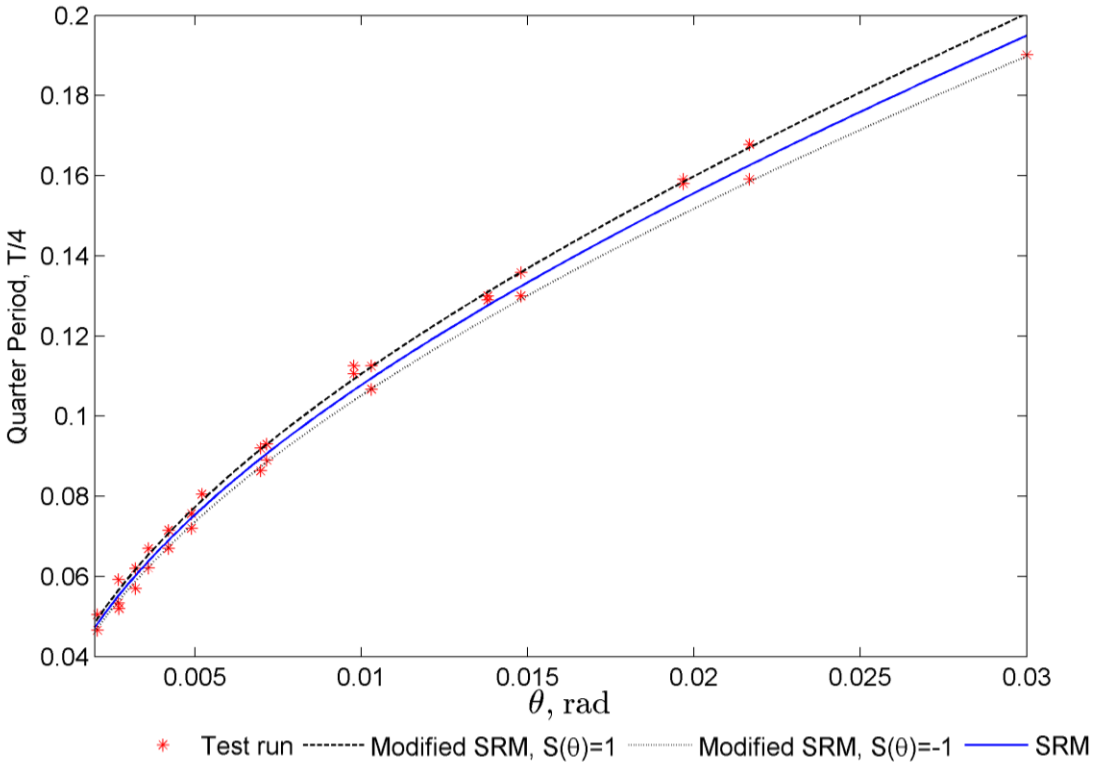

Figure 3-11. Quarter period of *Rocking System 3*; Modified SRM used β=1%

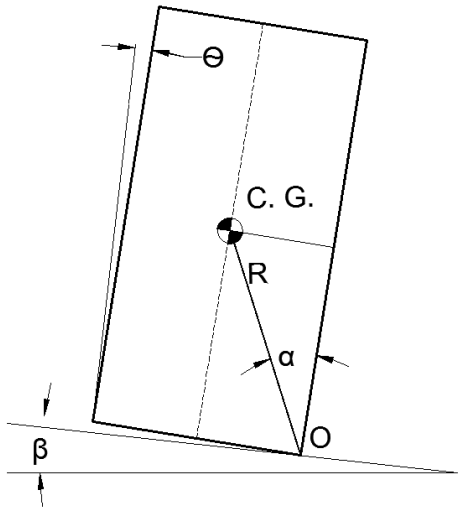

Figure 3-12. Free-standing block rocking on an inclined base

Following this modification, the modified SRM was applied to estimate the response of *Rocking System 2*, while the FE model was also reformed to accommodate the grout pad

inclination. The comparison between the three oscillations is presented in Figure 3-14, where the modified SRM was clearly unable to provide an acceptable estimation of the rocking quarter period. This outcome was initially attributed to the flexibility characteristics exhibited by this unit since the concrete mass located at the top of the column may have led to a more flexible rocking configuration, resulting in its relative in-phase oscillation.

Because this part of the experimental investigation was conducted using the first instrumentation configuration, flexibility effects was not experimentally captured. In contrast, the respective FE model was employed to justify the existence of a flexible response. Accordingly, the angular displacement time histories of the top and bottom edge of the column were calculated based on the FEA results demonstrating that the top and bottom edges of the column are characterized by a non-zero relative angular displacement, as can be inferred from Figure 3-13. This relative motion between top and bottom edge signifies that the top part of the unit may have been subjected to another in-phase motion besides rocking due to the flexibility effect induced by the location of the concrete mass in this unit.

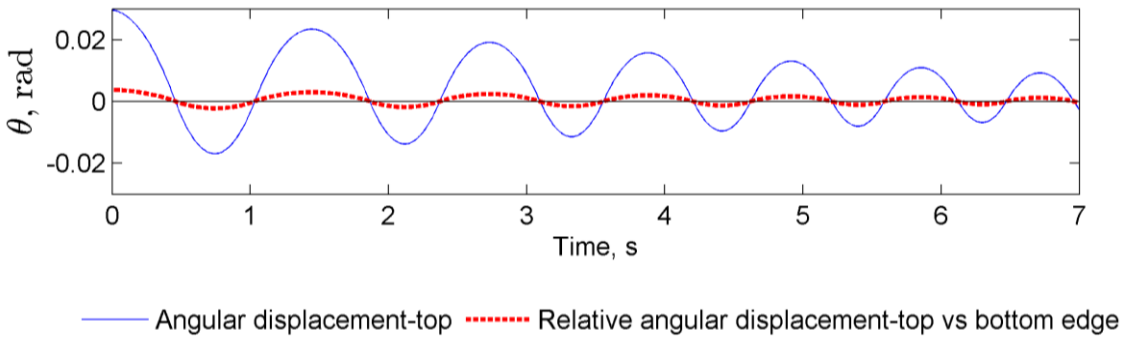

Figure 3-13. Angular displacement at the top vs. relative angular displacement between top and bottom edges of the FE model

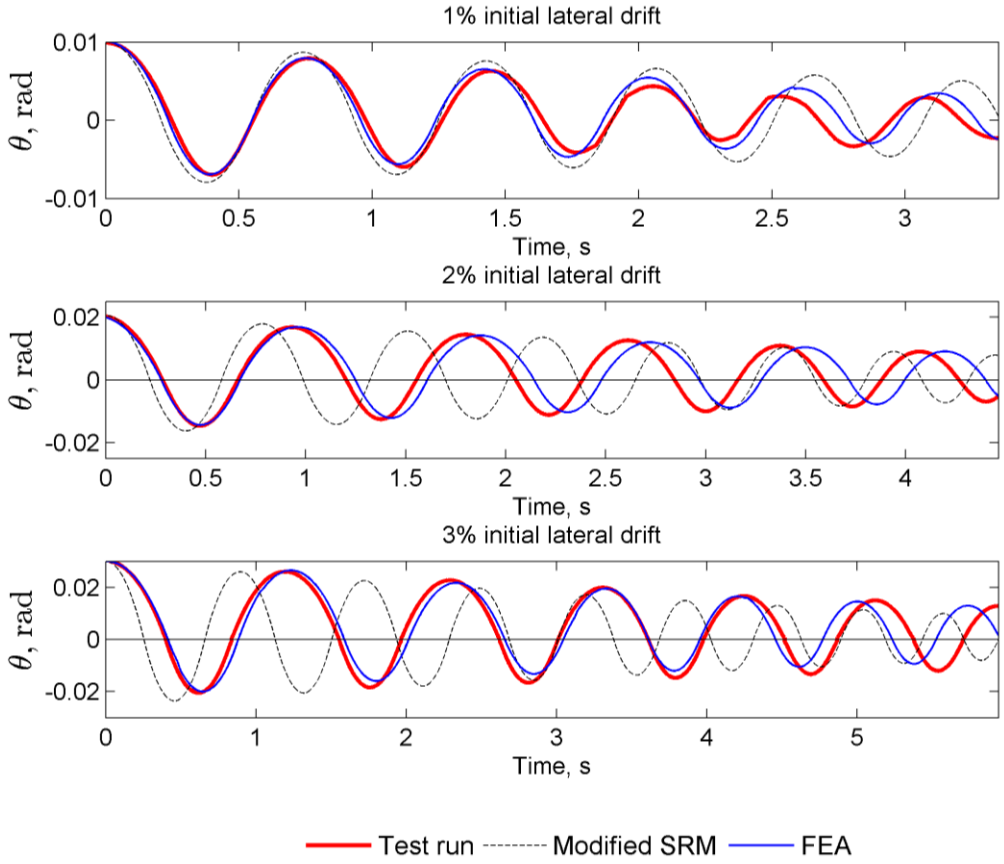

Figure 3-14. Angular displacement response of *Rocking System 2*

The angular displacement time histories comparison for *Rocking System 3* which is presented in Figure 3-15 shows that the three responses exhibit a similar displacement decay in time series with the SRM predicting a shorter quarter period with respect to an angular displacement peak compared to the actual response and FEA results. Even though *Rocking Systems 3* is characterized by a COR value by SRM which is close to the one of *Rocking System 1* (Table 3-1), SRM was able to provide a better prediction in its decay of motion. Consequently, it follows that this result may signify that the removal of the concrete mass in order to produce *Rocking System 3* was a parameter that influenced the decay of motion in this system by increasing its energy dissipation capabilities. Finally, FEA was able to capture

this behavior in the 2% and 3% ITLD cases, while its efficiency reduced in the 1% ITLD case.

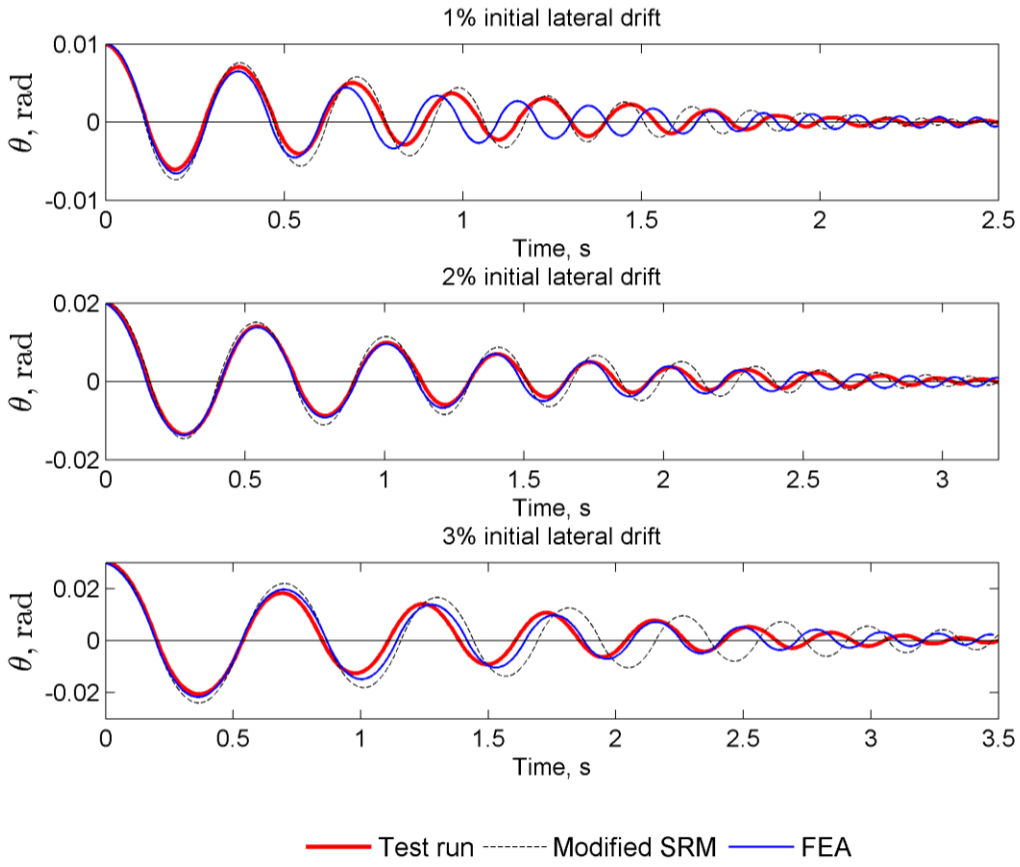

Figure 3-15. Angular displacement response of *Rocking System 3*

Overall, the proposed FE model was able to provide a sufficient estimation of the angular displacement time histories in all rocking systems for the 3% and 2% ITLDs, while its efficiency was lower for the 1% ITLD oscillation. Local imperfections on the rocking interface which apparently are more critical for smaller displacements may have affected the periodic and damping characteristics of the rocking units, creating difficulties in predicting their behavior in this region.

3.7.2 Phase diagrams

For a closer inspection of the behavior exhibited by these free rocking systems, their angular velocities are plotted against the respective angular displacements. The resulting relationships, referred to as phase diagrams, can provide a clear picture of the impact phase; the velocities associated with the impact; and the "energy" path followed by a rocking structure during the impact and continuous phase of its motion, providing an understanding of the dissipation mechanisms occurring in these phases. A comparison of the theoretical idealizations (SRM, FEA) with the experimental results through these diagrams was also necessary at this point in order to investigate their ability to follow the actual velocity responses and consequently, estimate the windows of free rocking motion (i.e. the nonlinear impact phase and the continuous phase of the rotating motion) in which energy dissipation takes place.

Before investigating the phase diagram responses, it was prominent to eliminate noise which typically appear in the velocity data and create difficulties in reading the velocity peak values associated with the impact phenomenon. This was implemented by using a smoothing technique in order to filter the raw velocity data. Figure 3-16 presents a typical filtered velocity time history showing that the instantaneous drops of the velocity peaks that occur once the rocking system enters the impact phase, while at the end of an impact, the velocity has built up and the system enters the continuous phase of rocking motion.

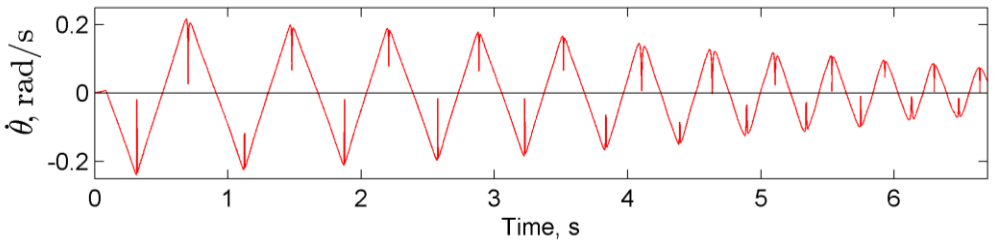

Figure 3-16. A smoothed velocity response for *Rocking System 1*, for 3% ITLD using an LED sensor of the first configuration

After ensuring reliable experimental velocity data, phase diagrams were plotted for all test runs and compared with SRM and FEA results, as shown in Figures 3-18, 3-19, and 3-20. Several observations can be made herein:

- SRM did not provide an acceptable estimation of the angular velocity-displacement relationship during the continuous phase of the motion. The deviation of SRM prediction from the actual behavior increases with decrease in ITLD. For $\theta(t) \leq 1\%$, SRM significantly overestimates the impact velocities.
- There may be an energy dissipation mechanism acting during the continuous phase of the motion in *Rocking Systems 1* and *3*. This is deduced by the fact their experimental angular velocity versus displacement relationships do not follow the "energy dissipation free" path of the continuous phase as suggested by SRM; and these systems were not subjected to a flexible rocking motion that could influence their velocity performance. On the contrary, the experimental results for *Rocking System 2* present the largest deviation from the SRM, a behavior which was attributed to its flexible rocking motion. Since an estimation of this secondary effect was not experimentally captured, accurate separation between the continuous dissipation and flexibility effects on *Rocking System 2* was not

feasible. Therefore, concrete conclusions regarding potential continuous energy dissipation in this system could not be made.

- The effect of this continuous dissipation in *Rocking Systems 1* and *3* is higher for 1% and decreases with increase in ITLD. In contrast, the impact dissipation component seems to dominate the rocking response for higher drifts, i.e. 3%, where the rocking systems tend to follow the "energy dissipation free" path advocating a minimum participation of the continuous dissipation component.
- There is a large drop in the experimental velocity value when angular displacement is close to zero at the middle part of an impact. The velocity recovers and reaches a second peak at the end of the impact. In general, the velocity reaches its maximum value while the displacement has not reached a zero value. This behavior signifies that the rocking system exhibits its velocity decay slightly before reaching $\theta(t) = 0$.
- The FEA predicts angular velocity versus displacement relationships, which adequately follow the experimental phase diagrams. This confirms the FE model not only provided a sufficient estimation of the displacement time histories but was able to simulate the intrinsic behavior and decay of motion characteristics, which were exhibited by the three rocking systems. A small difference appears only in the 1% ITLD cases where the FEA peak velocities are slightly higher compared to the experimental peaks, while the FEA predicts also an idealized abrupt drop in the angular velocity at an impact.

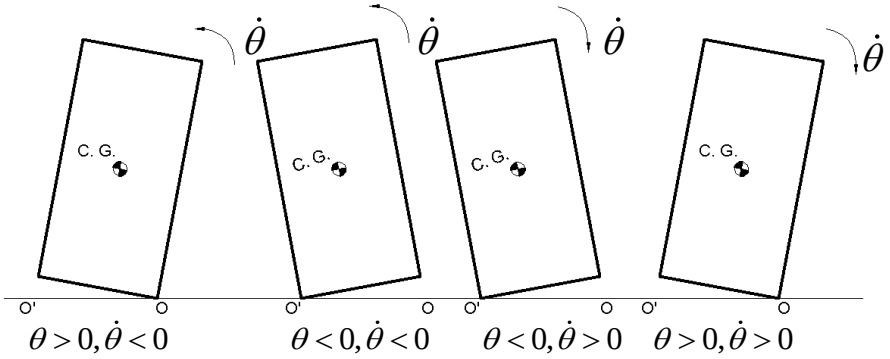

Figure 3-17. Sign convention followed in the phase diagrams

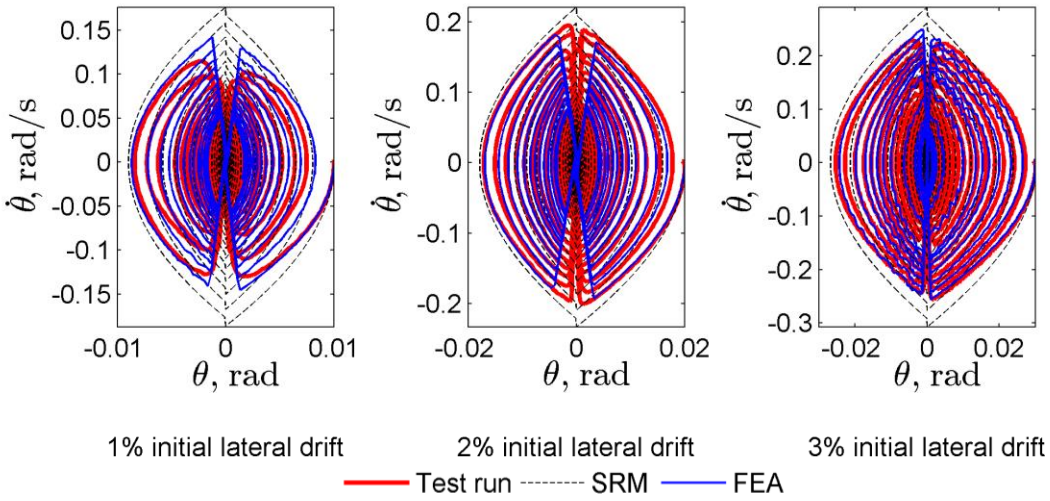

Figure 3-18. Phase diagram of *Rocking System 1*

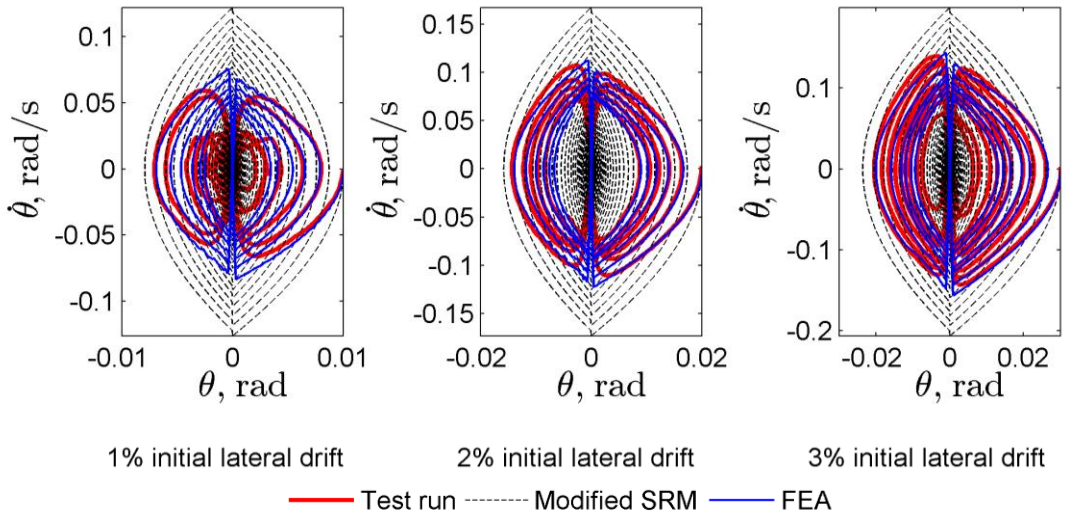

Figure 19. Phase diagram of *Rocking System 2*

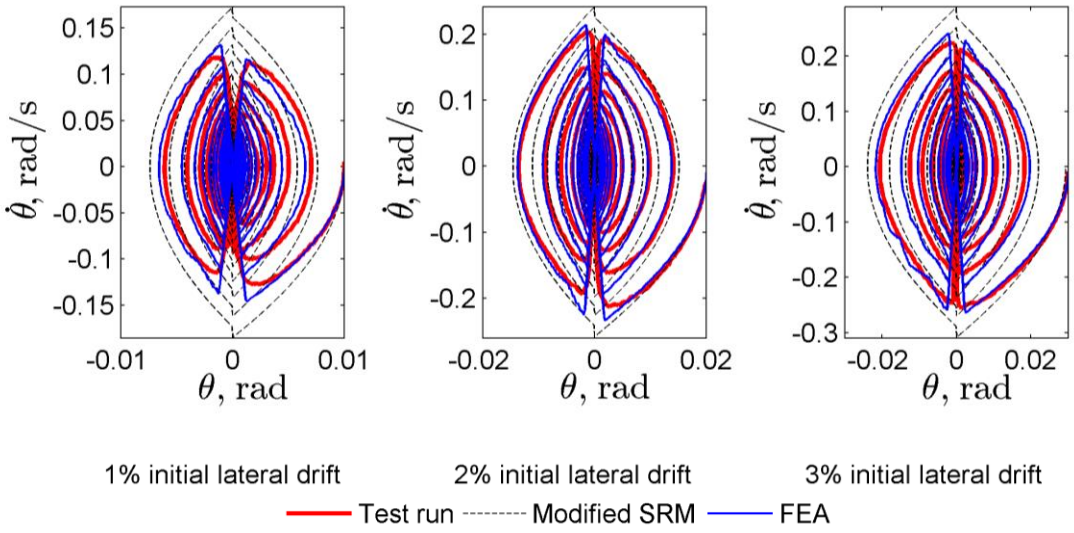

Figure 20. Phase diagram of *Rocking System 3*

3.7.3 Energy dissipation

Equation of motion proposed by Housner was used to quantify the two main energy components of free rocking. By SRM's idealization, these components are gravitational potential energy, U , in Eq. 3-11 and 3-12; and rocking kinetic energy, K , in Eq. 3-13. Eq. 3-12 was specifically produced to account for the grout pad inclinations observed in *Rocking Systems 2* and *3*.

$$U = MgR(\cos(\alpha - |\theta|) - \cos(\alpha)) \tag{3-11}$$

$$U = MgR(\cos(\alpha - |\theta| - S(\theta)\beta) - \cos(\alpha)) \tag{3-12}$$

$$K = \frac{1}{2} I_o \dot{\theta}^2 \tag{3-13}$$

Energy content of rocking is defined as the summation of K and U ,

$$E_{total} = K + U \tag{3-14}$$

A typical time history of free rocking energy content is plotted in Figure 3-21. In agreement with the angular velocity versus displacement relationships presented above,

kinetic energy reaches its highest value just before the impact; it significantly drops at the middle part of the impact and reaches another peak value just after the impact. At the same time, gravitational potential energy reaches its maximum value when kinetic energy reaches a zero value. The two energy components constitute the energy content of the free rocking system.

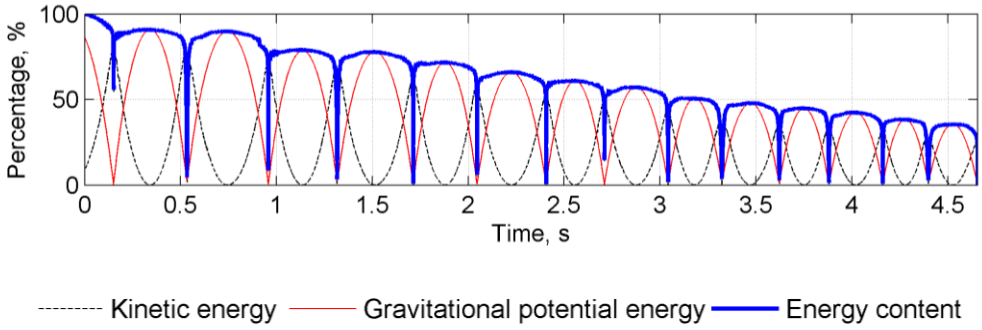

Figure 3-21. Typical time history of the Kinetic rocking energy; Gravitational potential energy; and Energy content of a concrete rocking system

Following the observations made previously regarding energy dissipation in these free rocking members, it is of interest to experimentally quantify the potential decay of motion mechanisms which may be referred to as, impact-instantaneous dissipation; and continuous dissipation. Impact dissipation is defined as the difference between kinetic energy before and after an impact,

$$\Delta K = \mid K_2 - K_1 \mid = \mid \frac{1}{2} I_o \dot{\theta}_2^{\,2} - \frac{1}{2} I_o \dot{\theta}_1^{\,2} \mid \qquad (3\text{-}15)$$

It was found that the clear reading of impact energy dissipation was not feasible only for a few impact interaction cases. In these particular cases, a minimal error was induced in the estimation of the accumulated impact dissipation.

In order to estimate the energy lost in a continuous fashion, the difference was calculated from the total energy content and the amount of impact dissipation per half a cycle to obtain an estimate of the remaining energy dissipated by the rocking system during this interval. For simplicity, this component was approximated to develop in a linear fashion, within this time increment.

Finally, the two energy dissipation components were calculated till a clear reading of the velocity time history was feasible considering noise effects became more pronounce for smaller angular displacements. Unfortunately, an out-of-plane mode was pronounce in the response of *Rocking System 2*, which restricted the quantification of its energy dissipation to a short portion of the time history.

Figures 3-22, 3-23, and 3-24 present time histories of the energy content and the two energy dissipation components for the three rocking systems. From the energy dissipation standpoint, the presented quantification of the two components is in good qualitative agreement with rocking behavior, which was previously displayed in the phase diagrams. In all three members, the percentage of continuous dissipation is lowest for 3% ITLD response, but increases with decrease in the ITLD. As it is also shown in these figures, this increase in continuous dissipation as the angular displacement decreases, is associated with a window where energy content is strongly controlled by the gravitational potential energy. During this part of the response, the rocking system exhibits an energy exchange; in other words, energy is continuously transferred in and out of the system during its motion.

Based on Figures 3-22 and 3-24, it can be furthermore inferred free rocking energy content decays in an exponential fashion in the region of small angular displacements (i.e. 1% ITLD), a fact that may trigger the consideration of a viscous type continuous energy

dissipation mechanism acting in these rocking systems. On the other hand, an approximately linear decay of motion is observed for the 3% ITLD free vibration response advocating that a different decay mechanism may control this response, evidently associated with the higher impact dissipation observed in this case.

In the comparison of the three systems, *Rocking System 1* has the minimum influence by continuous dissipation. This dissipation component becomes more pronounce in the dynamic response of *Rocking System 2*, where its flexural response has apparently contributed to this trend. Finally, continuous dissipation participates significantly in decay of motion of *Rocking System 3*, a result that can be linked with this system's ability to dissipate a higher amount of energy per cycle compared to *Rocking System 1* as previously discussed in the comparison of these two rocking systems.

As far as modeling of the impact mechanism is concerned, the results in Figures 3-22, 3-23 and 3-24 confirm that impact dissipation cannot be expressed through a constant COR value as the amount of energy loss per impact is not always analogous to the kinetic energy at the respective time instant. Accordingly and because of the influence by continuous dissipation, SRM was not able to provide a successful estimation for the angular displacement time histories; while this outcome should be also tied up with the velocity overestimations shown in the phase diagrams, possibly leading to erroneous estimations of the energy dissipation by SRM even with the use of an accurate COR.

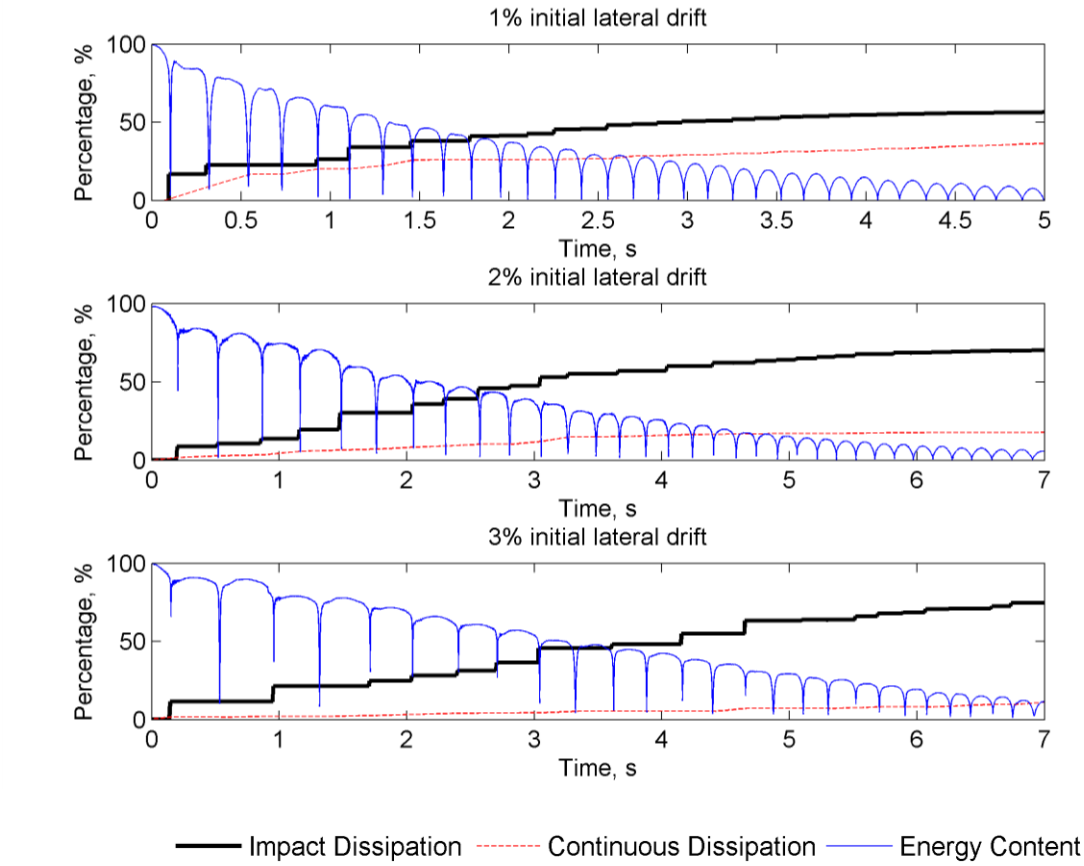

Figure 3-22. Experimental energy dissipation components and energy content of *Rocking System 1*

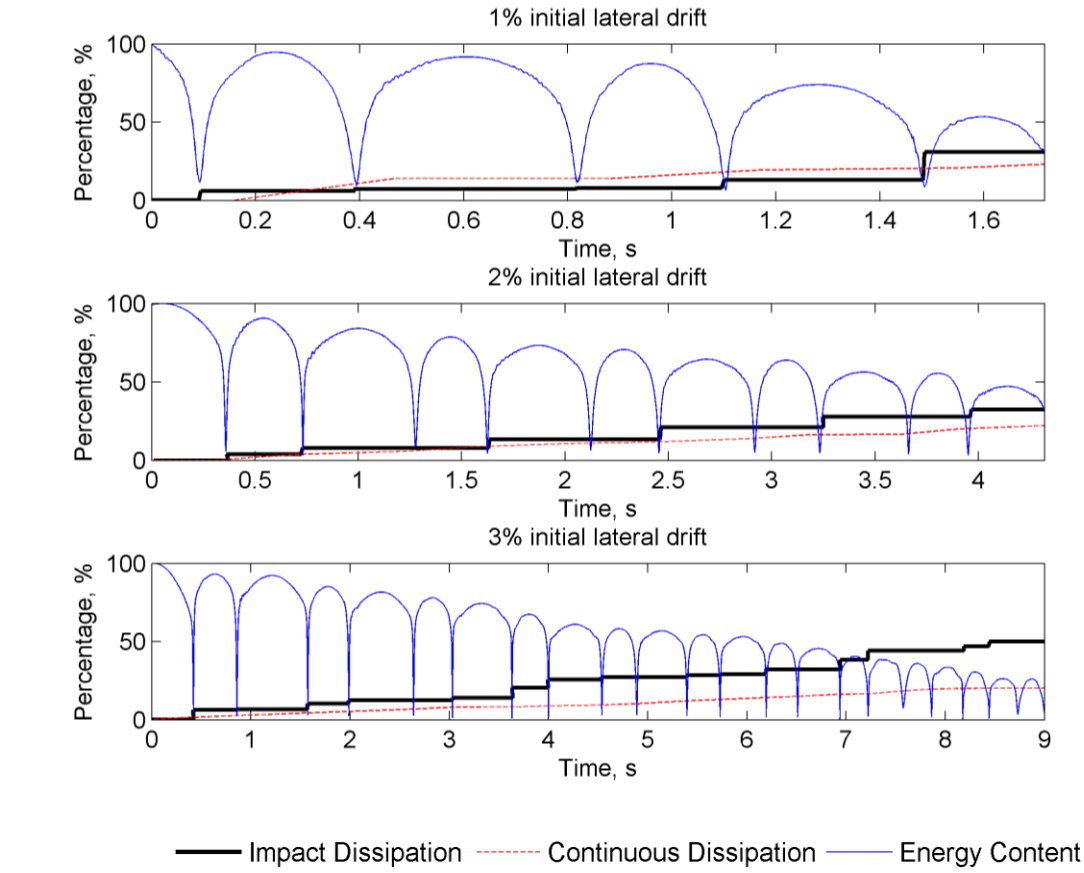

Figure 3-23. Experimental energy dissipation components and energy content of *Rocking System 2*

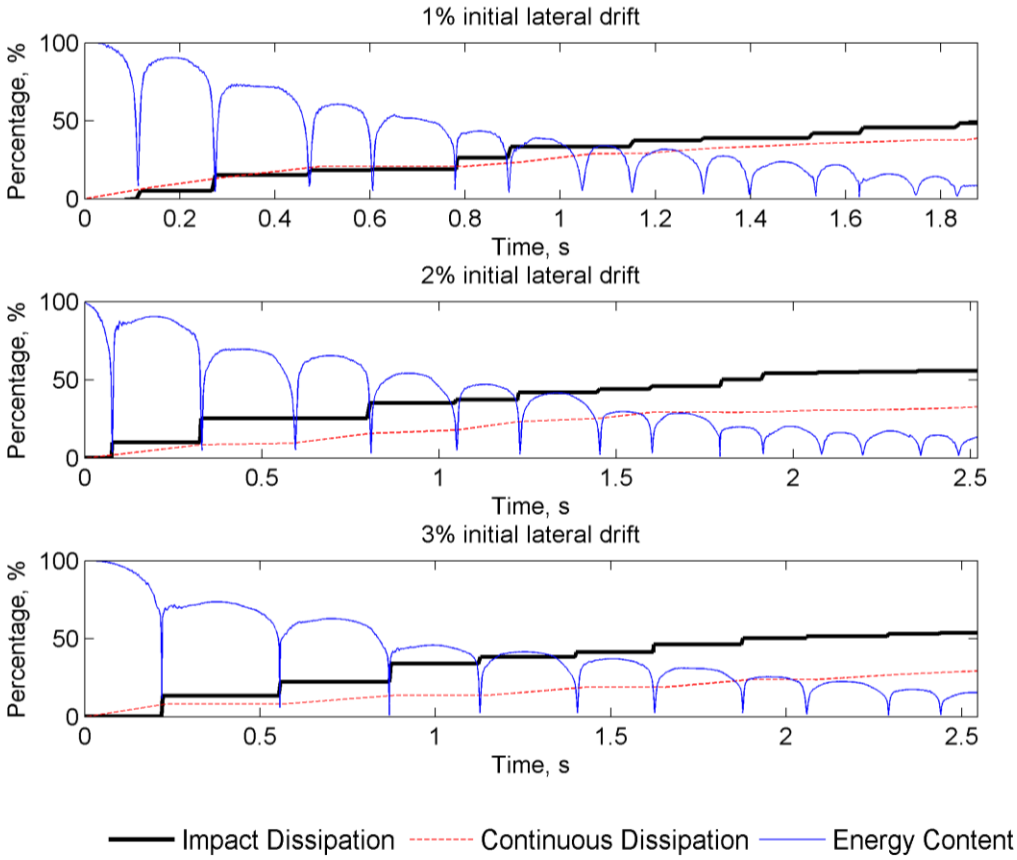

Figure 3-24. Experimental energy dissipation components and energy content of *Rocking System 3*

In order to further examine the capacity of the FE model, its results were used to quantify energy dissipation in the experimental rocking units. With the ability to unlimitedly increase the FEA sampling frequency, a more accurate estimation of the velocity response was targeted at this point by collecting 2,000 linear displacement data points per second, aiming at a consequent improved quantification of the kinetic energy and impact dissipation. Even by using a higher sampling frequency, a noise effect was unavoidably present in the FEA velocity data and smoothing was similarly applied to overcome this issue.

As initially argued, the FE model was able to approximately estimate decay of motion despite its deficiency to specifically predict the exact quarter periods of free rocking in the

region of very small angular displacements ($\theta(t) \leq 1\%$). This primary observation is verified in Figure 3-26 where a good energy content estimation was achieved for the 3% ITLD case and an adequate approximation of the energy loss per cycle was attained for the 1% and 2% ITLD cases. Parallel to this result, the experimental and FEA estimations for the two accumulated energy dissipation components unfold in the same fashion in all cases.

These results suggest that modeling of free rocking behavior by using the proposed FE model provided a tool not only for estimating the actual free rocking angular displacement, but for accurately capturing the associated actual decay of motion, as well. As energy dissipation in the FEA did not follow a predetermined energy dissipation pattern i.e. an impact, viscous or frictional dissipation mechanism in contrast to the majority of mathematical rocking models, the use of a Rayleigh material damping model provided an opportunity to recognize the existence of these two discrete decay of motion mechanisms.

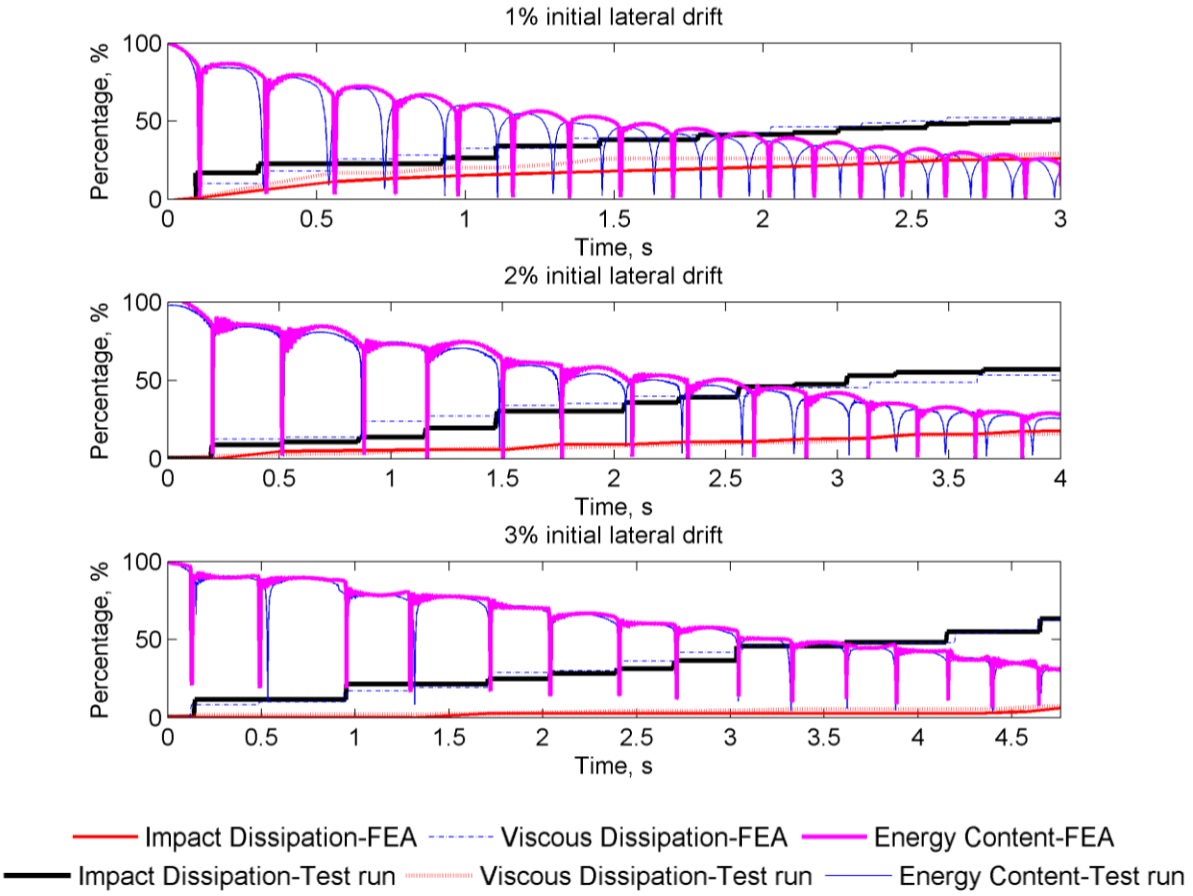

Figure 3-25. Typical experimental energy dissipation time history in comparison with FEA for *Rocking System 1*

Impact dissipation mechanism. The finding that free rocking concrete members are in parallel influenced by a continuous energy dissipation mechanism has created the need for another investigation, which is the comparison between the SRM and the experimental impact mechanisms in order to specifically examine the efficiency of SRM to model rocking impact, given the impact approaching angular velocity.

By literature, a common approach followed by previous researchers to conduct this investigation was the comparison between the experimental and theoretical COR. An equivalent approach that directly demonstrates the quantification of energy dissipation per impact was followed herein by employing the relationship between amount of energy

dissipation per impact (designated as ΔK) and respective impact approaching angular velocity. This relationship was developed by using the experimental and FEA, SRM simulations results.

ΔK by SRM was calculated per Eq. 3-16 which expresses the amount of energy dissipation per impact associated with COR, moment of inertia of the rocking body and its angular velocity just before the impact.

$$\Delta K = \frac{1}{2} I_o \dot{\theta}_1^2 (1-r) \tag{3-16}$$

Simultaneously, amount of impact dissipation and impact approaching angular velocity data sets were collected from the test runs and FEA, and plotted in comparison with the SRM estimations in Figure 3-26. In contrast to what might be expected, Figure 3-26 shows that the impact model of COR by SRM provided a lower-bound limit for energy dissipation per impact with respect to the corresponding approaching angular velocity in all cases. This observation is true even for *Rocking System 1* where Housner's model was initially showed to overestimate its free rocking decay of motion. In retrospect, this result may be linked with the previous findings that free rocking of these three rocking systems should be influenced by another dissipation mechanism, which is not associated with the instantaneous-impact phenomenon. Also, comparing real time angular displacement time history with SRM simulation does not necessarily provide a reliable indication for the originally proposed COR model as overestimating impact approaching angular velocity by SRM leads to erroneous estimations for ΔK.

The results in Figure 3-26 advocate that the SRM can be readily utilized as an efficient tool to provide a conservative estimation for the dissipated energy per impact given

the correct impact approaching angular velocity. It can also be inferred that FEA ΔK results have effectively fluctuated within the "boundaries" indicated by the experimental data.

In general, the ΔK - $\dot{\theta}$ relationship as extracted from the experimental study in Figure 3-26 supports the statement that impact dissipation is strongly dependent on the approaching angular velocity value; however, the large scatter in this relationship, which is higher for the flexible configuration of *Rocking System 2*, may implicitly suggest a relationship directly connecting these two variables cannot be formed.

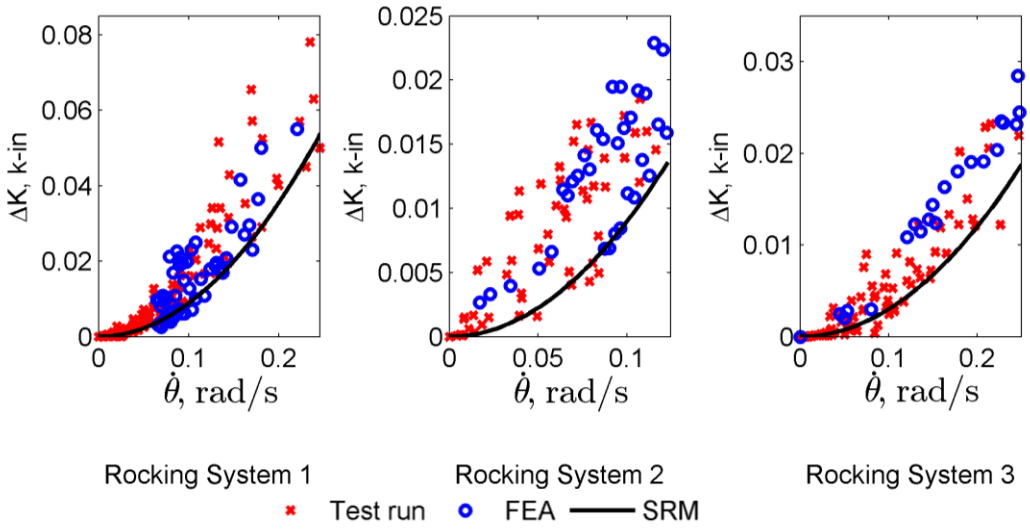

Figure 3-26. Impact dissipation versus approaching angular velocity

By SRM, COR and impact approaching angular velocity serve as the only parameters associated with the impact phenomenon. Since it has been shown that actual impact energy dissipation cannot be effectively characterized by its relationship with the approaching angular velocity, this study focused on exploring other parameters which can be associated with the impact mechanism.

Based on impact dynamics, impact dissipation may be linked with the impulsive force response taking place during an impact of the rocking system with its foundation. In order to estimate the support forces applied to the rocking system during a free rocking motion, Housner's fundamental assumptions of (1) rigid body motion; (2) no sliding between the rocking body and its foundation occurs; (3) no bouncing of the rocking body occurs; and (4) two-dimensional free rocking motion, were used to estimate the horizontal and vertical support forces applied to a free rocking system. Accordingly, the support force applied at its bottom corners can be divided into (1) a horizontal, F_h and (2) a vertical, F_v, component. These components were estimated by Newton's 2nd law and are presented in Eq. 3-17 and 3-18.

$$F_h = M(S(\theta)R\dot{\theta}^2 \sin(a-|\theta|) + R\ddot{\theta}\cos(a-|\theta|)) \tag{3-17}$$

$$F_v = M(g - R\dot{\theta}^2 \cos(\alpha-|\theta|) + S(\theta)R\ddot{\theta}\sin(\alpha-|\theta|)) \tag{3-18}$$

The total base force was then calculated as,

$$F_T = \sqrt{F_h^{\,2} + F_v^{\,2}} \tag{3-19}$$

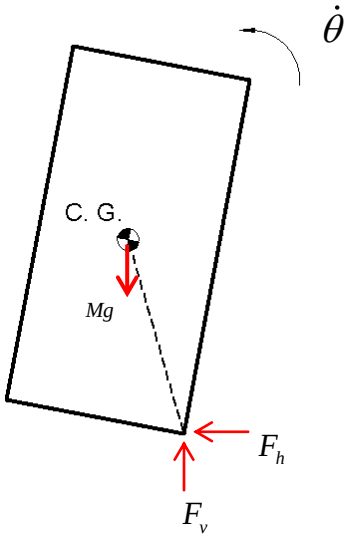

Figure 3-27. Free body diagram of a free rocking block

In order to experimentally determine the time histories of these forces, the smoothed velocity data was used, while experimental acceleration time histories were calculated by double differentiating raw displacement data. For an accurate estimation of the impulsive impact responses in acceleration time history, raw acceleration data was directly inputted in Eq. 3-17 and 3-18 without the use of any filtering technique in order to avoid corruption of the impulsive peak values.

Figure 3-28 shows typical smoothed velocity and raw acceleration time histories. Following the acceleration and velocity time series in this figure, the rocking impact phenomenon which corresponds to the peak values of angular velocity; and the impulsive responses of angular acceleration can be divided into two phases. First, at the outset of an impact the rocking body exhibits a high decelerating angular acceleration that causes an instantaneous drop in velocity and second, when angular velocity reaches a minimum value inside the impact phase of motion, angular acceleration starts to build up towards the opposite direction, leading to an increase in angular velocity and ultimately resulting in the just after impact angular velocity.

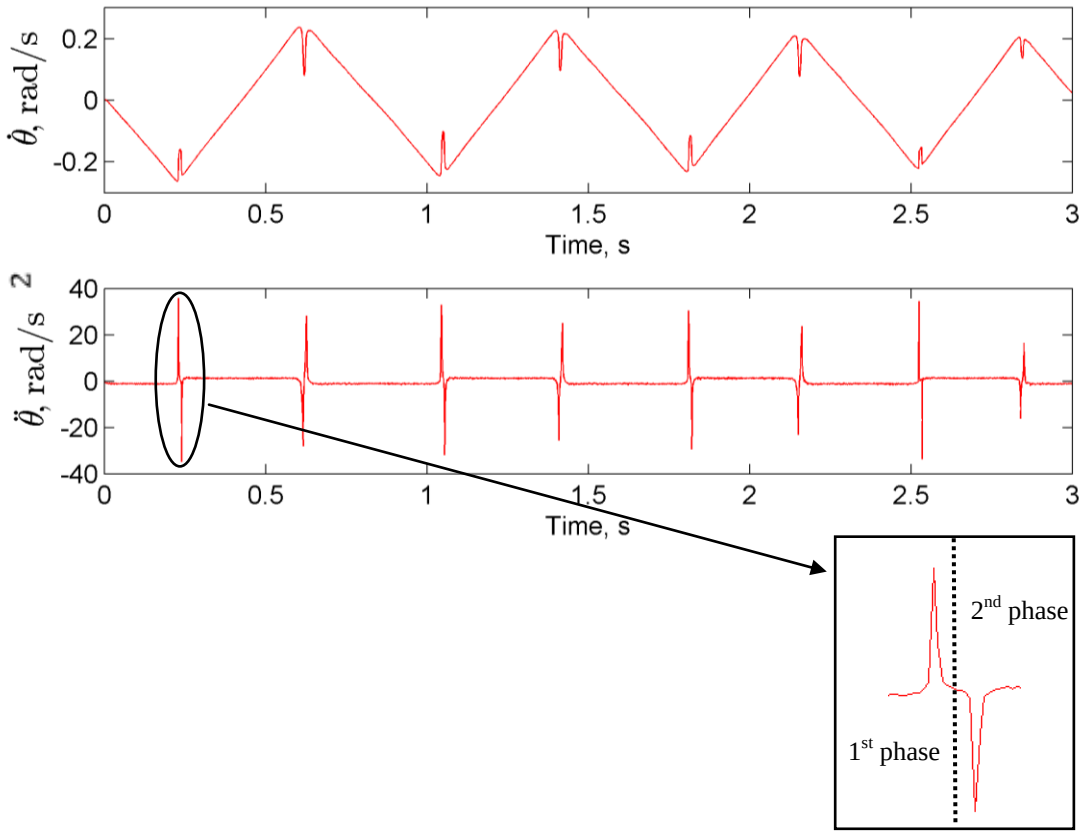

Figure 3-28. Typical experimental velocity and acceleration time histories

From SRM standpoint, rocking acceleration time history is, by contrast, an impulse free response. For $\theta(t) \geq 0$ and by using Eq. 3-5, theoretical angular acceleration becomes an angular displacement dependent variable, as shown in the resulting Eq. 3-20.

$$\ddot{\theta} = p^2(\theta - a) \tag{3-20}$$

According to this result and considering that an actual impact takes place at approximately $\theta(t) = 0$, the theoretical impact acceleration becomes a parameter dependent on the geometric properties of the rocking system.

Figure 3-29 presents the comparison between the theoretical estimations and the experimental results for angular acceleration, horizontal and vertical forces time histories. It

is shown despite their phase lag, actual and theoretical responses present an identical behavior during the continuous phase of free rocking motion; however, they exhibit fundamental differences during the impact phase. Theoretical horizontal force and angular acceleration are essentially constant during the continuous phase and they face a sign reversal as an impact takes place and the body starts to oscillate with respect to the opposite rotation center. Theoretical vertical force is always pointed upwards, as expected, and oscillates between a maximum value occurring at the peak angular displacement and a minimum value that takes place at the instant of impact. While these trends are in close agreement with the respective experimental responses during the continuous phase, experimental forces exhibit a nonlinear impulsive response during the impact phase characterized by sharp peaks analogous to the response observed in angular acceleration time history. The peak of these impulsive forces presents significant fluctuations in time series; nevertheless, from a careful inspection it experiences a gradual decay as the rocking body approaches its rest condition.

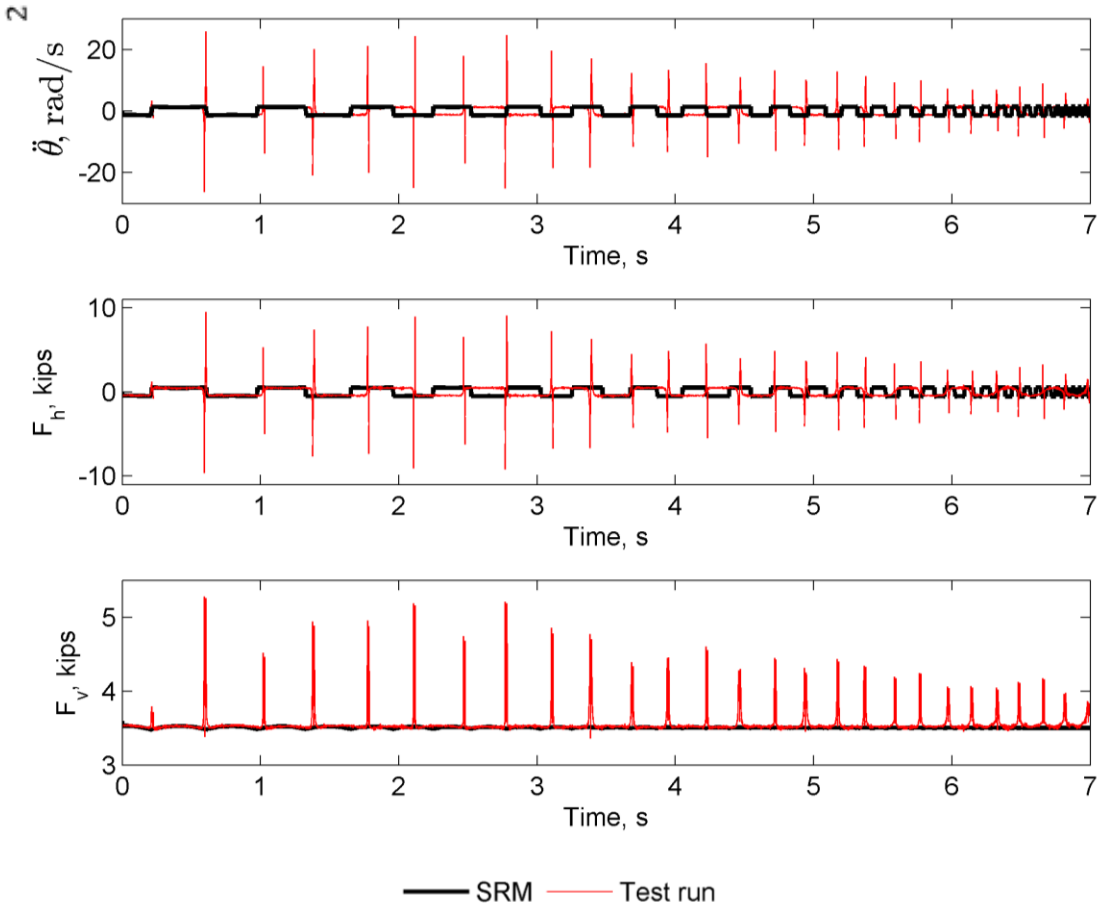

Figure 3-29. Typical angular acceleration and base forces (*Rocking System 1*)

Eq. 3-17 and 3-18 indicate that horizontal and vertical support forces are velocity and acceleration dependent quantities. After combining these two components into the total impact force, its peak values that take place during the 1st phase of an impact were collected and compared with the angular velocity and acceleration respective peak values, as shown in Figure 3-30. Looking at this figure, the total impact force appears essentially insensitive to changes in impact approaching angular velocity and acceleration values for a window that corresponds to very small F_T values (i.e. also corresponds to approximately $\theta(t) \le 0.5\%$). As higher forces are applied to the free rocking system, a linear relationship builds up revealing a dependence of the total force on angular velocity and acceleration values. This linear

relationship is clearer in the acceleration plot, and characterized by a slight scatter in the velocity plot due to the corruption induced by noise effect in this data series.

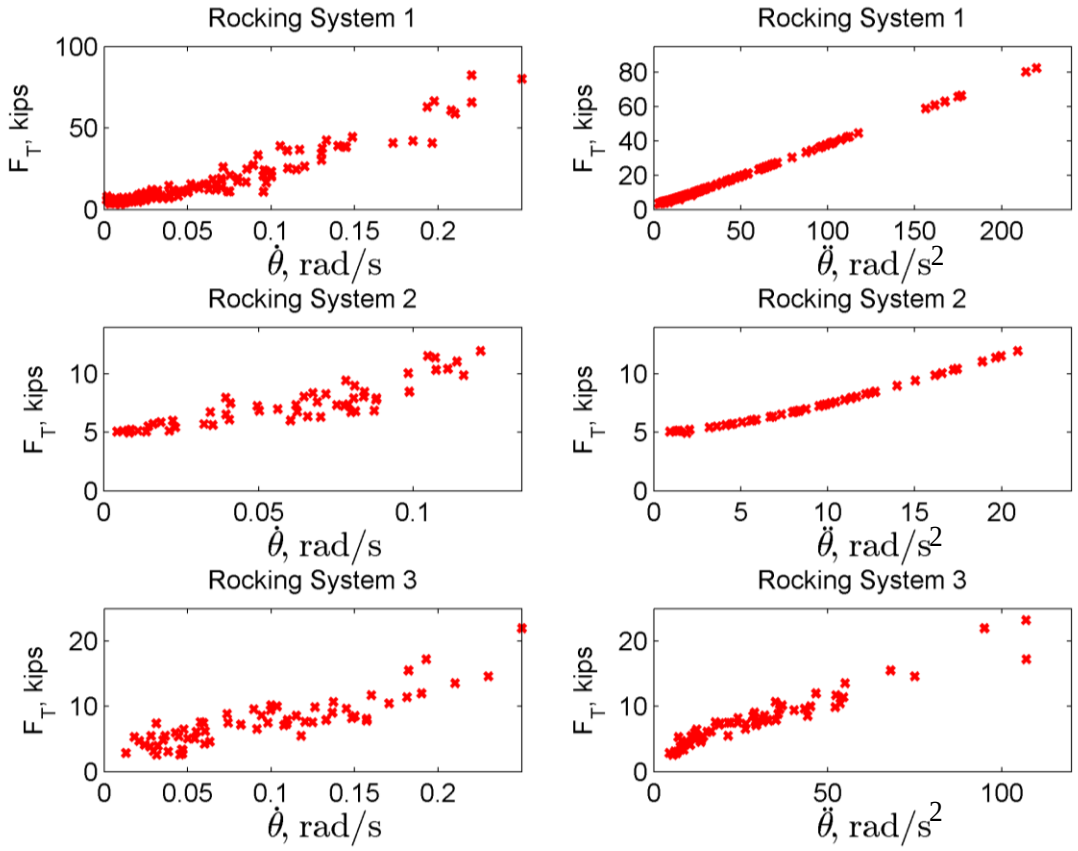

Figure 3-30. Experimental impact total force vs. impact approaching velocity and acceleration values

Using the experimental total force results together with the respective quantities from FEA, the impact force was plotted against the respective amount of impact energy dissipation, ΔK, in Figure 3-31. According to this plot, ΔK is less sensitive to impact force changes for the window of very small force values, while it becomes more dependent on the impact force variation at higher values where an approximately linear relationship is formed and is described by a different slope for each of the free rocking systems.

Ignoring the significantly scattered part corresponding to small F_T values in the graphs of Figures 3-30 and 3-31, approximately linear relationships may be assumed for the ΔK - F_T and F_T - $\dot{\theta}$ data sets. The slopes of these relationships can be consequently linked with the real time COR values. Assuming this approximation, it can be inferred that a slope increase either in the ΔK - F_T or F_T - $\dot{\theta}$ graph corresponds to decrease in the real time COR.

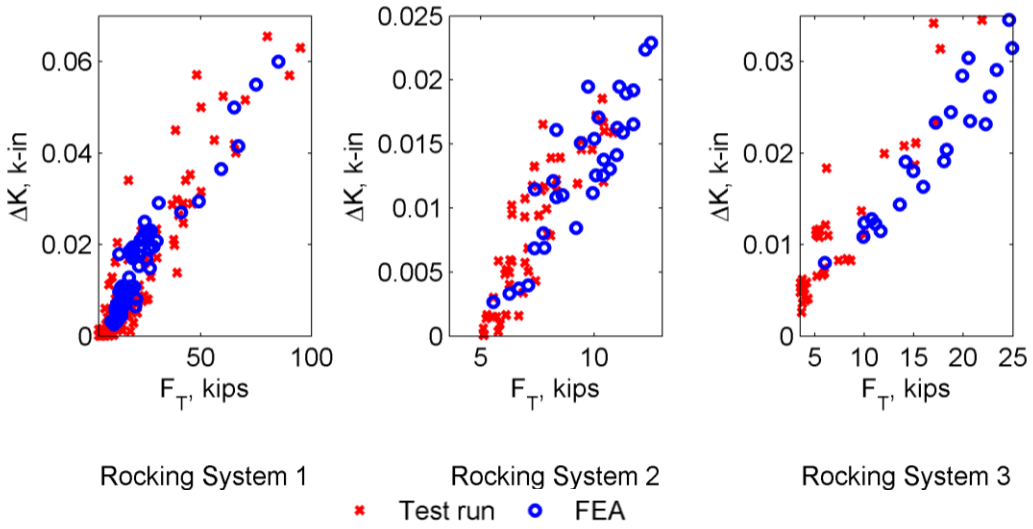

Figure 3-31. Impact energy dissipation vs. total support force just before an impact

Let s_1 being the slope in the F_T - $\dot{\theta}$ graph, and s_2 the slope in the ΔK - F_T graph. These two relationships are expressed as,

$$F_T = s_1 \dot{\theta} \tag{3-21}$$

$$\Delta K = s_2 F_T \tag{3-22}$$

Using Eq. 3-16, 3-21, and 3-22, the two slopes can be used to create an alternative empirical equation for COR, as shown below.

$$r = 1 - \frac{2 s_1 s_2}{I_o \dot{\theta}} \tag{3-23}$$

Given that s_1 and s_2 are constant for a particular free rocking precast concrete member, COR becomes a velocity dependent variable.

Continuous dissipation mechanism. From a qualitative assessment, participation of the continuous dissipation in the decay of motion was shown to decrease with increase in ITLD of the free vibration response. This component of the free rocking decay of motion was also shown to play a more significant role within a region of small angular displacement peaks, where angular displacement time history experiences an exponential decay. It can be due to the influence of a continuous dissipation mechanism that an energy transfer in and out of the rocking system was identified within the window of small angular displacement peaks, a behavior which may signify the existence of two regions where the rocking system losses energy in a continuous manner; and a portion of the "dissipated" energy is gradually returned to the rocking system. Following this assumption, it is suggested that continuous dissipation could be expressed through a continuous dissipation term supplementing the original linearized equation of motion, Eq. 3-3.

In order to develop a velocity-dependent free rocking model which follows the fundamental assumptions of SRM (except from the assumption on decay of motion of a rocking rigid block), Eq. 3-3 was reformed and equation of free rocking motion was accordingly divided into four pieces with respect to the angular displacement and velocity directions (sign convention shown in Fig. 3-18): (1) $\theta > 0, \dot{\theta} < 0$; (2) $\theta < 0, \dot{\theta} < 0$; (3) $\theta < 0, \dot{\theta} > 0$; and (4) $\theta > 0, \dot{\theta} > 0$. Presented are the first and second phases as the next two can be respectively derived.

Given that $\theta(t) \geq 0$, Eq. 3-24 describes the motion with initial conditions of $\theta(t) = \theta_o$ and $\dot{\theta}(t) = 0$ and terminates at $\theta(t) = 0$. Next, Eq. 3-25 describes the motion starting with $\theta(t) = 0$ and $\dot{\theta}(t) = \dot{\theta}_o$ and terminates at $\dot{\theta}(t) = 0$. A coefficient c was used to describe continuous energy dissipation during the first phase, while the second phase assumes that a portion of the dissipated energy is recovered by the rocking system, a behavior which is modeled through the r' parameter expressing the percentage of the c coefficient which now operates in a recovering manner.

$$I_o\ddot{\theta} + MgR\sin(\alpha - \theta) + c\dot{\theta} = 0 \tag{3-24}$$

$$I_o\ddot{\theta} + MgR\sin(\alpha - \theta) - r'c\dot{\theta} = 0 \tag{3-25}$$

These two equations of free rocking motion were solved for $\theta(t)$ by applying the aforementioned initial conditions leading to Eq. 3-26 for the first phase and Eq. 3-27 for the second phase.

$$\theta(t) = \alpha + e^{(-\beta t/2)}(\theta_o - \alpha)(\cosh(p't) + \frac{\beta}{2p'}\sinh(p't)) \tag{3-26}$$

$$\theta_r(t) = \alpha + e^{(r'\beta t/2)}(-\alpha\cosh(p_r't) + (\frac{\dot{\theta}_o}{p_r'} + \frac{r'\beta\alpha}{2p_r'})\sinh(p_r't)) \tag{3-27}$$

The dynamic parameters p' and p_r' which represent the "natural" frequencies of the free rocking system are dependent on the coefficient, c and the recovery parameter, r', as shown in Eq. 3-28 and 3-29.

$$p' = p\sqrt{(\frac{\beta}{2p})^2 + 1} \tag{3-28}$$

$$p_r' = p\sqrt{(\frac{r'\beta}{2p})^2 + 1} \tag{3-29}$$

Where β is defined as,

$$\beta = \frac{c}{I_o} \tag{3-30}$$

The described free rocking model (designated as MFRM) was subsequently tested for its applicability in *Rocking Systems 1 & 3*, while *Rocking System 2* was omitted at this point due to its flexibility properties which violate the fundamental assumption of a rigid body motion initially taken for developing MFRM. The above-referenced piecewise equations were implemented by using MATLAB software. Two dissipation mechanisms were assumed in this model: impact dissipation and continuous dissipation. As this section focused only on evaluating the applicability of the continuous-dissipation model in free rocking concrete members, impact dissipation expressed through COR was accordingly adjusted for each impact.

As far as *Rocking System 1* is concerned, a $c = 20$ k-in-s and $r' = 80\%$ were finally selected as the most suitable values to model the 3% ITLD response. Figure 3-33 shows the phase diagram and angular displacement time history comparisons between MFRM and the respective test run. It is demonstrated MFRM produced an accurate estimation of the continuous phase, being able to closely follow the experimental results till the boundaries of impact phase. The impact approaching velocity estimation was also improved compared to the results by SRM; however there was still a significant deviation between the MFRM and the real time response within the impact-dependent region.

In addition, MFRM was applied to simulate the 1% ITLD response. In contrast to what would be expected, an increased coefficient value of $c = 30$ k-in-s was selected this time as the most accurate value to estimate this experimental response. Considering the experimental conditions established at the beginning of each test run, it is likely the rocking

interface was essentially deteriorated as the testing process was moving from 1% to the 3% ITLD test runs. This effect may have damaged the damping abilities of the free rocking system leading to a decreased damping as well as COR, as indicated by comparing Figures 3-33 and 3-34.

Figure 3-34 shows that MFRM was able to effectively simulate the continuous phase of free rocking motion and better estimate the impact approaching angular velocities of the actual system; nevertheless, this improvement presented in the phase diagram was not accompanied by an accurate estimate of the actual angular displacement time history, as this behavior is also strongly influenced by the "natural" period of the actual free rocking system which was not captured by the MFRM simulation.

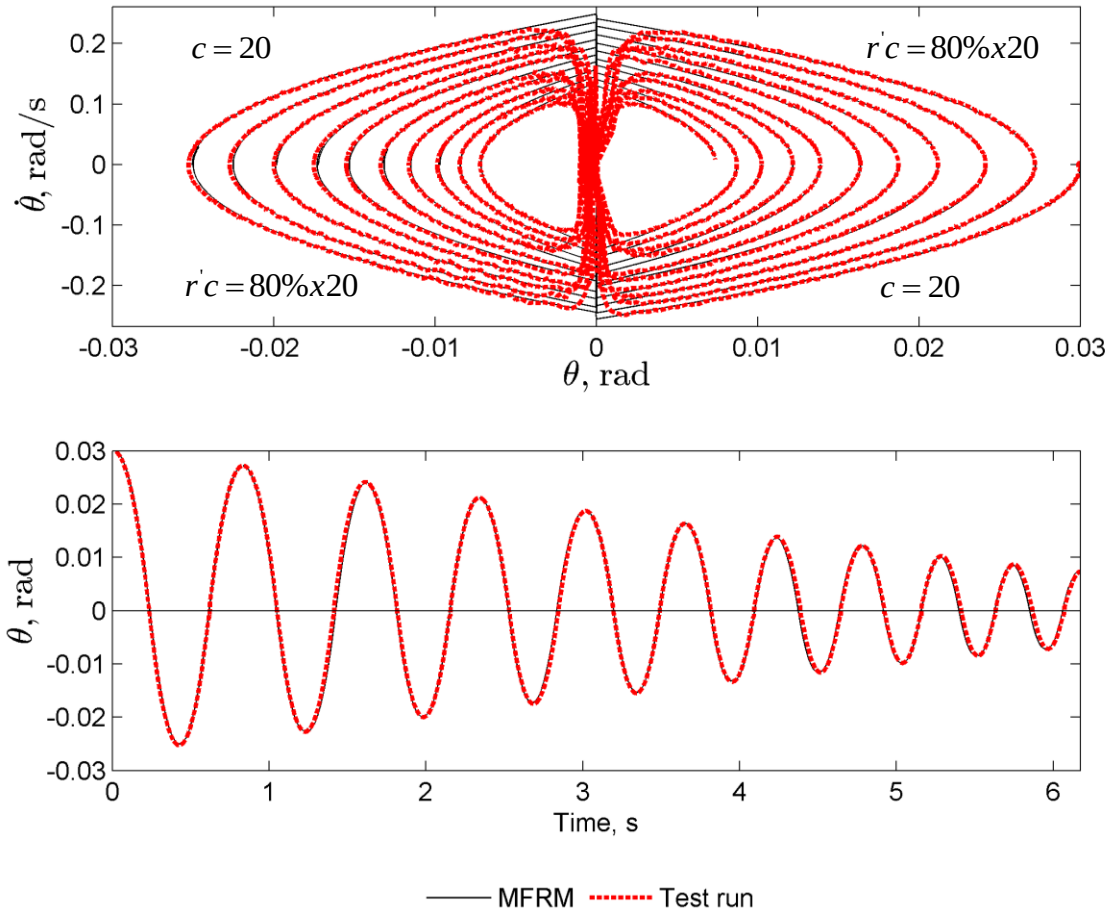

Figure 3-33. MFRM compared with test run for 3% initial lateral drift free vibration test on *Rocking System 1*

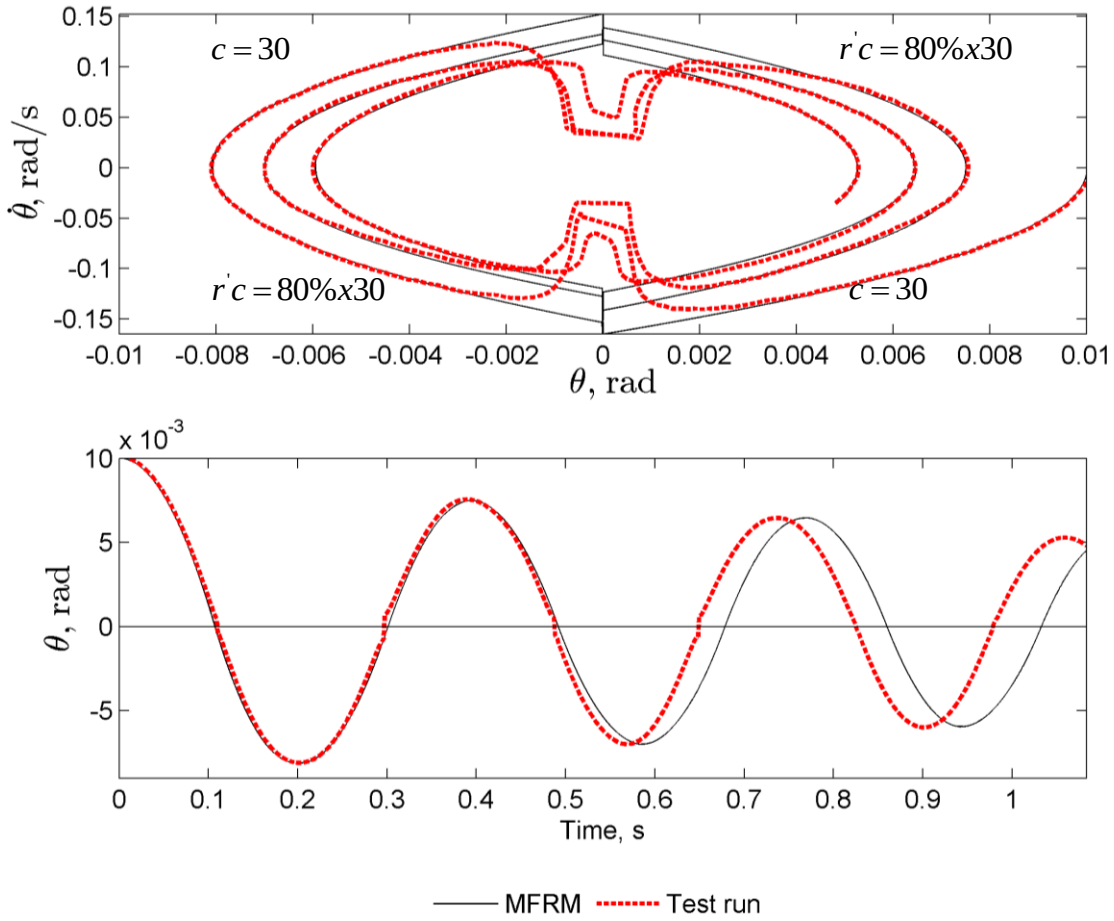

Figure 3-34. MFRM compared with test run for 1% initial lateral drift free vibration test on *Rocking System 1*

In the initial evaluation of *Rocking Systems 1 & 3*, it was shown that the latter is able dissipate a higher percentage of energy by its continuous dissipation mechanism. This behavior is also depicted in the phase diagram produced by MFRM which demonstrates that the 3% ITLD response of *Rocking System 3* is associated with a different pattern with lower c and r' values.

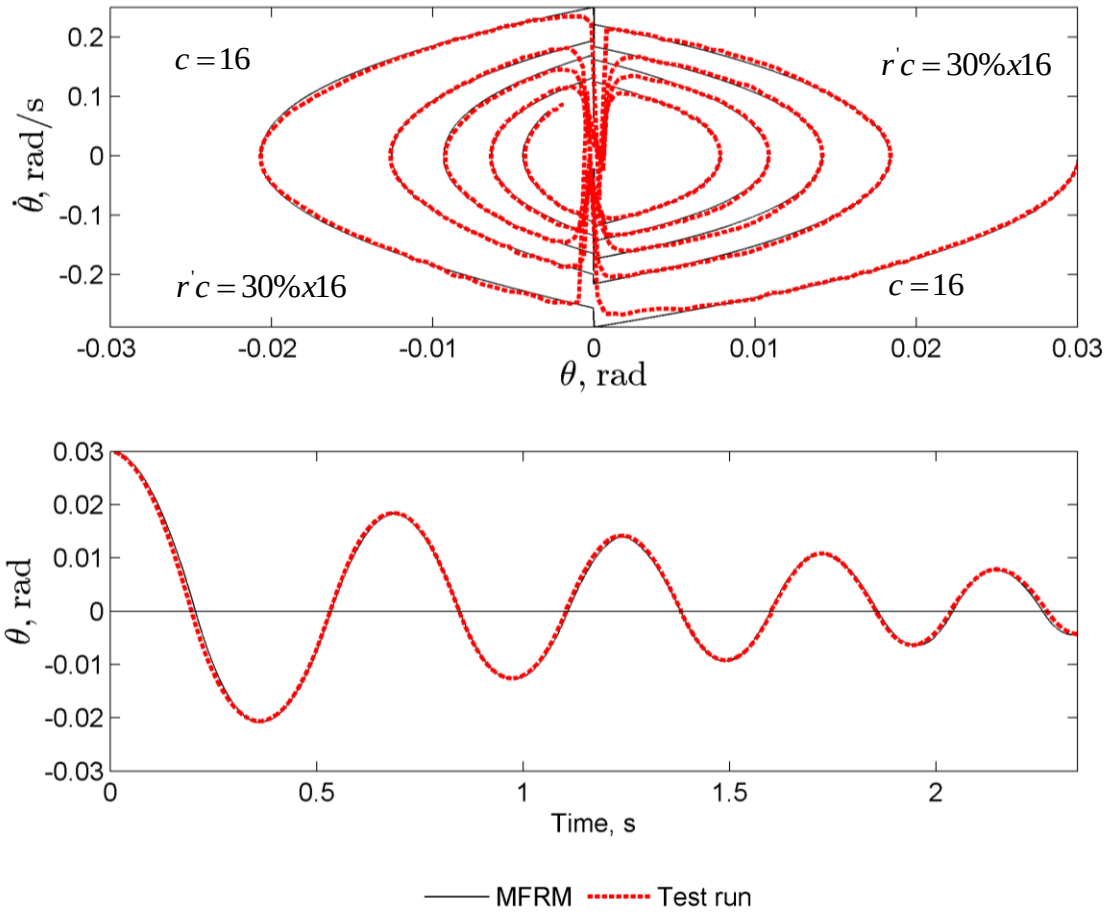

Figure 3-35. MFRM compared with test run for 3% initial lateral drift free vibration test on *Rocking System 3*

For a closer inspection of this behavior by *Rocking System 3*, the results extracted from the second instrumentation configuration were employed to investigate local behavior at the rocking interface, which was believed to be the location strongly associated with energy dissipation in a rocking motion. The four LED sensors attached along the column's bottom edge were used to find the dynamic neutral axis (NA) response as exhibited by the free rocking concrete units. Figure 3-37 presents a typical time history of the dynamic NA and its relationship with angular displacement. A more chaotic response is shown for the 1% ITLD case where the dynamic NA response would have been significantly affected by local imperfections of the rocking interface. It is also indicated that free rocking concrete systems

are not subjected to an abrupt NA variation as assumed by SRM, as is typically shown in Figure 3-37; in contrast, dynamic NA oscillates between a minimum (top angular displacement peak) and maximum (during impact phase) value during its motion. This behavior signifies an intense and continuous interaction between the unit's bottom edge and foundation's surface which is dependent on the magnitude of the support forces developed during rocking motion. As *Rocking Systems 1 & 3* experience a different range of support forces due to their mass difference, the resulting local behavior of the rocking interface produces a continuous-dissipation mechanism which may be different for each system. Even though the assumption of this dissipation mechanism was shown to be a promising approach for supplementing energy dissipation modeling in these free rocking systems, this complex behavior experienced by these systems advocates a continuous dissipation which is not a purely velocity dependent parameter but its controlling variables of c and r' can be also influenced by other properties of the rocking structural configuration associated with the material conditions and the interactions taking place along the rocking interface.

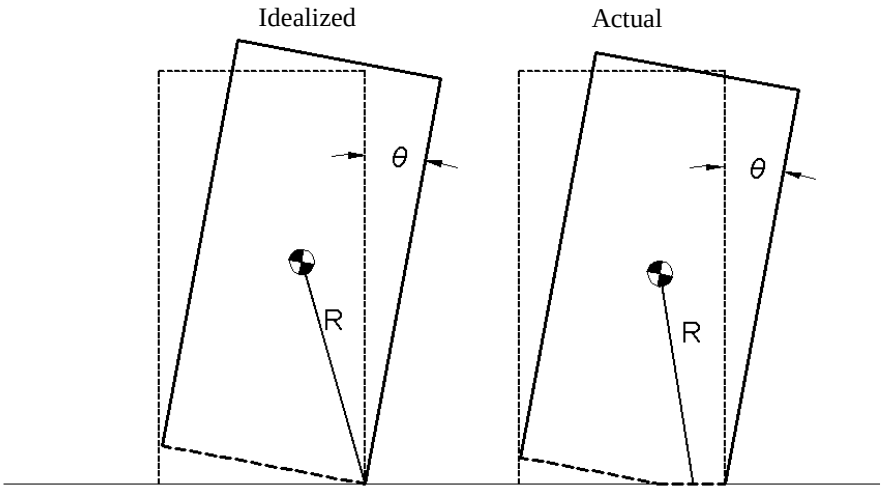

Figure 3-36. Typical (1) idealized; and (2) actual behavior of the rocking bottom edge

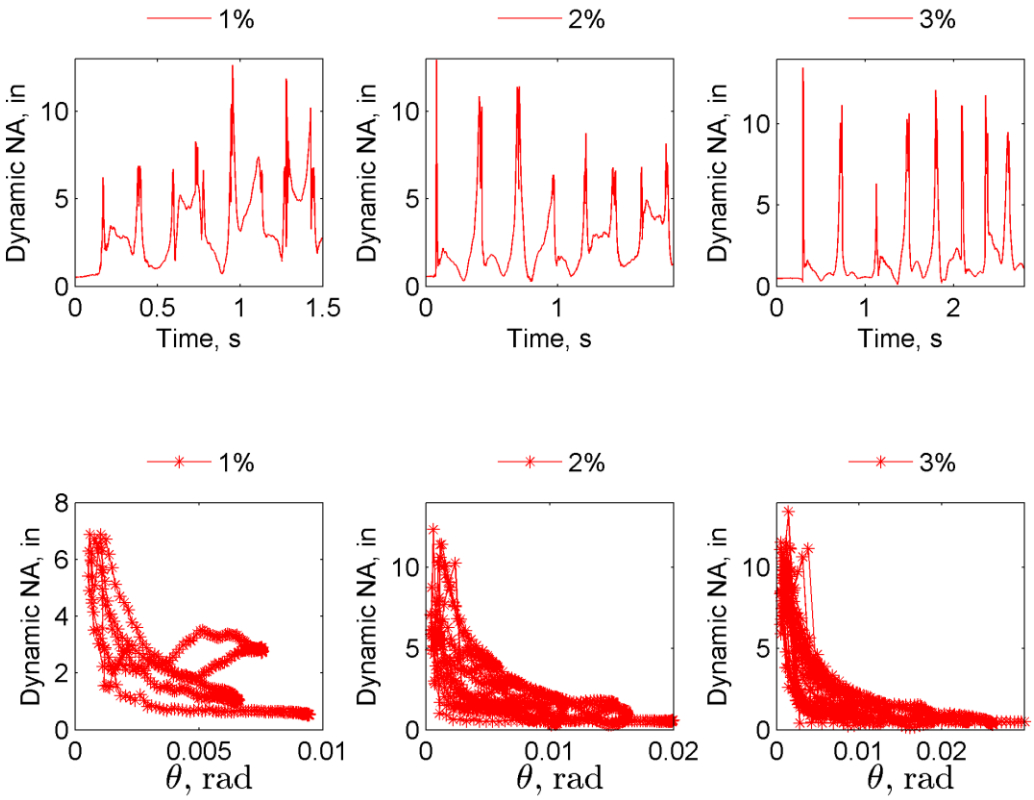

Figure 3-37. Typical dynamic neutral axis variation with respect to time and angular displacement

3.8 Conclusions

The likelihood of structural systems to enter free rocking under seismic load underscores the need to better understand and accurately model free rocking motion. This study investigated the dynamic characteristics of this behavior. It was experimentally and analytically shown that free rocking members can exhibit complicated energy dissipation features, which are not addressed in previous modelling techniques.

Two energy dissipation mechanisms were identified, namely: 1) impact; and 2) continuous. Housner's COR model was shown to provide the conservative boundary for impact dissipation. It was next shown that continuous dissipation can be modeled in terms of velocity-dependent parameters. This mechanism operates in two phases, in which it 1)

dissipates rocking energy; and 2) recovers part of the "dissipated" energy. Despite that findings of this study suggest continuous dissipation may not significantly participate in the total amount of energy dissipation, it must be recognized that its importance hinges on the gradual decay of angular velocity as the free rocking member approaches an impact. Consequently it follows, continuous and impact mechanisms interact with each other in such a way that modelling of both mechanisms is necessary for an effective use of the COR approach by SRM and in order to obtain reasonable estimation of the expected free rocking response.

A reasonable analysis method for free rocking motion of precast concrete columns may include the introduced continuous dissipation with empirically selected parameters, while impact model 1) by an empirical approach as presented or 2) by SRM may be employed to provide average or conservative estimations for impact dissipation, respectively.

3.9 Acknowledgements

This work presented in the paper was undertaken as part of the "*NEES* Rocking Wall" project, with funding from the National Science Foundation under Grant No. 1041650 and Precast/ Prestressed Concrete Institute (PCI). Any opinions, findings, and conclusions or recommendations expressed in this material are those of the authors and do not necessarily reflect the views of the National Science Foundation or PCI. The authors would also like to thank Owen Steffens and Douglas Wood of Iowa State University laboratory for their help with completing the rocking system tests.

3.10 References

Abaqus analysis user's guide version 6.13. *Dassault Systemes Simulia Corp.*

Andreaus, U., and Casini, P., 1999. On the rocking-uplifting motion of a rigid block in free and forced motion: Influence of sliding and bouncing, *Acta Mechanica*, 138, 219-241.

Ardila-Giraldo, O., 2013. Contact interface modeling in the dynamic response of rigid blocks subjected to base excitation, *4th ECCOMAS Them. Conf. on COMPDYN*.

Aslam, M., Godden, W.G., and Scalise, D. T., 1980. Earthquake rocking response of rigid bodies, *J. Struct. Eng.*, ASCE, 106, 377-392.

Belleri, A., Torquati, M., and Riva, P., 2013. Finite element modeling of 'Rocking walls', *4th ECCOMAS Them. Conf. on COMPDYN*.

Chatzis, M., and Smyth, A., 2012. Robust modeling of the rocking problem, *J. Eng. Mech.*, ASCE, 138, 247-262.

Chopra, A., and Yim, S., 1985. Simplified earthquake analysis of structures with foundation uplift, *J. Struct. Eng.*, ASCE, 111, 906-930.

Fielder, W., T., Virgin, L., N., and Plaut, R., H., 1997. Experiments and simulation of overturning of an asymmetric rocking block on an oscillating foundation, *Eur. J. Mech, A/Solids*, 16, 905-923.

Housner, G. W., 1963. The behavior of inverted pendulum structures during earthquakes, *Bulletin of the Seismological Society of America*, 53, 403-417.

Kalliontzis, D., and Sritharan, S., 2014. A finite element approach for modelling controlled rocking systems, *2nd European Conference on Earthquake Eng. and Seismology*

Lipscombe, P. R., and Pellegrino, S., 1993. Free rocking of prismatic blocks, *J. Eng. Mech.*, ASCE, 119, 1387-1410.

Ma, Q., 2009. The mechanics of rocking structures subjected to ground motion, *PhD Thesis, Department of CEE, The University of Auckland, New Zealand.*

Manos, G., Petalas, A., and Demosthenous, M., 2013. Numerical and experimental study of the rocking response of unanchored body to horizontal base excitation, *4th ECCOMAS Them. Conf. on COMPDYN*.

Muto, K., Umemura, H., and Sonobe, Y. (1960). Study of the overturning vibrations of slender structures, *Proc. 2nd World Cong. Earthquake Eng.*, Tokyo, Japan, 1239-1261.

Pena, F., Prieto, F., Lourenco, P., B., Costa, A., C., and J. V. Lemos, 2007. On the dynamics of rocking motion of single rigid-block structures, *Earthquake Eng. Struct. Dyn.*, 36, 2383-2399.

Priestley, M. J. N., Evison, R. J., and Carr, A. J., 1978. Seismic response of structures free to rock on their foundations, *Bulletin of the New Zealand National Society for Earthquake Eng.*, 11, 141-150.

Spanos, P., D., and Koh, A., S., 1984. Rocking of rigid blocks due to harmonic shaking, *J. Eng. Mech.*, ASCE, 106, 377-392.

Tso, W. K., and Wong, C. M., 1989. Steady state rocking response of rigid blocks, Part 1: Analysis, *Earthquake Eng. Struct. Dyn***.,** 18, 89-106.

Yim, C., S., and Lin, H., 1991. Nonlinear impact and chaotic response of slender rocking objects, *J. Eng. Mech.*, ASCE, 117, 2079-2100.

CHAPTER 4: ON THE DYNAMIC DECAY OF CONTROLLED ROCKING MEMBERS

A reduced version to be submitted to Journal of Structural Engineering, ASCE

Dimitrios KALLIONTZIS and Sri SRITHARAN

4.1 Abstract

Their self-centering capacity and the use of supplemental damping mechanisms to ensure adequate hysteretic energy dissipation have introduced unbonded post-tensioned rocking concrete systems as a contemporary design philosophy in the realm of seismic-resisting mechanisms. Accurate estimation of their seismic response is dependent on their inherent damping capabilities which cannot effectively addressed by the simple rocking model which has been commonly applied to free rocking motion of rigid blocks. This study presents an experimental investigation on free and controlled rocking behavior highlighting precast concrete members subjected to controlled rocking experience lower dynamic energy dissipation per cycle compared to their free rocking response. Accordingly, the original energy dissipation model by the free rocking theory is reformed for estimating controlled rocking dynamic decay of motion. Finally, a finite element modeling approach for controlled rocking is validated with experimental results of discrete controlled rocking systems.

4.2 Introduction

4.2.1 Free rocking

The first steps towards understanding free rocking motion of a rectangular block were taken by Housner (1963) who introduced the simple rocking model (SRM) for estimating dynamic response of free rocking rigid blocks. This modeling method was developed based on the assumptions that (1) both the rocking block and the underlying base are rigid; (2) the motion is free from sliding; (3) no bouncing of the block takes place; (4) energy dissipation due to free rocking is attributed to a mechanism associated with the impact of the block with its base; (5) the impact occurs at the corner of the bottom edge of the block; and (6) the rocking motion takes place in a two-dimensional fashion. Following these assumptions, Housner suggested free rocking motion may be considered dependent on the geometric properties of the block with the aspect ratio, α, of the block and the distance, R, between its center of gravity and the rotation center on the foundation being the critical variables of its behavior. These two variables are shown in Figures 4-1.

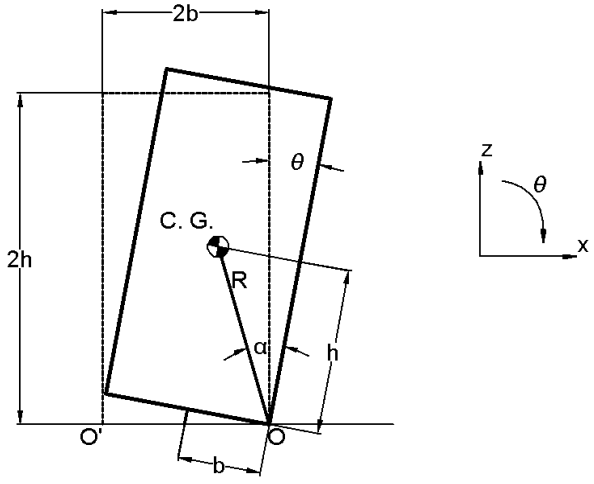

Figure 4-1. A free rocking block

$$R = \sqrt{\frac{(2b)^2 + (2h)^2}{2}} \tag{4-1}$$

$$\alpha = \arctan(\frac{2b}{2h}) \tag{4-2}$$

Equation of motion for free rocking may be described by the following Eq. 4-3,

$$I_o\ddot{\theta} + S(\theta)MgR\sin(\alpha - |\theta|) = 0 \tag{4-3}$$

where $I_o = \frac{4}{3}MR^2$ is the moment of inertia of the block with respect to the rotation center (O or O') and M is the total mass of the rocking block. The $S(\theta)$ parameter in Eq. 4-4 below is used to express the sign convention adopted for free rocking motion, as specified in Figure 4-1.

$$S(\theta) = \begin{cases} 1, for\ \theta > 0 \\ -1, for\ \theta < 0 \end{cases} \tag{4-4}$$

As far as slender blocks are concerned (a block is designated as slender when $a \le 20^o$), Housner suggested that Eq. 4-3 can be linearized as,

$$I_o\ddot{\theta} + S(\theta)MgR(\alpha - |\theta|) = 0 \tag{4-5}$$

By applying the initial conditions of $\theta(0) = \theta_o$ and $\dot{\theta}(0) = 0$ to Eq. 4-5, the solution for $\theta(t)$ becomes,

$$\theta(t) = a - (a - \theta_o)\cosh pt \tag{4-6}$$

Where p is the so-called *dynamic parameter* of the block defined as,

$$p = \sqrt{\frac{3g}{4R}} \tag{4-7}$$

Eq. 4-6 applies till $\theta(0)=0$, a condition that is reached at $t=\frac{T}{4}$, and the $\frac{T}{4}$ quantity expresses the quarter period of free rocking motion which is estimated from Eq. 4-8.

$$\frac{T}{4}=\frac{1}{p}\cosh^{-1}\left(\frac{1}{1-\theta_o/a}\right) \tag{4-8}$$

At the point of $\theta(0)=0$, the free rocking block reaches its peak velocity and consequently dissipates part of its energy content through the impact with the base. The parameter that associates the impact dissipation with the impact approaching velocity is the coefficient of restitution, *r* (designated as COR), which is an aspect ratio dependent variable, as shown in Eq. 4-9.

$$r=\left[1-\frac{MR^2}{I_o}(1-\cos(2a))\right]^2 \tag{4-9}$$

As explained by Housner, Eq. 4-9 was derived by equating the moment of momentum just before an impact to the moment of momentum just after the impact about the rotation center after the impact. At the end of an impact, free rocking motion continues with respect to the opposite bottom corner, while the source of energy dissipation during the entire free rocking motion is the impact mechanism expressed through COR.

4.2.2 Controlled rocking

Controlled rocking is designated as the rocking motion of a block supplemented with a re-centering mechanism produced by an unbonded strand connecting the top edge of the block with the underlying base, as shown in Figure 4-2. Following Housner's assumptions, the original SRM can be modified to account for this re-centering effect induced by an unbonded post-tensioned (PT) strand. The controlled rocking block of Figure 4-2 is supplemented with

a force comprised of two components: (1) one is due to the initial prestressing force (designated as F_{PT}); and (2) a second is due to the added force produced by the elongation of the strand, when $\theta(t) \neq 0$ (designated as F_{el}). For small angular displacements for which the vector of the total re-centering force can be approximately oriented along the centerline of the rocking block, F_{el} can be estimated as,

$$F_{el} = kbS(\theta)\theta \tag{4-10}$$

where k is the axial stiffness of the PT strand.

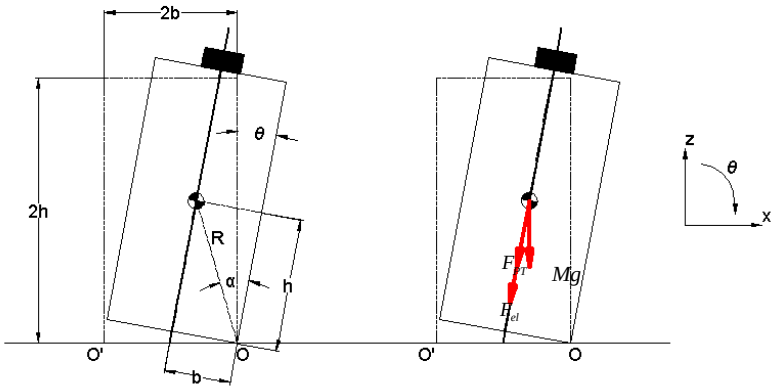

Figure 4-2. A controlled rocking block

For $\theta(t) \geq 0$, the linearized form for the equation of controlled rocking motion may be expressed as,

$$I_o\ddot{\theta} + MgR(\alpha - \theta) + F_{PT}b + kb^2\theta = 0 \tag{4-11}$$

Assuming that $kb^2 \geq MgR$ and for the initial conditions of $\theta(0) = \theta_o$ and $\dot{\theta}(0) = 0$, equation for $\theta(t)$ becomes,

$$\theta(t) = -\frac{\beta}{p_c^{\,2}} + (\theta_o + \frac{\beta}{p_c^{\,2}})\cos p_c t \tag{4-12}$$

Where

$$\beta = \frac{MgR\alpha + F_{PT}b}{I_o} \tag{4-13}$$

And

$$p_c = \sqrt{\frac{kb^2 - MgR}{I_o}} \tag{4-14}$$

p_c expresses the *dynamic parameter* of the rigid block in its controlled rocking motion. The quarter period of controlled rocking motion which starts with the initial conditions of $\theta(0) = \theta_o$ and $\dot{\theta}(0) = 0$ may be described by Eq. 4-15.

$$\frac{T}{4} = \frac{1}{p_c}\cos^{-1}\left(\frac{\beta}{\beta + \theta_o {p_c}^2}\right) \tag{4-15}$$

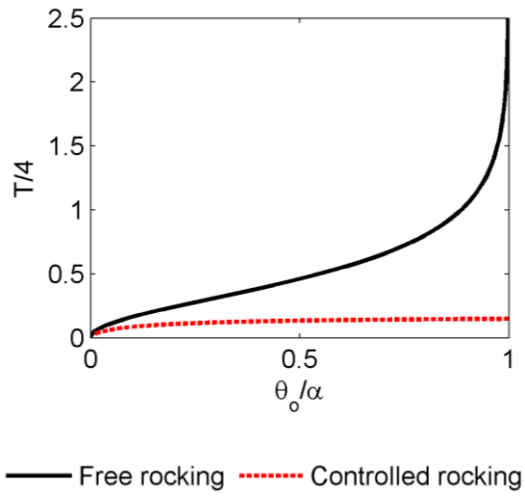

Figure 4-3. Typical behavior of the free and controlled rocking quarter periods

Figure 4-3 shows that the natural quarter period in a controlled rocking system as defined in Eq. 4-15 is dependent on the initial angular displacement uplift. However, when compared with natural quarter period in free rocking motion, the influence of angular

displacement uplift is estimated to be less significant. In controlled rocking motion, the associated quarter period is more dependent on the re-centering force applied through the PT strand, an effect which is specifically expressed through the controlled rocking dynamic parameter, p_c and the constant, β, in Eq. 4-15.

Now, assuming a controlled rocking system with geometric properties of $R = 40$ in and $\alpha = 10.1^o$, $M = 9.3$ lb-s^2/in and a PT strand with $k = 35$ k/in, Figure 4-4 presents the variation of its natural quarter period with respect to different levels of initial prestressing force applied to the PT strand. It is seen that changes in this variable would influence the quarter period of the system most significantly in the region of small θ_o / α ratios (i.e. $\theta_o / \alpha < 0.5$). On the other hand, considering a controlled rocking system with the aforementioned geometric and mass properties, and $F_{PT} = 5$ k, Figure 4-5 shows the variation of natural quarter period with respect to changes in axial stiffness of the PT strand. Interestingly, variation of this parameter, which is critical in estimation of p_c, would influence the quarter period in controlled rocking mostly within the window of higher θ_o / α ratios (i.e. $\theta_o / \alpha > 0.5$).

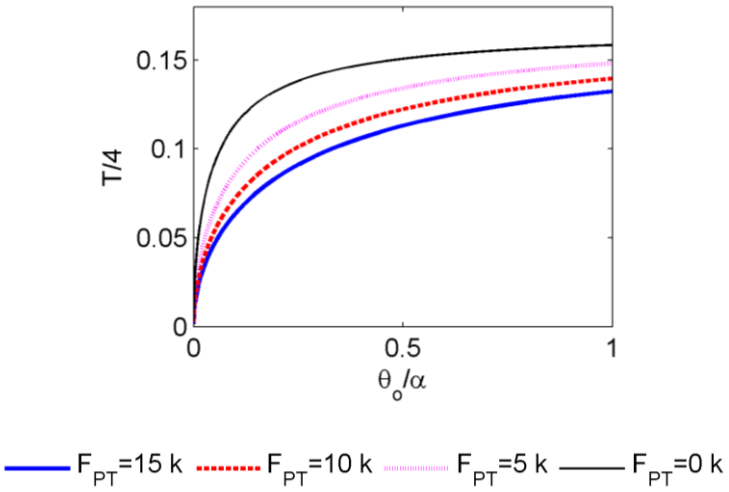

Figure 4-4. Variation of $\frac{T}{4}$ with respect to F_{PT}

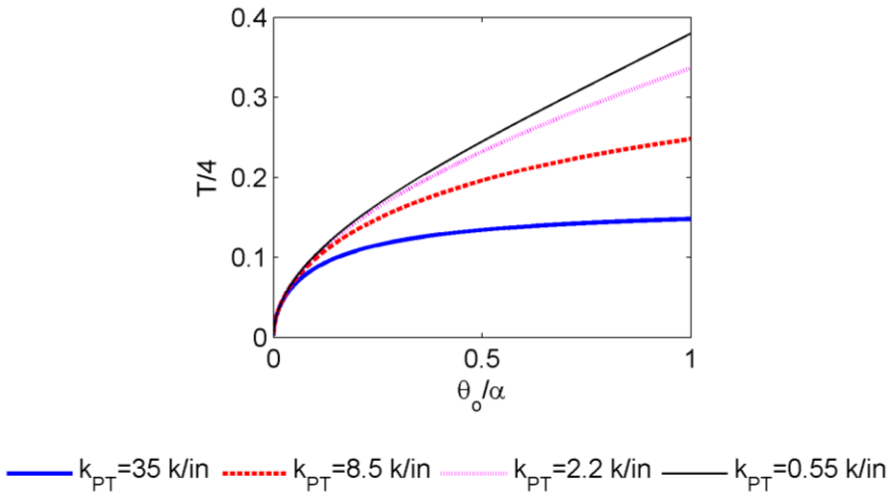

Figure 4-5. Variation of $\frac{T}{4}$ with respect to k (k is designated as k_{PT})

As far as decay of motion in controlled rocking is concerned, energy dissipation at the impact can be similarly described by COR of Eq. 3-9.

The simple rocking model adjusted to account for controlled rocking (designated as SRM-CR) was used herein to compare with experimental and finite element analyses (FEA) results of precast concrete units subjected to controlled rocking motion under free vibration.

Accordingly, these comparisons were used to examine the capacity of SRM-CR to estimate an actual controlled rocking response and subsequently suggest methods to appropriately reform this approach.

4.3 Background

The first steps towards a comprehensive modeling of free rocking motion are attributed to Housner (1963); however, alternative modeling approaches were later developed by several researchers. Chopra and Yim (1985) introduced three SDOF models for simulating the response of a structural system free to rock on the soil under horizontal ground excitation: (1) assuming a rigid rocking interface; (2) rocking interface was modeled as two vertical spring-dashpot elements located at the two bottom corners of the free rocking system; and (3) rocking interface was modeled as distributed vertical spring-dashpot elements along the bottom edge of the free rocking system, designated as Winkler Foundation model. Depending on the structural system's and underlying soil's flexibility characteristics, the most suitable of these modeling approaches may be used for estimating its seismic performance, given the system would be able to enter free rocking motion under earthquake load. Chatzis and Smyth (2012) extended the understanding on behavior of free-standing blocks rocking on a flexible foundation. The foundation was modeled with vertical spring-dashpot elements in two ways: (1) spring-dashpots were located at the bottom corners of the rocking block; and (2) spring-dashpots were used to formulate a Winkler Foundation model. In addition, these rocking models incorporated geometric nonlinearities, uplift and shear sliding effects, assumed to influence free-standing blocks' motions under base

excitation. It was concluded selection of the stiffness and damping properties of the spring-dashpots, as well as coefficient of static friction is critical to their responses.

The introduction of unbonded post-tensioning mechanisms in rocking systems has altered their dynamic characteristics and increased their re-centering capacity. Behavior of these systems under earthquake load was investigated in the Precast Seismic Structural Systems (PRESSS) research program by experimentally testing the response of a precast joint wall as part of a five story precast concrete building (Priestley et al, 1999). The wall was successfully tested up to lateral drift levels much higher than the design level (Zone 4), while experiencing insignificant damage and exhibiting sufficient self-centering capacity.

Following the promising experimental results of the PRESSS research program, the controlled rocking mechanism was implemented for creating innovative design solutions in the realm of seismic-resisting structural systems. After the experimental phase of the PRESSS research program, Stanton and Nakaki (2002) proposed guidelines for designing precast joint wall systems for seismic resistance. Even though these systems exhibited acceptable performance during experimental testing, they were considered uneconomical for use in design practice. This issue was successfully addressed by Aaleti and Sritharan (2007) who introduced a cost-effective precast wall system designated as the PreWEC system. PreWEC consisted of one or more controlled rocking precast walls which were connected with end columns by using special connectors, also operating as energy dissipating mechanisms.

Analytical modeling of controlled rocking motion under base excitation was conducted by Dimentberg et al. (1993) who suggested controlled rocking rigid blocks are less vulnerable to overturning compared to free rocking blocks. By conducting numerical

investigations, Makris and Zhang (2001) extended the understanding on stability of controlled rocking of rigid blocks showing there is a frequency window of horizontal pulse excitations where free rocking blocks are more stable.

Alternative methods for modeling controlled rocking were discussed by Belleri et al. (2013) who employed finite analyses techniques with (1)one; (2) two; and (3) three dimensional elements which were all given nonlinear material properties based on Mander's model (Mander et al. 1988) combined with material damping definitions which used the Rayleigh damping model.

Modeling of energy dissipation due to controlled rocking motion of concrete walls was investigated by O'Hagan et al. (2013) who tested three different damping models: (1) Coefficient of Restitution (COR); (2) Equivalent Viscous Damping (EVD); and (3) Coulomb Friction (CF). This research study suggested the use of a combination of (1) COR with CF; or (2) EVD with CF is necessary to ensure accurate estimation of a controlled rocking response under free vibration. However, the source of CF was not experimentally justified, while it was necessary to empirically adjust the COR and EVD parameters to produce a good fit with the experimental response.

Experimental work on controlled rocking motion was conducted by Cheng (2007) who investigated the effects of (1) aspect ratio and size of the rocking unit; (2) area of anchored steel; and (3) rocking interface materials. It was demonstrated that damping due to controlled rocking increases with increase in the area of anchored steel and decreases with increase in the aspect ratio. Ma (2009) extended the understanding on controlled rocking motion through an experimental study on a post-tensioned masonry wall (PCM). Ma showed that accurately estimating the location of the rotation center during rocking motion is of

critical importance for predicting the "natural" quarter period in controlled rocking motion of the PCM under free vibration. In addition, controlled rocking energy dissipation was shown to occur smoothly in the window of very small angular displacements; in contrast to free rocking where energy dissipation was shown to take place abruptly and during the impact.

4.4 Research Significance

The addition of a self-centering mechanism to the original free rocking concrete system has introduced controlled rocking as an attractive technology for seismic applications. Accordingly, novel design solutions have been proposed for the use of controlled rocking in practice by creating seismic-resisting systems able to sustain earthquake excitations with minimal damage. The limited knowledge on the ability of a simple controlled rocking concrete system to inherently dissipate energy during its dynamic motion has led researchers to supplement their controlled rocking models with additional hysteretic damping mechanisms which can ensure the required amount of energy dissipation under an earthquake load.

Given that the published literature has not concluded in a concrete methodology to quantify dynamic decay of motion in controlled rocking systems, implementing this parameter in the design procedures remains an unsolved problem. This study aimed at characterizing decay of motion in controlled rocking concrete systems based on their free vibration responses. By conducting experimental and analytical investigations on geometrically discrete controlled rocking concrete members, the goals of this study were to (1) conclude in a simple methodology which can provide a minimum amount of energy dissipation per impact given the level of lateral displacement peak reached by the controlled

rocking system; and (2) verify the capacity of an earlier proposed finite element technique for modeling controlled rocking (APPENDIX). Given these goals, this study may extend the current understanding on controlled rocking towards creating cost-effective seismic structural systems which make use of the minimum required hysteretic energy dissipation.

4.5 Experimental Investigation

4.5.1 Testing scheme

Figure 4-6 presents the two discrete precast concrete units, which were subjected to controlled rocking motion under free vibration. The experimental work took place in the structural laboratory at Iowa State University. The main feature of the two units was a 14x14x60 (width x length x height) cubic inches reinforced concrete column. The column was connected with a reinforced concrete mass with dimensions of 50x50x12 (width x length x height) cubic inches. As shown in Figure 4-7, the concrete mass consisted of two identical parts which were firmly attached on the column to create the complete rocking unit. The first rocking system (*Rocking System 1*) was constructed by locating the center of gravity of the concrete mass 23 ½ inches lower from the top edge of the column. To construct *Rocking System 2*, the concrete mass was attached at the top of the column.

The two systems were subjected to controlled rocking motion on a 1 inch thick grout layer which was casted on a 24x24x24 cubic inches flat concrete foundation. The rocking column's bottom sides were surrounded by a ½ an inch high grout (1 ½ total grout height). A pump (power team electric hydraulic pump-double acting PE554S) and a hydraulic jack (power team 55 ton hydraulic 13"-double acting cylinder RD5513) were used to apply the initial top lateral displacement to the rocking units and the initial prestressing force to the

unbonded post-tensioned seven-wire strand (Grade 270), which was used to create the connection between the top edge of the rocking units and the foundation underneath.

4.5.2 Initial conditions of free vibration

Several levels of initial prestressing force were applied to the two controlled rocking units in order to investigate the effect of this parameter on the decay of controlled rocking motion. Table 4-1 presents the levels of initial prestressing force used as to what was deemed necessary to appropriately evaluate the F_{PT} influence in dynamic energy dissipation. The total prestressing force, F_T ($F_T = F_{el} + F_{PT}$), was monitored throughout the duration of all experimental tests showing negligible F_{PT} losses from the beginning to the end of the free vibrations. The two units were excited with 1%, 2% and 3% initial top lateral drifts (ITLD) in all cases of F_{PT}.

Table 4-1. Levels of initial prestressing force applied to *Rocking Systems 1* and *2* for the free vibration tests

Levels of F_{PT} for *Rocking System 1*, kips	0.18	5.5	9	10.85
Levels of F_{PT} for *Rocking System 2*, kips	0.8	2.2	6.8	

4.5.3 Instrumentation

Two string pots acting in the horizontal direction were attached on the rocking column to ensure the desired ITLD for each of the free vibration tests. Analysis of the experimental results was based on experimental data extracted from a group of light emitting diodes (LED). As the value of the available sampling frequency used by the acquisition

system decreases with increase in the number of the LED sensors employed for a test run, the testing process was divided into two phases to ensure appropriate monitoring of the controlled rocking response with an effective combination of sampling frequency and number of LED sensors. Accordingly, (1) in the first phase, four LED sensors were attached on the top of the column to ensure linear displacement data with a minimum noise intrusion; and (2) in the second phase, four LED sensors were imposed along the bottom edge of the rocking column to provide displacement data for determining the dynamic neutral axis response.

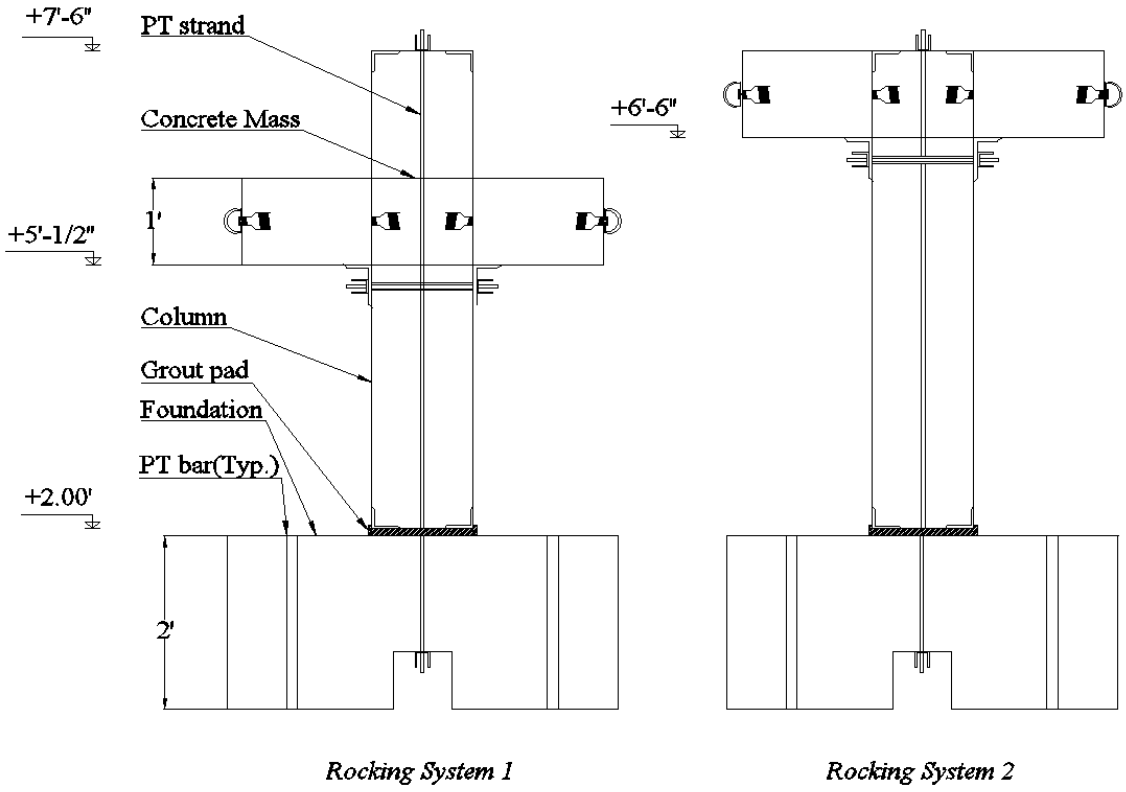

Figure 3-6. The two rocking systems subjected to controlled rocking motion under free vibration

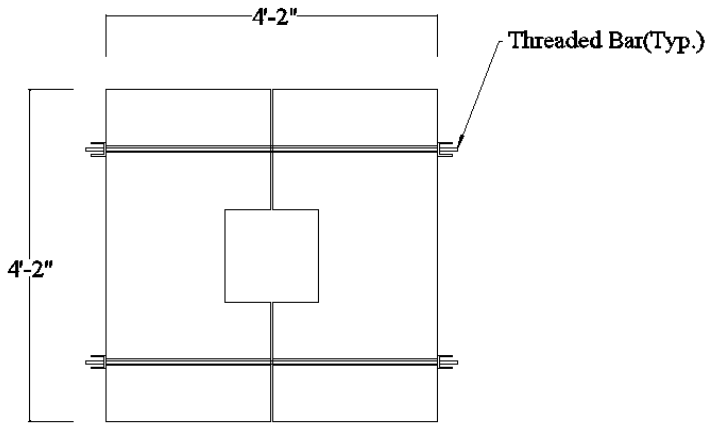

Figure 3-7. Top view of the concrete mass

4.6 Finite Element Modeling

The finite element analysis (FEA) technique presented in APPENDIX was used to simulate the controlled rocking response of the two systems under free vibration. Two FE rocking models were similarly created to simulate the responses of *Rocking Systems 1* and *2*, as shown in Figure 4-8. These models used the same Rayleigh damping model parameters as was suggested in the original study (Table 4-2). *FE Rocking model 1* was simulated for an initial prestressing force of 5.5 kips and *FE Rocking System 2* was simulated for an initial prestressing force of 2.2 kips. Note that the experimental and FEA results of *Rocking System 2* with an initial prestressing force of 6.8 kips have already been presented in the aforementioned study. Six simulations were executed during this study to estimate controlled rocking responses for 1%, 2% and 3% ITLDs for each system. The linear displacement time histories were collected with a sampling frequency of 2,000 Hz.

FE Rocking Model 1 *FE Rocking Model 2*

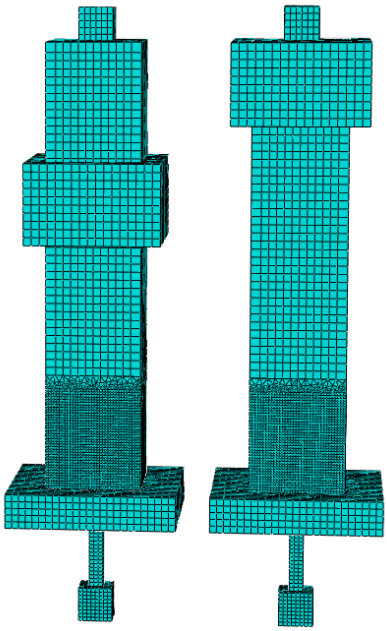

Figure 4-8. The two FE models used to simulate the controlled rocking responses of *Rocking Systems 1* and *2*

Table 4-2. The Rayleigh damping model coefficients used to define the material damping properties in the *FE Rocking Models 1* and *2*

FE Rocking Model	1% initial lateral drift	2% initial lateral drift	3% initial lateral drift
1	ALPHA=0.9, BETA=0	ALPHA=0.5, BETA=0	ALPHA=0.5, BETA=0
2	ALPHA=0.9, BETA=0	ALPHA=0.5, BETA=0	ALPHA=0.5, BETA=0

4.7 Comparison of Results

This section presents the experimental results of controlled rocking responses for *Rocking Systems 1* and *2*. Comparison of these results with free rocking motion, and the FEA and SRM-CR simulations for an initial prestressing force of 5.5 kips – *Rocking System 1* – and 2.2 kips – *Rocking System 2* are also included herein.

4.7.1 Free and controlled rocking motion

Figure 4-9 demonstrates a typical comparison between free and controlled rocking responses of a concrete member. Looking at their angular displacement time histories, it can be inferred that controlled rocking motion is characterized by a shorter natural quarter period and the decrease in the controlled rocking $\frac{T}{4}$ is not necessarily followed by an equivalent increase in the amount of energy dissipation per cycle; conversely, controlled rocking exhibits a smaller drop in its angular displacement peaks per cycle compared to the respective free rocking motion. These observations may define two fundamental differences between controlled and free rocking of concrete members.

The angular velocity time histories in Figure 4-9 show the controlled rocking member experiences higher levels of velocity amplitude during an impact, due to the prestressing effect. Discrete trends are also demonstrated for the two angular acceleration responses where controlled rocking response presents higher values during the continuous phase of its motion and a sinusoidal type of oscillation primarily due to the F_{el} response which is dependent on the angular displacement response, according to Eq. 4-10; however, nonlinear discontinuities occur in both free and controlled rocking during the impact phase of their motion.

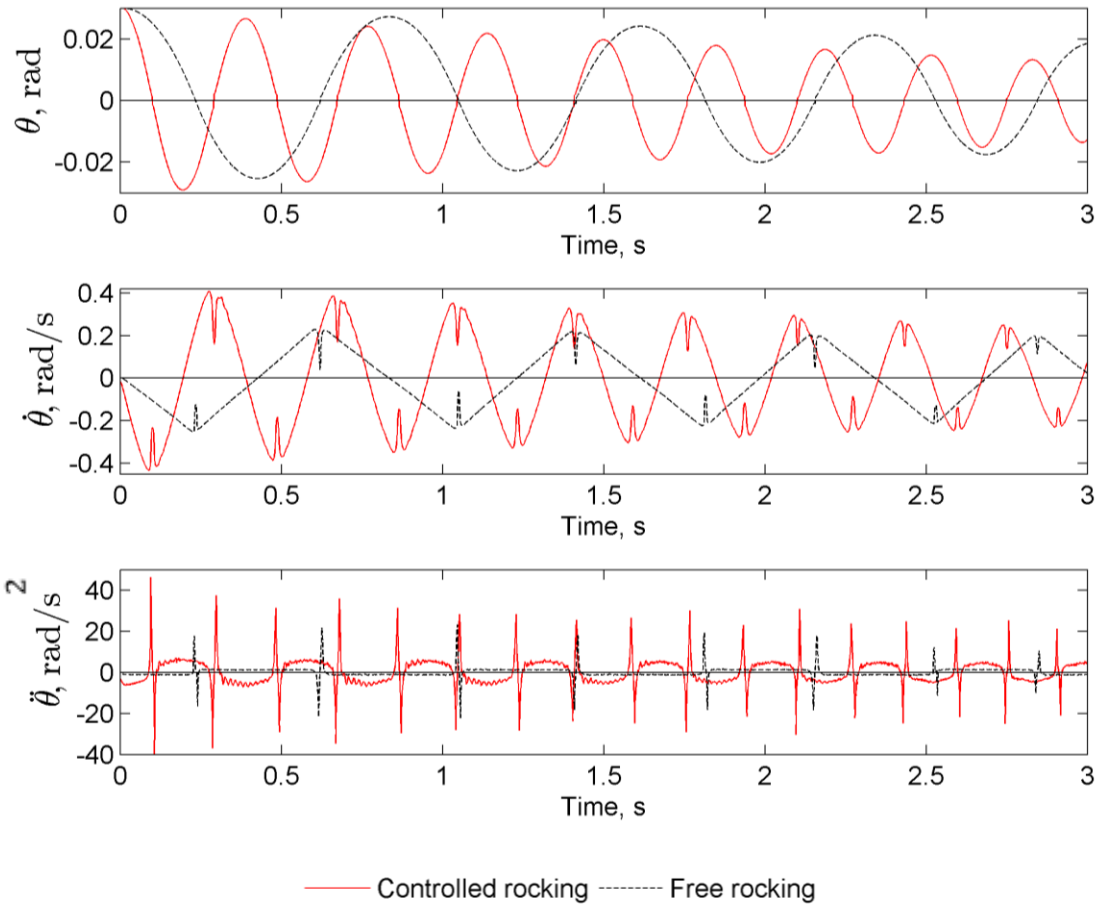

Figure 4-9. Experimental angular displacement, velocity and acceleration time histories for controlled and free rocking motion; *Rocking System 1*

4.7.2 Quarter period in controlled rocking

Accurate estimation of the natural quarter period in controlled rocking structural systems is of paramount importance for predicting their dynamic response. The SRM-CR is employed to investigate its ability in appropriately estimating this parameter. The properties of the two controlled rocking systems as used in SRM-CR simulations are presented in Table 4-3.

Table 4-3. Geometric, mass and impact energy dissipation properties of the two rocking systems as used in the SRM-CR simulations. COR was estimated from equation (4-9)

Rocking System	Total Mass, $k-s^2/in$	Moment of Inertia *Io*, $k-s^2-in$	R, *in*	Aspect ratio, α	Xcg, *in*	COR, *r*
1	0.0093	17.43	39.97	0.176	39.35	0.898
2	0.0093	28.49	51.53	0.136	51.05	0.937

A typical comparison between experimental and SRM-CR displacement time histories is presented in Figure 4-10, showing that the use of COR originally proposed by Housner to simulate impact energy dissipation in a free rocking block can lead to overestimation of the actual controlled rocking decay of motion. Furthermore, the SRM-CR simulation predicts a significantly shorter quarter period for controlled rocking motion as it can be clearly discerned by specifically comparing the first quarter cycles of the two angular displacement time histories.

Since $\frac{T}{4}$ has been shown to be strongly dependent on the magnitude of the total prestressing force applied to a controlled rocking structure, this discrepancy may be construed as an overestimation of the F_{el} component dependent on the PT strand elongation. An error in the F_{el} estimation can take place by assuming a rigid body motion which oscillates with respect to a constant rotation center (RC) – the bottom corner of the rocking body. In reality, RC may move along the rocking bottom edge with respect to the rocking angular displacement (Ma 2009). Consequently, the RC motion can influence the level of elongation of the PT strand. In order to determine the actual F_{el}, displacement data from the second experimental phase were used to investigate the experimental dynamic neutral axis (NA) response associated with the dynamic behavior of the rocking column's bottom edge.

The first graph in Figure 4-11 demonstrates that a structural system subjected to controlled rocking oscillates having a portion of its bottom edge under compression (i.e. indicated as the displaced portion of the rocking bottom edge which is negative in sign), while rocking motion takes place with respect to a RC which remains essentially constant during the most part and is shown to be located approximately in the middle of the compressed portion of the bottom edge. When the rocking system reaches a smaller angular displacement, RC starts to immigrate towards the opposite side of the bottom edge.

The first graph in Figure 4-11 also indicates that the decompression point of the bottom edge, which is apparently a different point than its RC, is moving towards the center of the bottom edge as angular displacement decreases. This motion of the decompression point is clearly demonstrated in the second graph of Figure 4-11 which presents the variation of the neutral axis depth with respect to angular displacement. Neutral axis reaches its minimum value at the angular displacement peak and is smoothly increasing till it reaches the total length of the bottom edge, which is when the rocking body completes its dynamic motion corresponding to a quarter cycle time period.

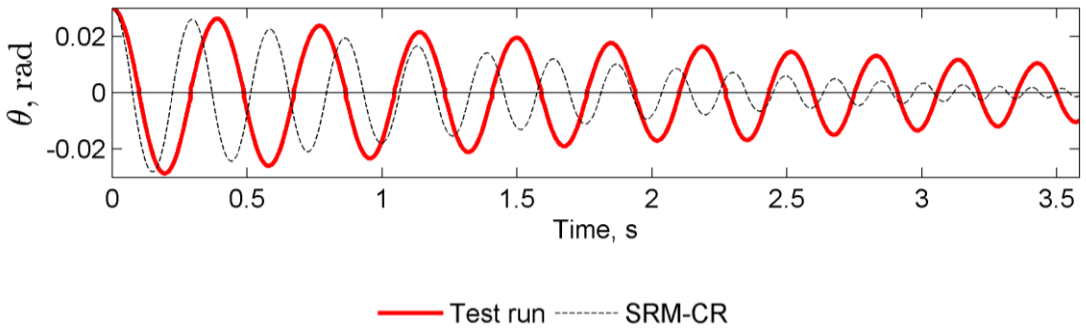

Figure 4-10. Typical experimental and SRM-CR displacement time histories of *Rocking System 1*

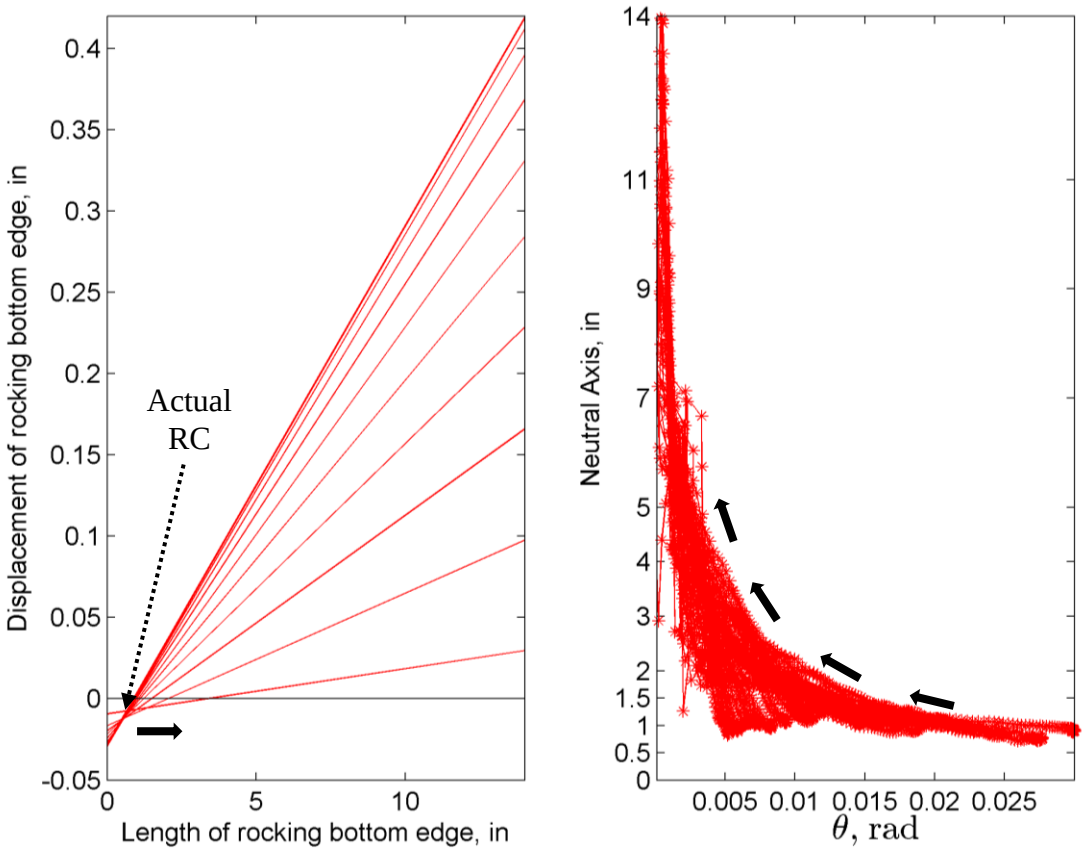

Figure 4-11. Neutral axis response in controlled rocking motion of *Rocking System 1*

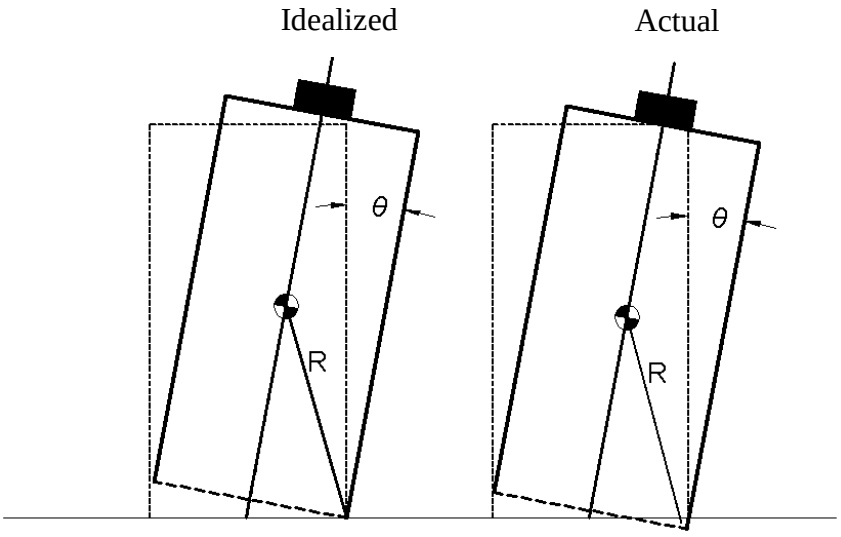

Figure 4-12. Representation of the (1) idealized; and (2) actual behavior of the controlled rocking bottom edge

In order to deal with this problematic aspect of the SRM-CR and being able to accurately estimate the actual elongation of the strand and the controlled rocking quarter period, the original SRM-CR is modified by empirically applying a reduction coefficient, r_{PT}, to the theoretically estimated elongation of the PT strand, which is critical for calculating F_{el}, as seen in Eq. 4-10. It was experimentally found that this simple method for calculating the PT strand elongation can provide a significantly improved estimation for both the actual total prestressing force and natural quarter period of the two controlled rocking systems expressed as functions of angular displacement. Typical comparisons of these relationships between the experimental, SRM-CR and modified SRM-CR simulation results are presented in Figures 4-13 and 4-14 for *Rocking Systems 1* and *2*; while the improved estimation of the quarter period is also demonstrated in Figure 4-15 through the typical angular displacement time histories.

$$x = r_{PT} b\theta \tag{4-16}$$

$$F_{el} = kxS(\theta) \tag{4-17}$$

Where x is the elongation of the PT strand.

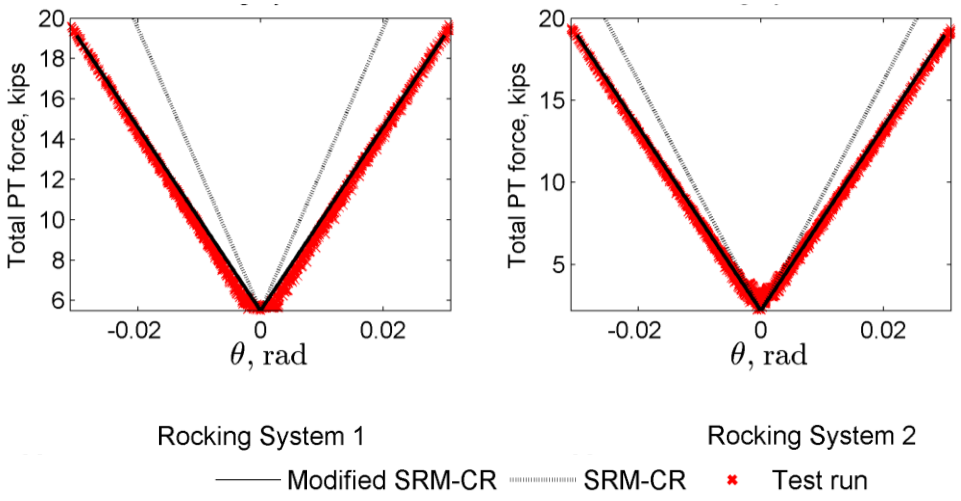

Figure 4-13. Typical comparisons between the modified SRM-CR, SRM-CR simulations and experimental total prestressing forces with F_{PT} = 5.5 kips – *Rocking System 1* – and F_{PT} = 2.2 kips – *Rocking System 2* –with respect to angular displacement

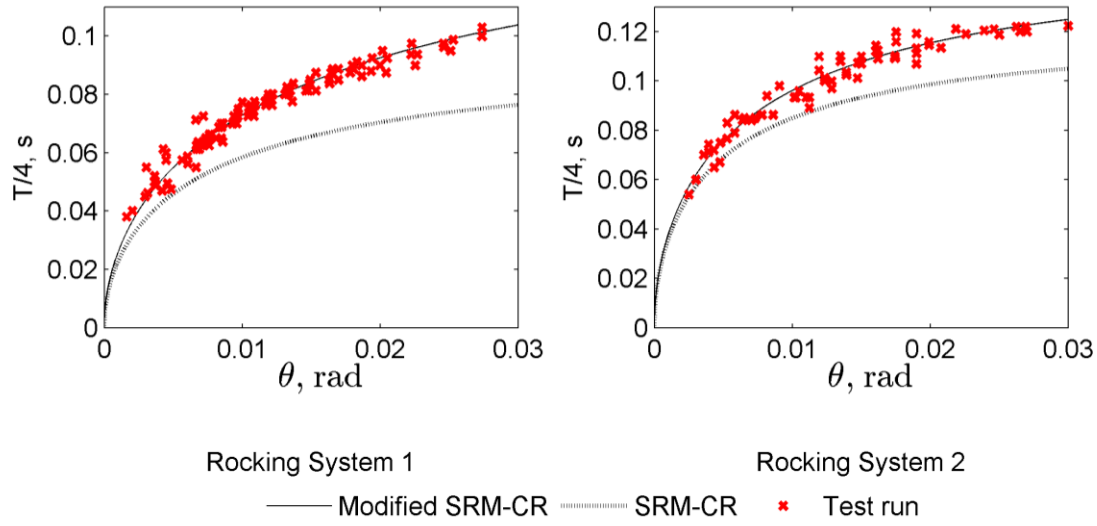

Figure 4-14. Typical comparisons between the modified SRM-CR, SRM-CR simulations and experimental quarter periods with F_{PT} = 5.5 kips – *Rocking System 1* – and F_{PT} = 2.2 kips – *Rocking System 2* – with respect to angular displacement peaks

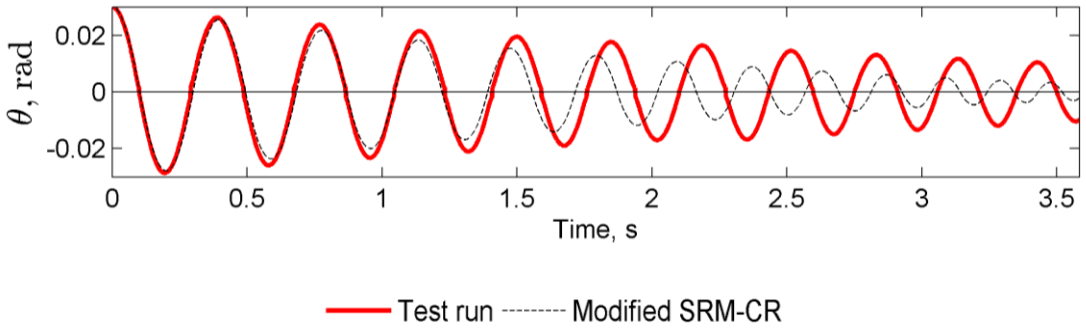

Figure 4-15. Typical experimental and modified SRM-CR displacement time histories

Next, the variation of the aforementioned reduction coefficient, designated as r_{PT}, with respect to the initial prestressing force was examined. Figure 4-16 presents the empirically determined, r_{PT} values which may be adopted for an acceptable estimation of the controlled rocking quarter periods in all F_{PT} cases used in the experimental investigation for the two controlled rocking units. It is shown that a significant reduction should be applied in the idealized PT strand elongation, which is higher for *Rocking System 1*. As it might be

expected, it was also found that r_{PT} should decrease with increase in the initial prestressing force applied to a controlled rocking unit.

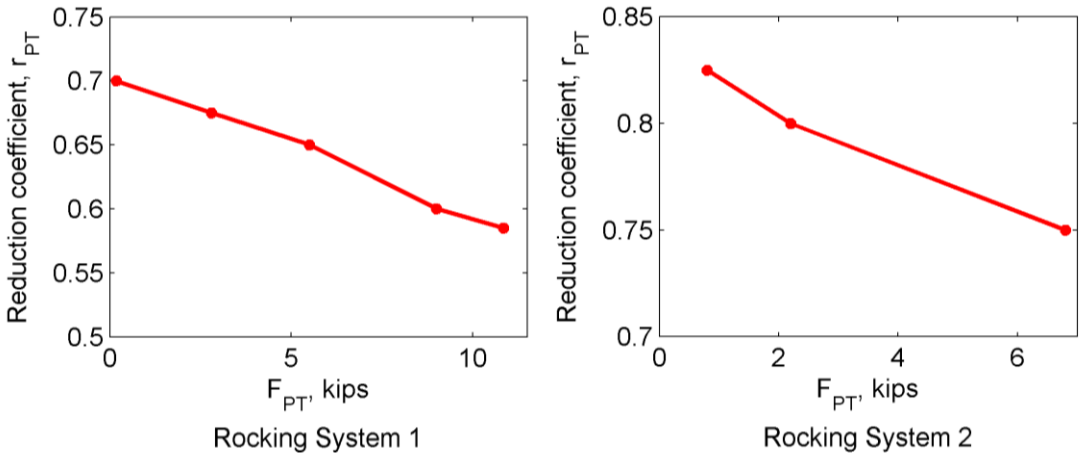

Figure 4-16. The empirically determined reduction coefficient, r_{PT} in comparison with the initial prestressing force

4.7.3 Angular displacement responses

It was previously explained that accurate modeling of controlled rocking is tied up with the accurate estimation of the dynamic energy dissipation and "natural" quarter period. As a simple method for adequately capturing the latter has already been presented, this section makes use of the modified SRM-CR for a comparison with experimental and FEA angular displacement responses mainly focusing on the energy dissipation characteristics of controlled rocking motion. Angular displacement responses are presented for free vibration excitations with 1%, 2% and 3% ITLDs. In particular, the free vibration responses with F_{PT} = 5.5 kips is presented for *Rocking System 1* and F_{PT} = 2.2 kips for *Rocking System 2*.

Figure 4-17 shows that the FE technique was able to provide an adequate estimation of the free vibration responses of *Rocking System 1*. The FEA results closely follow the

experimental responses, justifying the efficiency of this approach to capture the actual controlled rocking quarter period and the controlled rocking decay of motion. However, the modified SRM-CR grossly overestimated controlled rocking energy dissipation, signifying the need for a different analytical approach for estimating impact energy dissipation in controlled rocking motion.

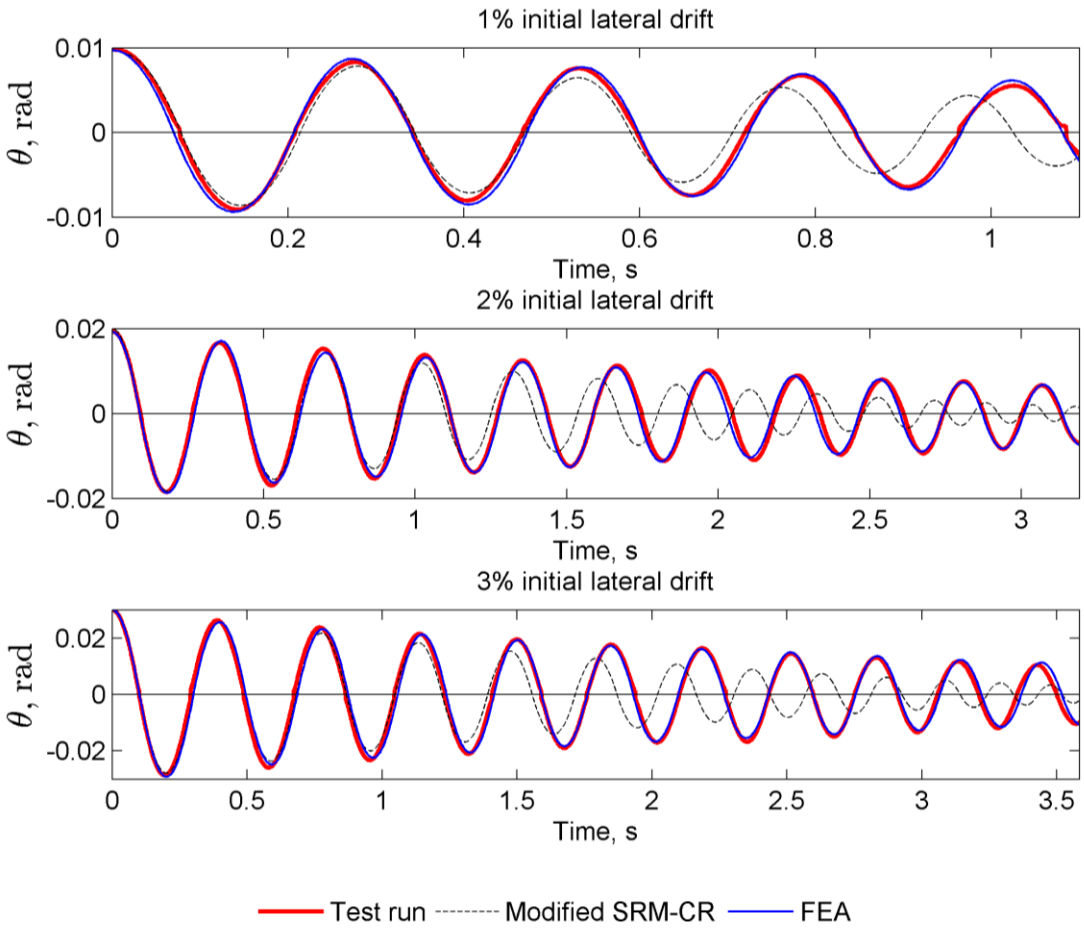

Figure 4-17. Angular displacement responses based on the experimental, modified SRM-CR and FEA results of *Rocking System 1* for F_{PT} = 5.5 kips

As shown in Figure 4-18, FEA provided acceptable estimations for the angular displacement responses of Rocking System 2, meaning that the FE technique originally used for modeling the controlled rocking behavior of *Rocking System 2* with F_{PT} = 6.8 kips

(APPENDIX) could be applicable for a case with different initial prestressing force, without any change in the original Rayleigh damping model.

On the other hand, SRM-CR was able to provide a better estimation for the actual decay of motion in *Rocking System 2* compared to its performance in estimating the displacement responses of *Rocking System 1*. In particular, SRM-CR was more efficient in the 3% ITLD displacement response, while its ability to capture the actual behavior decreased with decrease in the angular displacement peak. Similarly with the trend exhibited in *Rocking System 1*, SRM-CR predicted slightly overestimated energy dissipation.

The results of Figures 4-17 and 4-18 indicate that COR calculated from Eq. 4-9 cannot be safely used for estimating decay of motion in these two controlled rocking systems, as this approach predicted faster decay of the controlled rocking motions; results which did not reflect the actual decay in these units. These findings challenged the investigation of a different approach, more suitable for modeling controlled rocking. The relevant discussion is developed later in this paper.

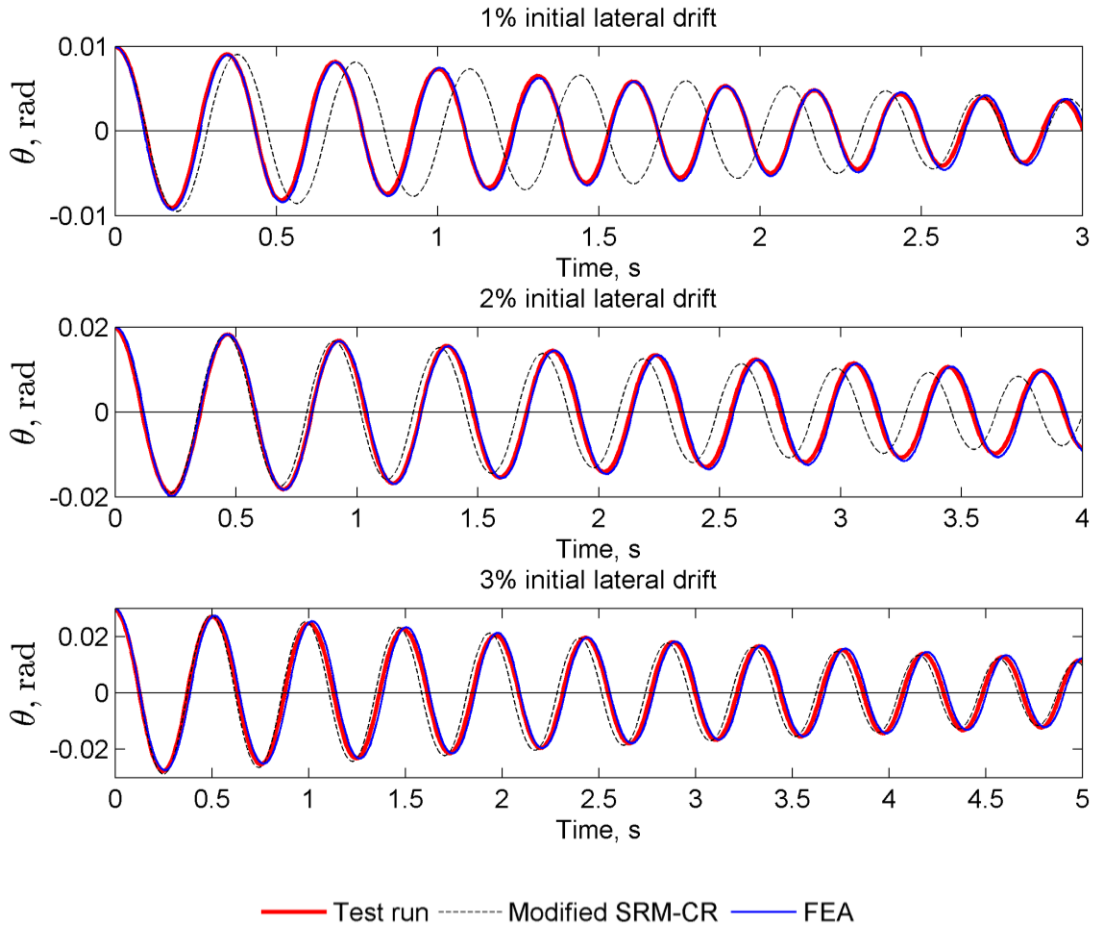

Figure 4-18. Angular displacement responses based on the experimental, modified SRM-CR and FEA results of *Rocking System 2* for F_{PT} = 2.2 kips

4.7.4 Phase diagrams

As a next step, an inspection of the angular velocity versus displacement responses, referred to as phase diagrams, was conducted. Figures 4-19 and 4-20 present the phase diagrams corresponding to *Rocking System 1* and *2*, respectively.

The phase diagrams presented in the above-referenced figures are, in general, characterized by a smooth, continuous motion which is interrupted by a discontinuity, which is typically experienced by a rocking concrete member during the impact (Chapter 3). As it would be expected, the impact phase is characterized by an abrupt velocity drop, a behavior

which is exhibited by both the FE models and experimental units. This aspect of controlled rocking motion constitutes a solid indication for the existence of an impact dissipation mechanism participating in its decay. Accordingly, the two controlled rocking systems exhibit a reduction in their angular velocity after an impact. This trend is adequately followed by both the SRM-CR and FEA simulations, with the FEA giving a noticeably better estimation for the velocity amplitudes before and after an impact.

Figures 4-19 and 4-20 demonstrate that experimental and FEA responses closely follow the continuous and free from energy dissipation paths as predicted by the modified SRM-CR, suggesting that decay of motion in these controlled rocking systems is not specifically influenced by a continuous dissipation mechanism. This result reveals another fundamental difference between the free and controlled rocking responses of these two concrete members, as it has been previously shown that a continuous dissipation mechanism is an integral part of their free rocking behavior (Chapter 3). In contrast, their controlled rocking responses indicate the use of an impact dissipation-based modeling approach for estimating their energy dissipation.

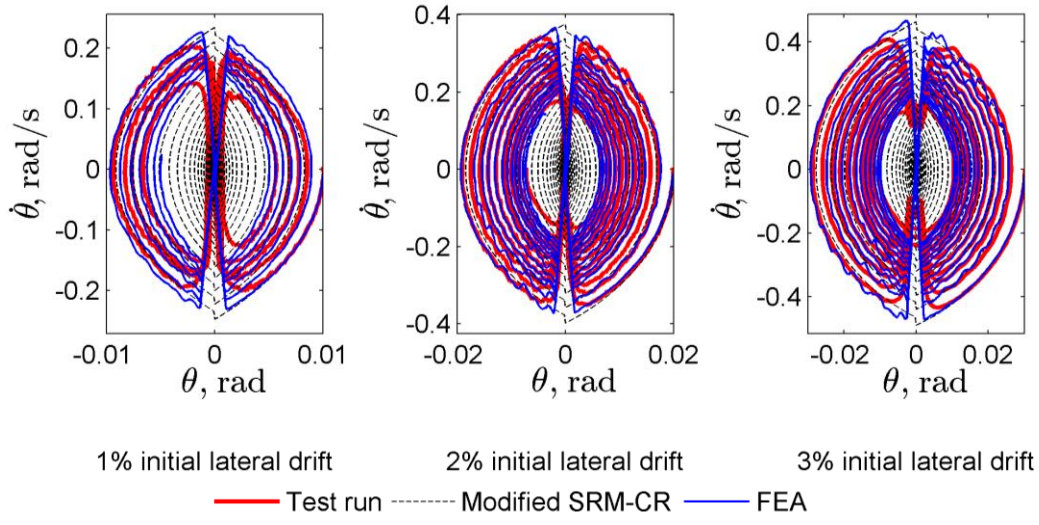

Figure 4-19. Phase diagrams of *Rocking System 1* with F_{PT} = 5.5 kips

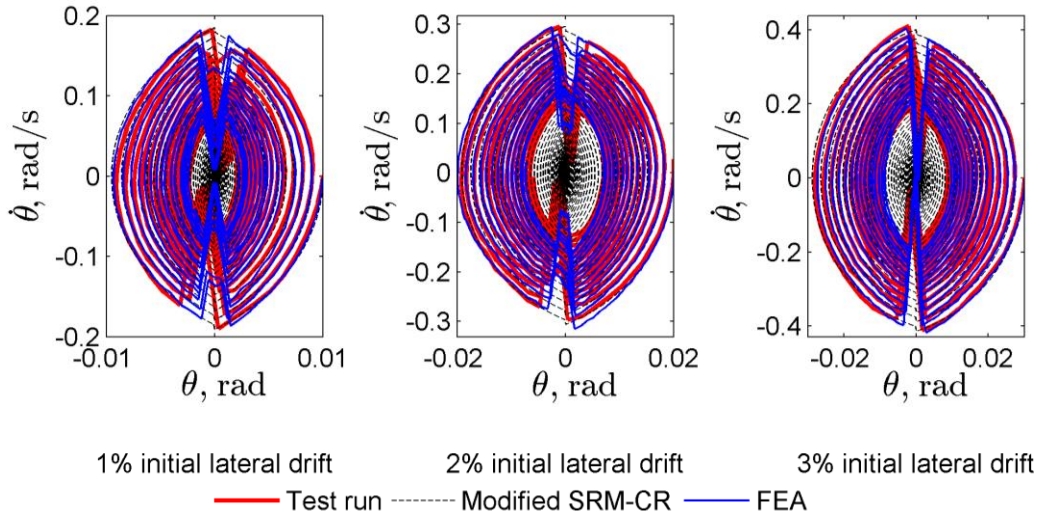

Figure 4-20. Phase diagrams of *Rocking System 2* with F_{PT} = 2.2 kips

4.7.5 Impact energy dissipation

Based on the results presented above, estimation of energy dissipation in the two controlled rocking systems should focus on their dissipation mechanism activated during the impact phase. In order to better understand the trends exhibited by the experimentally identified impact dissipation mechanism, experimental results were compared with theoretical modeling approaches with respect to the impact approaching angular velocities. The free rocking experimental results on impact energy dissipation, as presented in Chapter 3, were also used for comparison with controlled rocking.

Housner's model was initially employed to compare with the experimental results. Two variables were used for this comparison: the amount of energy dissipation per impact, ΔK and the associated COR, r.

For the experimental analyses, both variables were calculated by using the experimental kinetic energy, K, time histories, where kinetic energy responses were estimated from Eq. 4-18, presented below. COR was calculated as the ratio of the kinetic

energy of the rocking system just after the impact over the kinetic energy of the system just before the impact; while ΔK is defined as the absolute value of the difference of these quantities.

$$K = \frac{1}{2} I_o \dot{\theta}^2 \tag{4-18}$$

$$\Delta K = \frac{1}{2} I_o \dot{\theta}^2 (1 - r) \tag{4-19}$$

Figure 4-21 presents the comparison between free and controlled rocking experimental results, and the SRM's estimation for *Rocking System 1* with respect to the impact approaching angular velocities showing there are remarkably different trends between the actual free and controlled rocking impact dissipation mechanisms. As discussed in Chapter 3, experimental COR values in free rocking motion under free vibration with a maximum of 3% angular displacement uplift remain consistently below the SRM's COR for the most part, providing a lower-bound limit for the amount of energy dissipation per impact. In contrast, the experimental dynamic decay due to controlled rocking is characterized by significantly higher COR values, with SRM's COR overestimating the corresponding amounts of energy dissipation per impact for all F_{PT} cases and for $\dot{\theta} \geq 0.1$ rad/s . Given no bouncing of the rocking units occurred during the experimental tests, these results should not be expected if assuming a smooth transition between the before and after impact rocking phases with the rocking system continuing its oscillation after the impact with respect to the opposite RC, e.g. from point O to point O' as shown in Figure 4-2 (Housner 1963; Palmeri and Makris 2008). In other words, conservation of the moment of momentum about point O' – RC after the impact –, as originally used by Housner for determining the amount of energy

dissipation necessary for this smooth transition, may not be applicable to this controlled rocking system.

Alternatively, the second graph in Figure 4-21 presents the amount of energy dissipation per impact as calculated from the experimental analyses of *Rocking System 1*, in comparison with the respective estimations by SRM. A clearer picture of the ΔK - impact approaching $\dot{\theta}$ relationship for the region of higher angular velocities is provided through this graph, while it is similarly shown that the SRM's COR did not provide acceptable estimations for the experimental energy dissipation of *Rocking System 1*.

Looking at the experimental results of Figure 4-21, much higher amounts of energy were dissipated by free rocking motion for the same impact approaching velocities, signifying the two types of rocking motion exhibit differences in their impact dissipation mechanisms.

Regarding experimental controlled rocking motion, there were no noticeable differences in the COR trends between controlled rocking tests with different initial prestressing force values. In general, COR in controlled rocking essentially followed the same path in all F_{PT} cases.

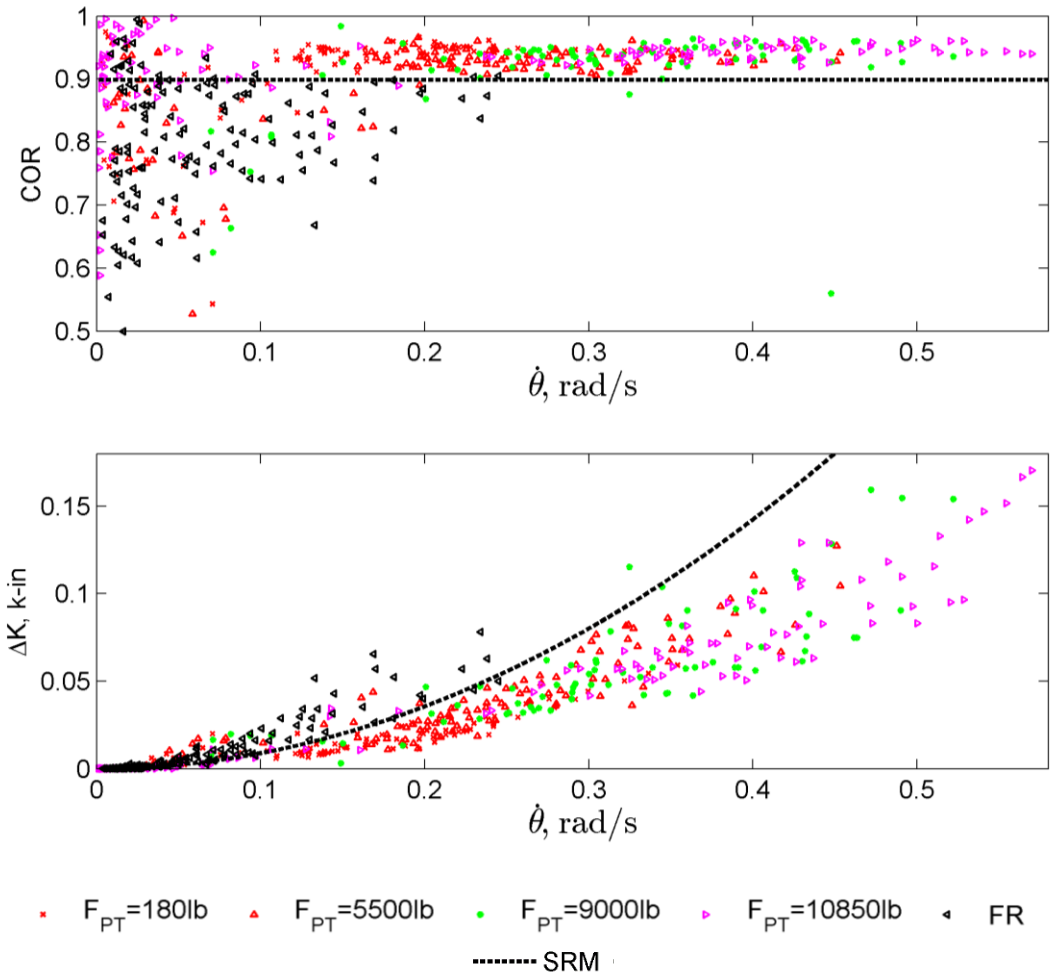

Figure 4-21. Energy dissipation expressed through COR and Δ*K* as functions of the impact approaching angular velocity for *Rocking System 1* under free and controlled rocking motions.

Similarly, *Rocking System 2* experienced higher COR values during its controlled rocking motion compared to its free rocking motion, as shown in Figure 4-22. In general, SRM's COR was unable to effectively predict decay of motion in this controlled rocking system, even though its deviation from the experimental COR values was less pronounce considering the results for *Rocking System 1*. A fair estimation of the actual COR and amount of energy dissipation per impact was achieved in the case of $F_{PT} = 2200\,\text{lb}$, as would be expected following the comparison of the angular displacement responses presented in

Figure 4-18. The experimental r and ΔK results for the case of $F_{PT} = 800\,\text{lb}$ exhibit a significant scatter with the majority of the data points showing a slightly higher energy dissipation compared to the SRM predictions. In contrast, COR for $F_{PT} = 6800\,\text{lb}$ is significantly underestimated by SRM's COR.

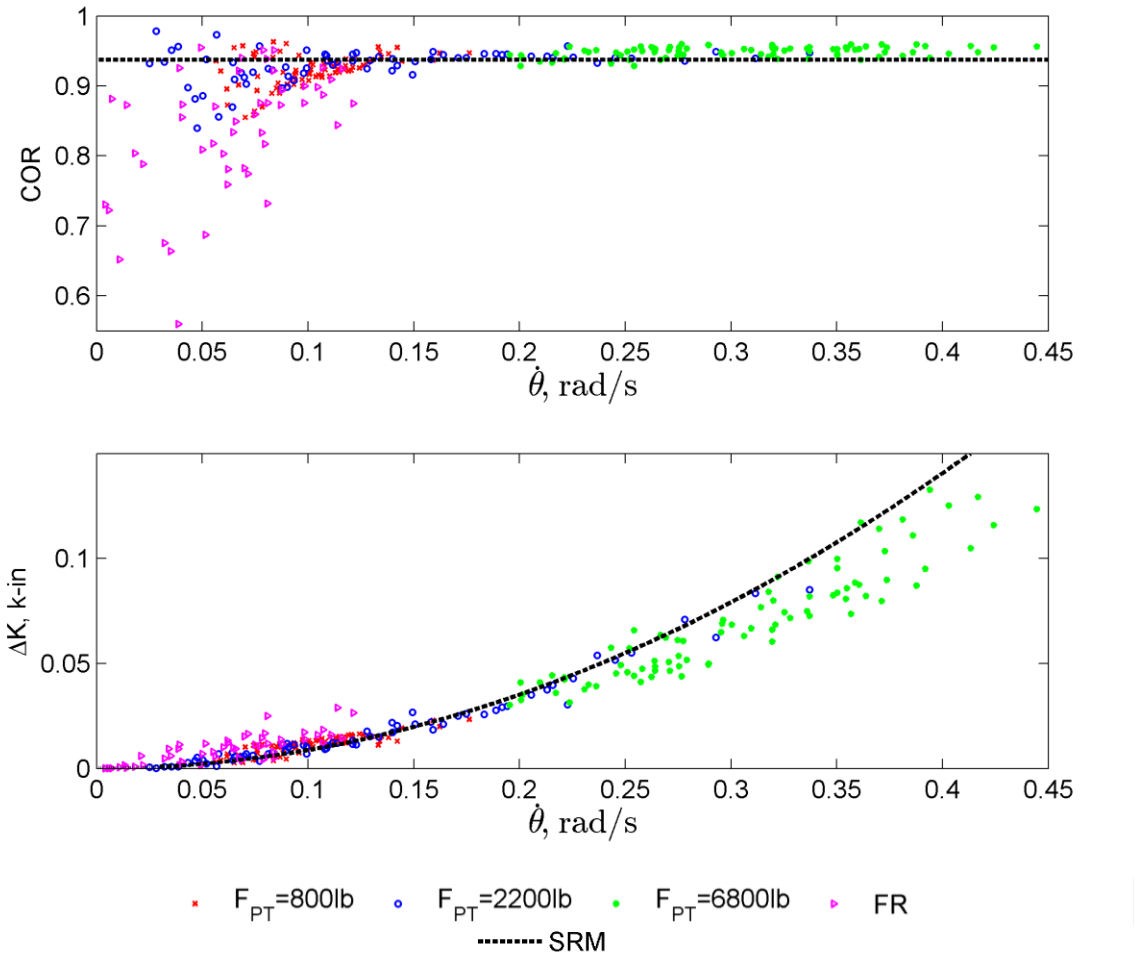

Figure 4-22. Energy dissipation expressed through COR and ΔK as functions of the impact approaching angular velocity for *Rocking System 2* under free and controlled rocking motions.

These results suggest that a safe estimation of the decay of motion in controlled rocking may not be feasible by using the above-referenced approach (SRM's COR), which was originally applied to free rocking motion.

Challenged by the outcome of the experimental investigation in controlled rocking, a new methodology to provide a lower-bound limit for energy dissipation in *Rocking Systems 1* and *2* during their controlled rocking motion was investigated, leading to a simplified approach for estimating COR.

Simplified Approach for COR. Considering COR in free rocking motion was calculated based on the geometric properties of the rocking body, estimation of COR in controlled rocking is assumed to be influenced by the supplemental prestressing force applied at the top of the rocking concrete member and may adopt the conclusion, made in the development of the FE modeling approach for controlled rocking (APPENDIX), that the angular displacement amplitude may influence energy dissipation in controlled rocking.

According to the simplified approach introduced herein, the total prestressing force applied to the rocking system at its angular displacement peak can be visualized as a point mass located at the center of the system's top edge, as shown in Figure 4-23. In order to calculate the COR value associated with the imminent impact event, this point mass is considered part of the geometric configuration and is accounted in re-estimating the "geometric" properties of the controlled rocking system. Using these fictitious "geometric" properties, the original approach proposed by Housner (1963) can be, next, step by step followed to calculate COR. As it would be expected, this approach leads to an increased COR value due to the fictitious "geometric" characteristics corresponding to a slenderer rocking block. Consequently follows that the use of this method suggests a COR which is strongly dependent on the initial prestressing force and the added force due to the strand elongation at the preceded angular displacement amplitude before the impact.

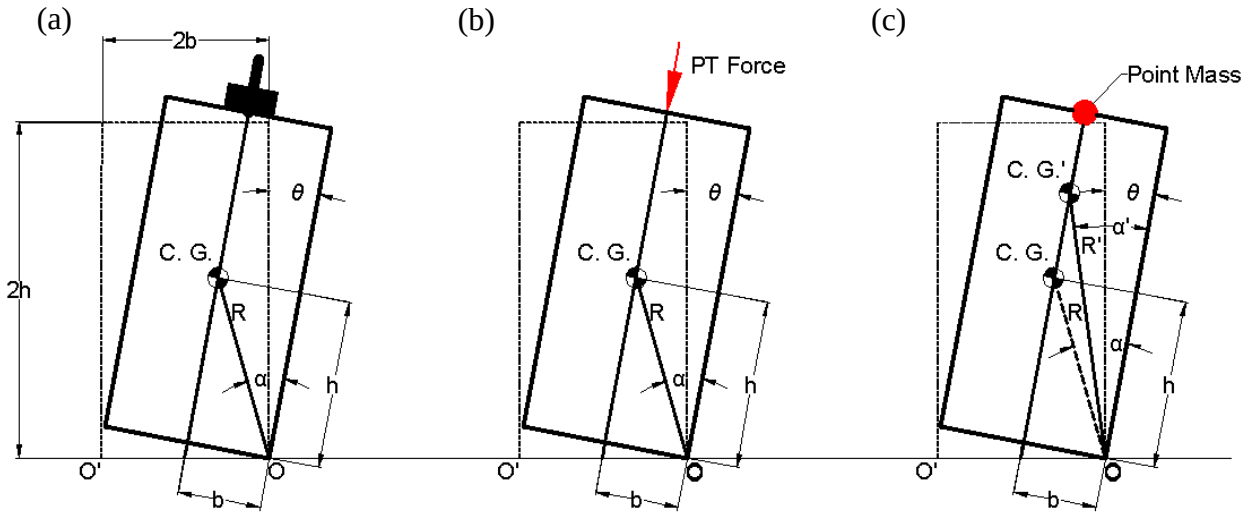

Figure 4-23. A controlled rocking block at its angular displacement peak (a). The total prestressing force is applied at the top of the block where the post-tensioned strand is anchored and it is directed along the centerline of the block for small angular displacements (b). This force is considered as a point mass located at the top of the block and the new "geometric" properties are calculated to estimate the COR value which corresponds to the imminent impact response (c).

This method was implemented to re-estimate the COR and ΔK values for *Rocking Systems 1* and *2*. As it is shown in Figure 4-24, an increase in COR was estimated for the first system which appears to be significantly dependent on the selected F_{PT} value, specifically for $\theta_o \leq 0.2$ rad/s. Respectively, it is indicated that COR by the simplified approach is sensitive to changes in the angular displacement amplitude, specifically for $\theta_o \leq 0.1$ rad.

Similar observations can be made by looking at Figure 4-25, where the COR trends by the simplified approach are presented for *Rocking System 2*; the simplified approach estimates COR values which are higher than the constant COR by SRM.

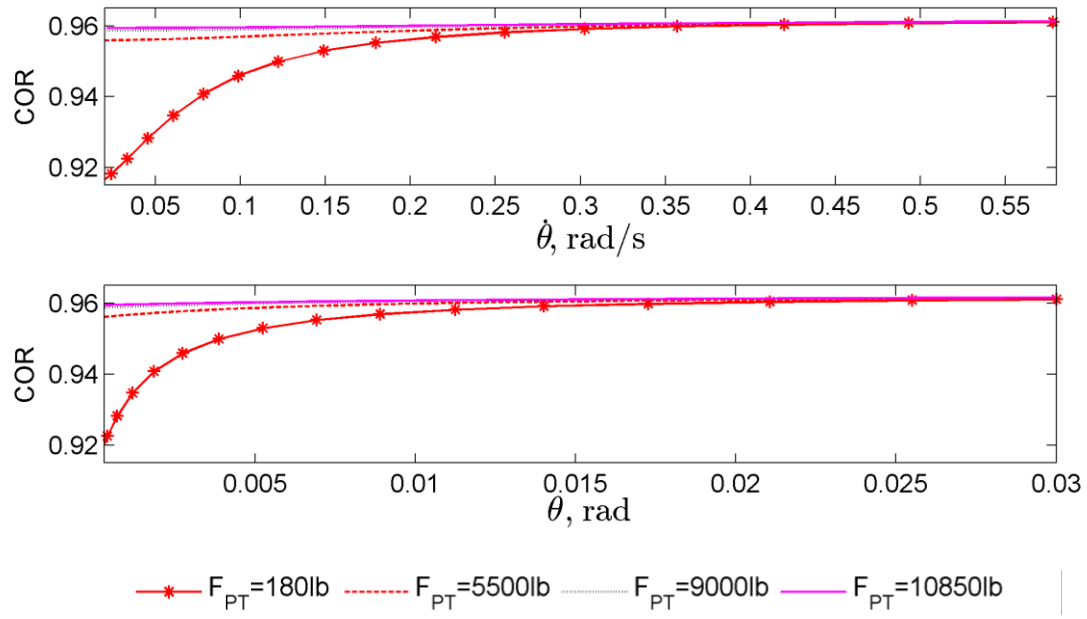

Figure 4-24. COR by the simplified approach for *Rocking System 1* in controlled rocking motion

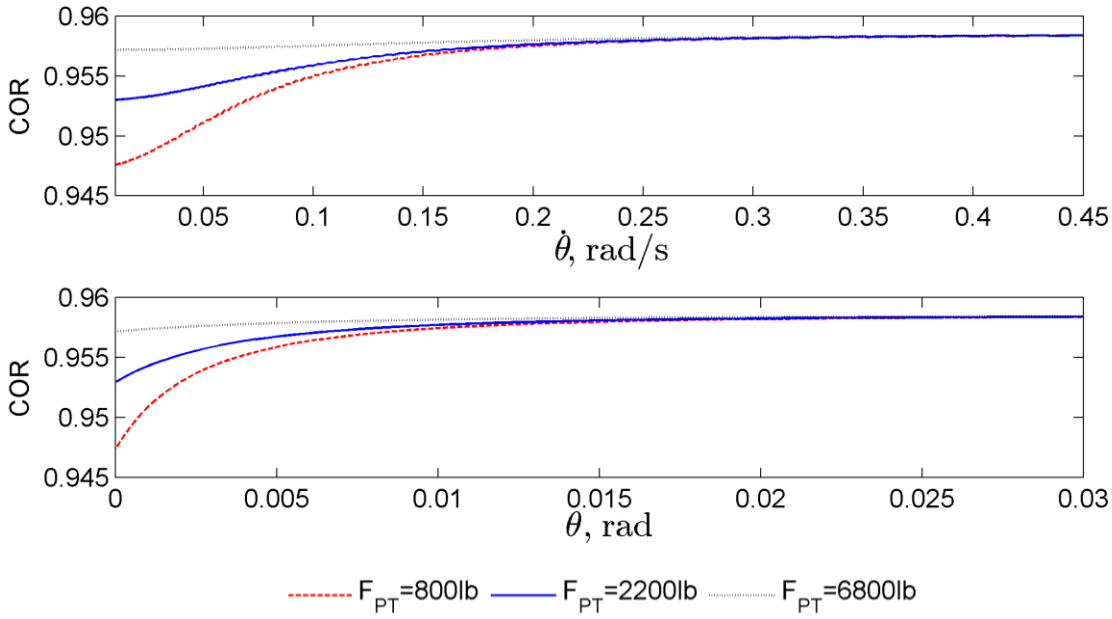

Figure 4-25. COR by the simplified approach for *Rocking System 2* in controlled rocking motion

Simplified approach for Rocking System 1. The efficiency of this approach was validated by comparing with the experimental data of COR and amount of energy dissipation per impact

for all F_{PT} cases implemented during the experimental work. As far as *Rocking System 1* is concerned, the simplified approach was able to provide the desired upper-bound and lower-bound limits for the COR and energy dissipation per impact, respectively, as shown in the Figures from 4-26 to 4-29. The simplified approach effectively provided these limits without significantly underestimating energy dissipation per impact for a large range of impact approaching angular velocities, i.e. $\dot{\theta} \geq 0.1$ rad/s. As the angular velocity decreases below this level, the simplified approach conservatively estimates decay of motion, while COR is underestimated only for very small angular velocity values.

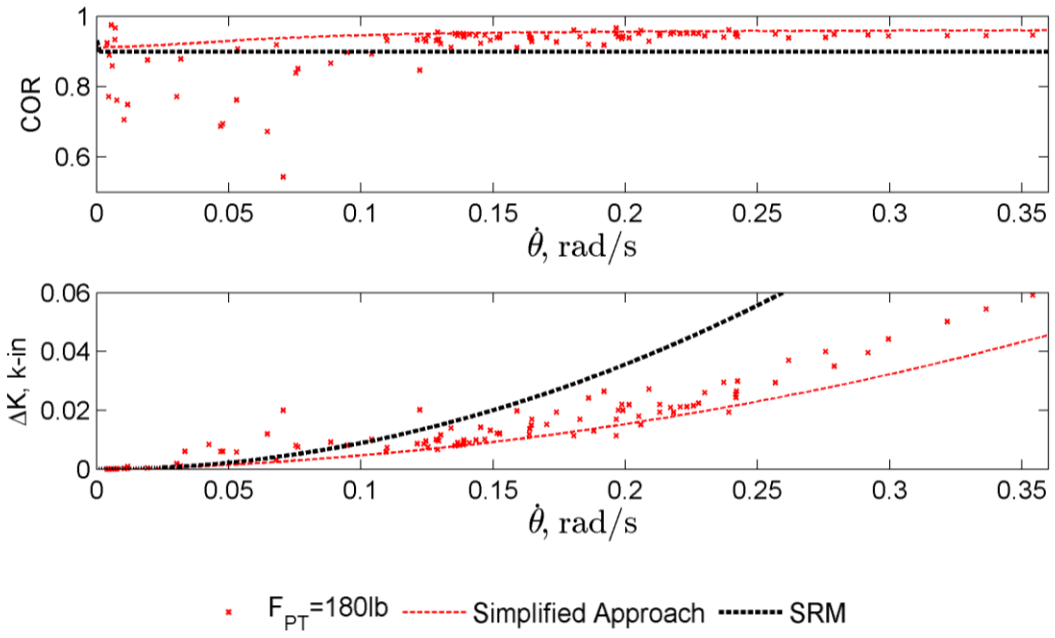

Figure 4-26. Energy dissipation expressed through COR and ΔK by (1) experimental results; (2) the simplified approach; (3) SRM for *Rocking System 1* in controlled rocking with $F_{PT} = 180$ lb.

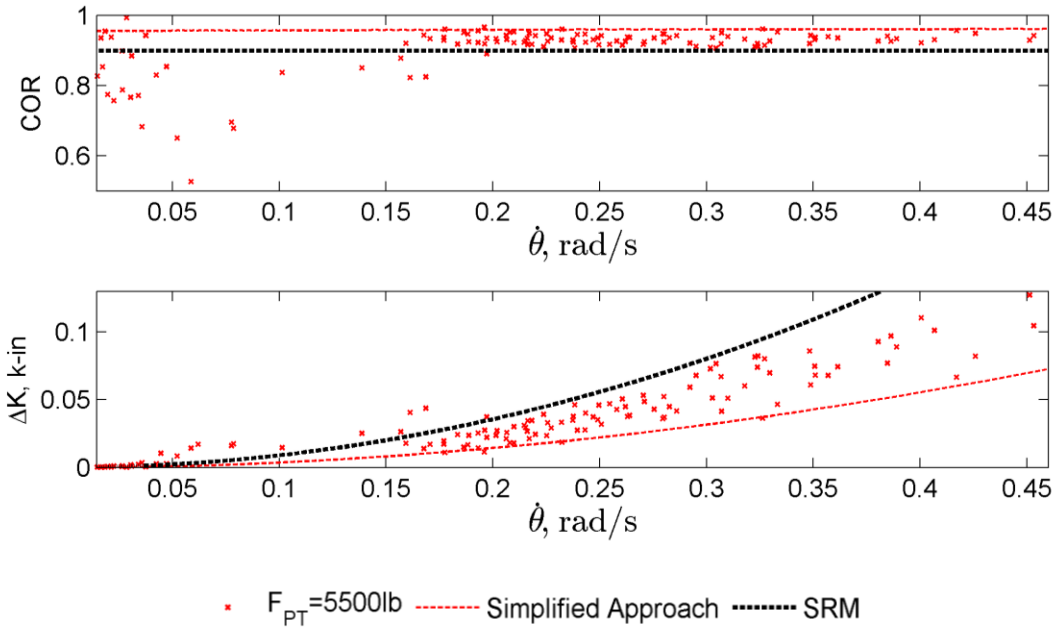

Figure 4-27. Energy dissipation expressed through COR and ΔK by (1) experimental results; (2) the simplified approach; (3) SRM for *Rocking System 1* in controlled rocking with $F_{PT} = 5500$ lb.

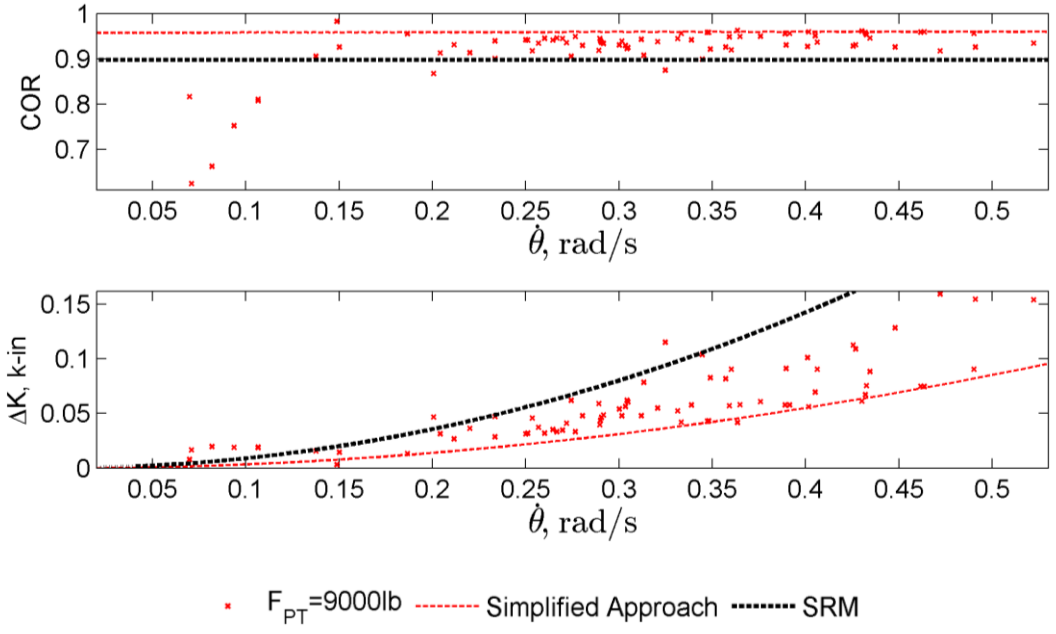

Figure 4-28. Energy dissipation expressed through COR and ΔK by (1) experimental results; (2) the simplified approach; (3) SRM for *Rocking System 1* in controlled rocking with $F_{PT} = 9000$ lb.

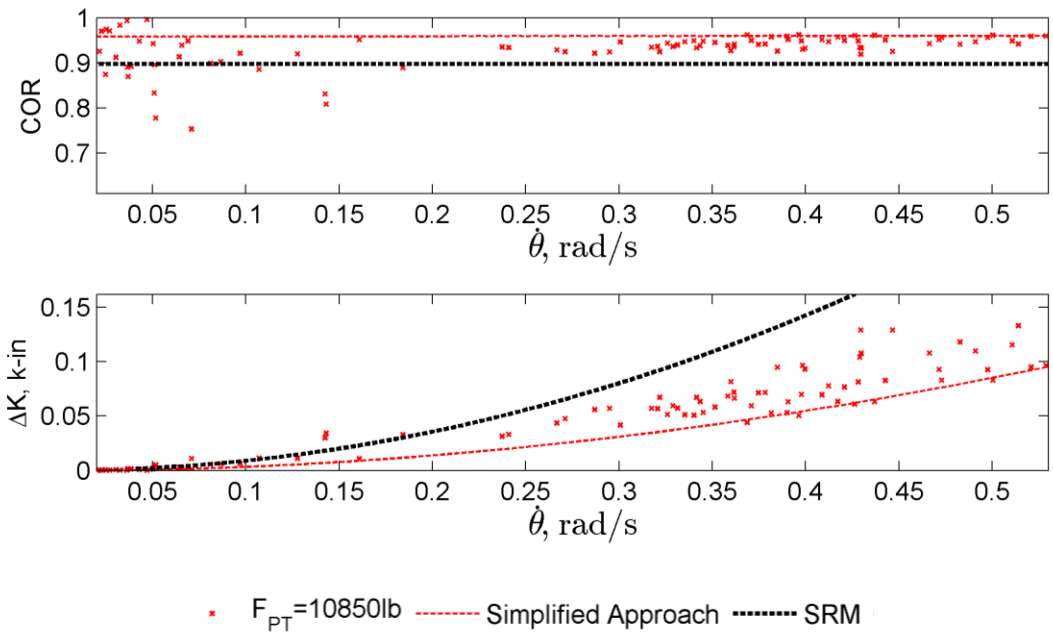

Figure 4-29. Energy dissipation expressed through COR and ΔK by (1) experimental results; (2) the simplified approach; (3) SRM for *Rocking System 1* in controlled rocking with $F_{PT} = 10850$ lb.

Simplified approach for Rocking System 2. The application of the simplified approach to Rocking System 2 shows it can be effectively used to safely estimate decay of motion for this controlled rocking system, as well (Fig. 4-30, 31 and 32). In particular, the efficiency of this approach increases with increase in the initial prestressing force, and finally, the most effective limit by the simplified approach is estimated for the case of $F_{PT} = 6800$ lb.

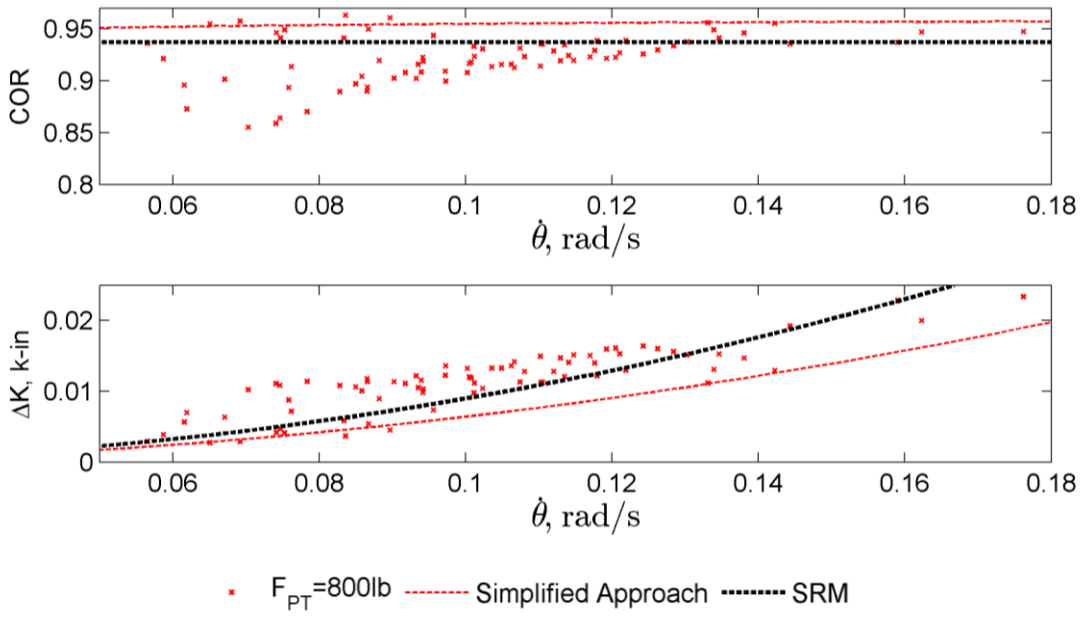

Figure 4-30. Energy dissipation expressed through COR and ΔK by (1) experimental results; (2) the simplified approach; (3) SRM for *Rocking System 2* in controlled rocking with $F_{PT} = 800\,\text{lb}$.

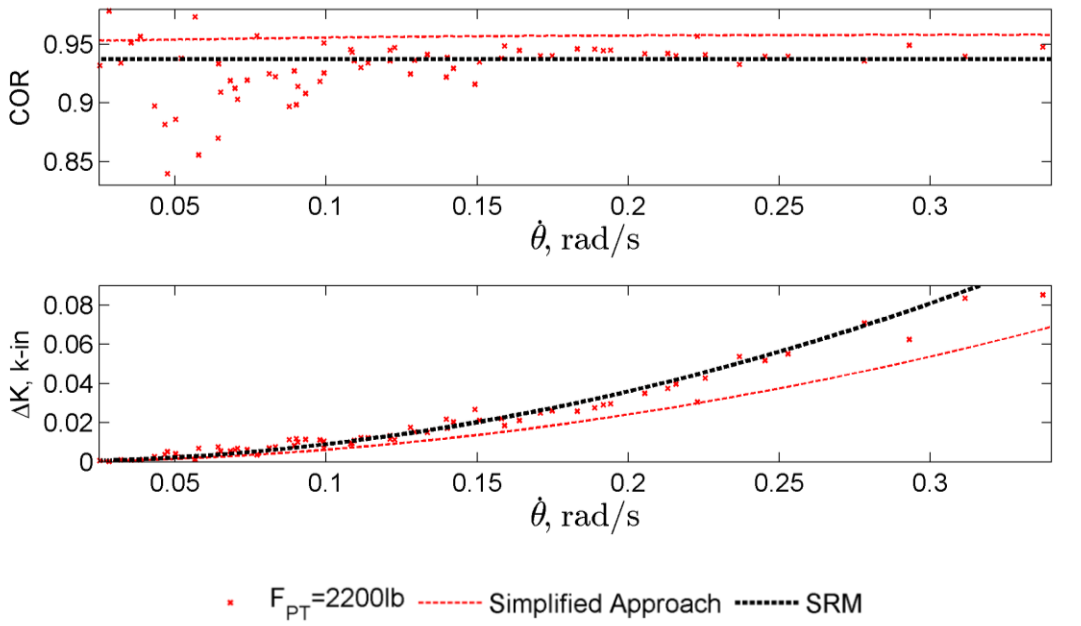

Figure 4-31. Energy dissipation expressed through COR and ΔK by (1) experimental results; (2) the simplified approach; (3) SRM for *Rocking System 2* in controlled rocking with $F_{PT} = 2200\,\text{lb}$.

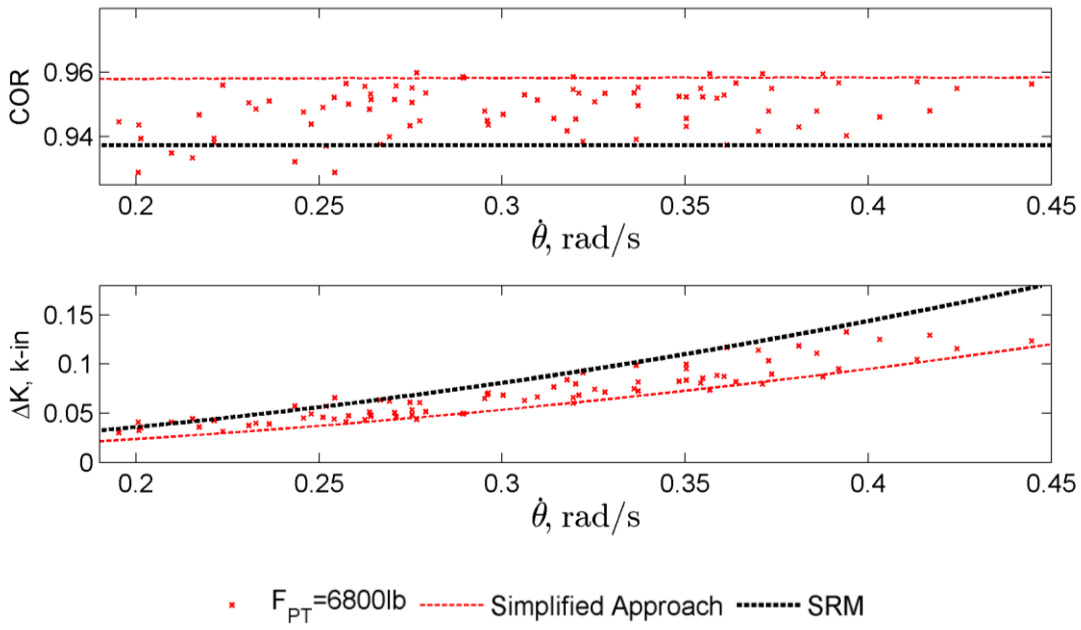

Figure 4-32. Energy dissipation expressed through COR and ΔK by (1) experimental results; (2) the simplified approach; (3) SRM for *Rocking System 2* in controlled rocking with $F_{PT} = 6800$ lb.

4.8 Conclusions

This work has focused on experimentally investigating decay of motion in controlled rocking of precast concrete members, and verifying an earlier introduced FE approach for modeling controlled rocking for its applicability to accurately estimate experimental controlled rocking motion of the originally examined controlled rocking system by applying a different initial prestressing force condition; and a geometrically discrete concrete unit.

By using the original SRM, a simplified approach for safely estimating decay of motion in the experimentally tested controlled rocking systems was proposed.

Following the outcome of this investigation several conclusions can be made:

- Controlled rocking fundamentally differs from free rocking motion in its "natural" quarter period, with controlled rocking being characterized by shorter quarter periods and its dynamic decay of motion characteristics with controlled rocking (a) being, in general,

characterized by higher COR values; (b) being primarily influenced by the impact dissipation mechanism, in contrast to free rocking where a continuous dissipation was shown to be part of the total decay of motion.

- It was found that COR in controlled rocking is underestimated by SRM's COR implying conservation of moment of momentum in a rocking body as defined by Housner (1963) may not be applicable to controlled rocking of the examined controlled rocking columns. Solid reasoning of this behavior would require very accurate experimental data able to step-by-step describe rocking response during the impact phase in order to confidently determine direction of the linear velocity just before and after an impact and the exact RC just after the impact. Since only a good approximation of these parameters was available after the experimental work, a simplified approach was developed, assuming an effect on COR due to the prestressing mechanism. The simplified approach was successfully verified by using experimental data of two geometrically different controlled rocking systems.
- The correct estimation of the elongation of the PT strand is of critical importance for accurately estimating the "natural" quarter period in controlled rocking. While adequate estimation of the controlled rocking quarter periods was achieved by empirically estimating the actual F_{el}, it is suggested this behavior mainly associated with the rocking base of the concrete member should be further investigated.

4.9 Acknowledgements

This work presented in the paper was undertaken as part of the "*NEES* Rocking Wall" project, with funding from the National Science Foundation under Grant No. 1041650 and

Precast/ Prestressed Concrete Institute (PCI). Any opinions, findings, and conclusions or recommendations expressed in this material are those of the authors and do not necessarily reflect the views of the National Science Foundation or PCI. The authors would also like to thank Owen Steffens and Douglas Wood of Iowa State University laboratory for their help with completing the rocking system tests.

4.10 References

Aaleti, S., Sritharan, S., 2007. A precast wall with end columns (PreWEC) for seismic application, *Proc. 8th Pacific Conf. Earthquake Eng.*

Abaqus analysis user's guide version 6.13. *Dassault Systemes Simulia Corp.*

Belleri, A., Torquati, M., Riva, P., 2013. Finite element modeling of 'Rocking walls', *4th ECCOMAS Them. Conf. on COMPDYN*.

Chatzis, M., and Smyth, A., 2012. Robust Modeling of the Rocking Problem, *J. Eng. Mech.*, ASCE, **138**(3), 247-262.

Cheng, C., T., 2007. Energy dissipation in rocking bridge piers under free vibration tests, *Earthquake Eng. Struct. Dyn.*, **36**(4), 503-518.

Chopra, A., and Yim, S., 1985. Simplified earthquake analysis of structures with foundation uplift, *J. Struct. Eng.*, ASCE, **111**(4), 906-930.

Dimentberg, M., F., Lin, Y., K., Zhang, R., 1993. Toppling of computer-type equipment under base excitation. *J. Eng. Mech.*, ASCE, **119**(1), 145-160.

Housner, G. W., 1963. The behavior of inverted pendulum structures during earthquakes, *Bull. Seismol. Soc. Am*, **53**(2), 403-417.

Ma, Q., 2009. The mechanics of rocking structures subjected to ground motion, *PhD Thesis, Department of CEE, The University of Auckland, New Zealand.*

Makris, N., and Zhang, J., 2001. Rocking response of anchored blocks under pulse-type motions, *J. Eng. Mech.*, ASCE, **127**(5), 484-493.

Mander, J., B., Priestley, M., J., N., Park, R., 1988. Theoretical stress-strain model for confined concrete, *J. Struct. Eng.*, **114**(8), 1804-1826.

O'Hagan, J., Twigden, K., Ma, Q., 2013. Sensitivity of post-tensioned concrete wall response to modeling of damping, *New Zealand Society for Earthquake Engineering Conference.*

Priestley, M., J., N., Sritharan, S., Conley, J., R., Pampanin, S., 1999. Preliminary results and conclusions from the PRESSS five-story precast concrete test building, *PCI J.*, **44**(6), 42-67.

Psycharis, I., and Jennings, P., 1983. Rocking of slender rigid bodies allowed to uplift, *Earthquake Eng. Struct. Dyn.*, **11**(1), 57-76.

Stanton, J., F., and Nakaki, S., D., 2002. Design guidelines for precast concrete seismic structural systems, *PRESSS report no. SM 02-02*, Department of Civil Engineering, University of Washington.

CHAPTER 5: SUMMARY, CONCLUSIONS AND FUTURE WORK

Main objective of this study was to provide a better understanding on decay of free and controlled rocking motion of precast concrete members. Considering the knowledge provided by the published literature, it was initially believed conclusions made by previous researchers on this topic could not solidly address the mechanisms behind free and controlled rocking energy dissipation; and the parameters which may influence these mechanisms, specifically in precast concrete members. In addition, none of the previous studies has discussed methods for estimating dynamic decay of controlled rocking for use in design practice; considering appropriate modeling of dynamic energy dissipation due to controlled rocking can be implemented in the design of precast concrete wall systems for minimizing the required hysteretic energy dissipation.

5.1 Summary and Conclusions for Free Rocking

A step-by-step examination of free rocking was deemed of critical importance to give an improved insight into the simplest type of rocking behavior, which is free rocking. Three geometrically discrete free rocking units were experimentally tested for different levels of initial conditions showing similar trends in their dynamic energy decay patterns. The experimental work was accompanied by analytical (FEA and mathematical modeling) studies in order to predict, estimate and reproduce the experimental observations. In the comparison of analytical and experimental results, it was found that there are two energy dissipation mechanisms influencing free rocking motion, namely, instantaneous and continuous energy dissipation.

By using a relatively high sampling frequency in the experimental set-up, it was achieved to adequately capture the impulsive force responses during the impact, and show the magnitude of the impact force is associated with the amount of impact energy dissipation through an approximately linear relationship. The magnitude of the impact force was also shown to linearly vary with respect to the impact approaching velocity. Consequently, an empirical equation, which makes use of these relationships, was introduced for calculating COR.

A new free rocking model, designated as MFRM, was introduced in order to account for the continuous dissipation mechanism, improve the estimation of the impact velocities and produce angular displacement responses which successfully fit the actual behavior.

5. 2 Summary and Conclusions for Controlled Rocking

For the analytical investigation of controlled rocking, an idealized equation of motion was created, showing controlled rocking quarter period can be significantly influenced by (1) the initial prestressing force applied to the unbonded post-tensioned strand; and (2) the stiffness of the strand. It was experimentally found the correct estimation of controlled rocking quarter periods is tied up with the accurate estimation of the elongation of the strand, which cannot be achieved by assuming a rigid body motion. In contrast, the bottom edge of the rocking member is under compression during controlled rocking motion causing the variation of the neutral axis depth with respect to the rocking angular displacement and the reduction in the elongation of the post-tensioned strand, in comparison with the initially idealized rigid bottom edge assumption. A simplified approach was employed to reform the original

equation of motion and succeed an accurate estimation of the controlled rocking quarter periods.

After achieving an improved estimation for the "natural" quarter periods, decay of controlled rocking motion was investigated. In contrast to what one would expect, dynamic decay of controlled rocking motion in precast concrete members may not be significantly influenced by any continuous-type energy dissipation mechanism, and it is characterized by lower energy dissipation per impact compared to free rocking. Assuming an effect of the post-tensioning mechanism on the impact dissipation due to controlled rocking, a simplified approach for safely estimating COR in controlled rocking was proposed. This approach was validated with experimental results of two geometrically discrete controlled rocking units showing its ability to provide an effective upper-bound limit for the experimentally determined COR values.

5.3 Future Work in Free Rocking

Free rocking of precast concrete members was surprisingly shown to be influenced by a continuous-type energy dissipation mechanism, which was then successfully simulated by an alternative free rocking model. By using the MFRM, an improved estimation of free rocking was achieved; however, the use of different coefficients was proven necessary for accurately modeling the experimental free rocking motions with different initial conditions and for different concrete units. Considering the intricacy associated with this continuous mechanism, a thorough investigation would be appropriate in order to clearly determine the parameters influencing its behavior.

5.4 Future Work in Controlled Rocking

This study has reached its ultimate goal by introducing and validating a simple approach for calculating a minimum amount of energy dissipated per impact during a controlled rocking motion. This approach could be used in design practice to account for an extra source of energy dissipation due to rocking motion. It is, however, believed that more experimental testing should be conducted to further investigate the applicability of this approach to other controlled rocking precast concrete systems. It is specifically suggested possible effects of different geometric variables should be examined such as aspect ratio, dimensions of rocking member's cross-section and size effect. Experimental validation of this method with shake table testing is also considered of critical importance.

This study researched controlled rocking by specifically using a Grade 270 unbonded post-tensioned strand. The two controlled rocking units were excited with various levels of initial prestressing force showing the initial prestressing force may influence the impact energy dissipation, an effect which was also had a slight effect in the theoretical estimation of COR by the simplified approach. Additional research examining the effect of the stiffness and dimensions of the unbonded post-tensioned strand on energy dissipation could provide a better understanding on the parameters influencing decay of controlled rocking motion and further investigate the capacity of the simplified method.

Finally, one of the major problems encountered in predicting controlled rocking motion was the accurate estimation of its "natural" quarter periods. This problem was empirically tackled in this study; however, a methodology able to predict the dynamic neutral axis depth and the corresponding elongation of the post-tensioned strand, is necessary to ensure accurate estimation of controlled rocking motion.

APPENDIX: A FINITE ELEMENT APPROACH FOR MODELLING CONTROLLED ROCKING SYSTEM

A paper published in the Second European Conference on Earthquake Engineering and Seismology, Istanbul August 24-29, 2014

Dimitrios KALLIONTZIS and Sri SRITHARAN

A.1 Abstract

Unbonded post-tensioned structural systems have gained momentum in recent years for seismic applications as they enable structures to re-center after experiencing an earthquake load. Accurate modelling of controlled rocking is of paramount importance for understanding the expected seismic performance of these structural systems. Considering the intricacy associated with rocking mechanisms, use of finite element models routinely employed for dynamic problems is inadequate to characterize the response of a system subjected to controlled rocking. This paper presents a study which has developed an efficient approach to quantify the dynamic response of a rocking system with unbonded post-tensioning. Details of a three-dimensional model combined with an explicit finite element technique are provided for a rocking column designed with unbonded post-tensioning. The analytical results are validated with experimental data to confirm the accuracy of the modelling technique.

A.2 Introduction

A.2.1 Free rocking

The survival of seemingly unstable structures during strong earthquake events of the past was attributed to their ability to enter rocking motion. This behaviour, associated with structural systems not firmly attached to the ground, triggered researchers to examine rocking as a potential mechanism for seismic protection. Housner (1963) was the first to present important steps for modelling of rocking behaviour by proposing piecewise equations that describe the free rocking motion of a uniform block rocking on its flat base. The work of this researcher was based on several assumptions: (a) both rocking block and base are rigid; (b) there is no sliding between the block and the base; (c) no bouncing of the block occurs; (d) energy dissipation takes place instantaneously at the time of the impact and is expressed through a coefficient of restitution (COR) dependent on the geometric properties of the block; (e) the impact takes place at the corners of the bottom edge; and (f) the block oscillates in a two-dimensional fashion. A novel approach to rigid body-rigid base modeling was proposed by Prieto and Lourenco (2005), who suggested that energy dissipation can be estimated by simulating the impulsive force response taking place at the impact. This way, these researchers were able to bridge the piece-wise equations introduced by Housner with the impact phenomenon by substituting the initially proposed COR approach with a Dirac-delta force function applied during the impact. The capacity of the simple rocking model (SRM) developed by Housner was investigated by Lipscombe and Pellegrino (1993) who conducted experimental tests on four unanchored blocks of various aspect ratios. It was shown that in many cases the SRM is insufficient to accurately predict the displacement response and energy dissipation of a free rocking system.

Other researchers suggested the dynamic modelling of a free rigid block motion should also account for different types of motion besides rocking, as the assumptions of no sliding and continuous contact between the base and the block can be violated under an earthquake excitation. Ishiyama (1992) classified the rigid body motions into six types, namely (a) rest; (b) slide; (c) rock; (d) slide-rock; (e) translation jump; and (f) rock jump. Ishiyama developed equations to describe these modes of motion, appropriately defined the limits to induce transition from one motion to another, and incorporated the idea of tangential COR into the proposed equations. A few years later, Shenton (1996) stated that a rigid body at an initial rest condition may be excited into five discrete modes of motion, namely, (a) rest; (b) slide; (c) rock; (d) slide-rock; and (e) free flight due to a horizontal ground motion. This work emphasized, sliding and rocking do not always occur separately and therefore; there is a mode in which these two motions occur simultaneously. The proposed condition which indicates the occurrence of this mode depends on (a) the coefficient of friction of the rigid block-rigid base interface; (b) the geometric properties of the block; and (c) the ground acceleration.

On the improvement of modelling free rocking motion, researchers eliminated the assumption of a rigid system suggested by the SRM and introduced alternative approaches to account for the flexibility effects, which spring from either the rocking interface or the self-deflection of the block. Psycharis and Jennings (1983) developed two models which accounted for the flexibility of the rocking base. The first model used two concentrated springs at the corners, while the second one followed the Winkler foundation type. Chopra and Yim (1985) studied the foundation uplift phenomenon of a structural system subjected to an earthquake excitation. Interface material flexibility was again modelled using spring-

dashpot mechanisms at two locations: (a) at the bottom corners of the foundation; and (b) in a distributed manner along the entire contact interface, while the rocking body was modelled as a single degree of freedom system. Chatzis and Smyth (2012) proposed two spring models considering the effects of sliding, uplift, base flexibility and geometric nonlinearities. The response of these models was shown to be very sensitive to the selection of damping and the spring stiffness parameters of the spring-dashpot mechanisms.

A.2.2 Controlled rocking

The introduction of post-tensioning in a rocking system creates additional challenges as it introduces a controlled mechanism and significantly alters the dynamic properties of the rocking system. This behaviour was examined by O'Hagan et al. (2013), who showed that energy dissipation of this system cannot be exclusively described by COR as defined by Housner and a combination of damping components may influence the response. Suggested supplemental damping components by O'Hagan et al. included equivalent viscous damping (EVD) and a Coulomb friction damping.

A.2.3 Finite element analysis

Finite Element Analysis (FEA) using implicit techniques has also been used by researchers to assess the response of free and controlled rocking systems. Ardila-Giraldo et al. (2013) developed a two-dimensional FE free rocking model using a fine uniform mesh for the block, where Rayleigh damping was used to simulate the decay of motion. In order to investigate the dynamic response of ancient structural monuments located in Greece and Italy, Manos et al. (2013) developed finite element models to simulate free rocking response

of scaled ancient columns. Again, a uniform meshing pattern was used in these models which were subjected to free vibration, sinusoidal and earthquake motion excitations. Belleri et al. (2013) conducted dynamic FEA of an unbonded post-tensioned rocking wall by using different FE techniques. A three-dimensional rocking wall model using brick elements was developed. Fine mesh was used only for the bottom corners and the contact surface definition was divided into tangential and normal behaviour. One-dimensional models with springs and fiber elements were also proposed; however, validation of these models with experimental results was not presented.

A.3 Research Significance

Previous work has produced significant information on modelling methodologies for simulating free rocking behaviour using mathematical approaches and FE analyses. As there is still a need to better understand the fundamentals of this behaviour, most of these studies have focused on characterizing rocking response of free-standing blocks and therefore, modelling of controlled rocking has received limited attention. The objective of this work is to propose and validate a FE approach for controlled rocking of a structural system which makes use of an explicit analysis – a suitable approach to model impact phenomena. In contrast to previous research work, the proposed model does not adopt a rigid or relatively rigid system, but incorporates the elastic material properties for both the rocking system and the foundation-base, as determined for laboratory test units. By following this approach, (a) the flexibility properties of the rocking system and their influence on the response are accounted; and (b) one can correlate the selected damping properties with the geometric, as well as, the material features of the controlled rocking system.

In addition, the study examines an appropriate meshing pattern and suitable analysis parameter selections to secure reliable outputs in order to (a) successfully fit the experimental displacement responses; (b) provide better understanding of damping under controlled rocking; and (c) ensure minimum solution time.

A.4 Modified SRM to account for Controlled Rocking

Comparison of the SRM proposed by Housner with the experimental and FEA results provides an understanding of its capacity to estimate the response of a controlled rocking system under free vibration. Following the fundamental assumptions of Housner's model and relying on the decay of motion mechanism expressed through a constant COR, the SRM is extended herein to account for the controlled rocking effect.

Housner's free rocking modelling technique was originally developed based on the geometric properties of the block which were taken as the controlling parameters of its rocking motion. The two critical geometric quantities are (a) the distance between the centre of gravity of the block and its rotation centre (R); and (b) the aspect ratio of the block (α), as shown in Figure 1. In controlled rocking, the block is supplemented with a re-centering force applied by the prestressed strand. This force can be divided into two components, (1) the initial prestressing force (F_{PT}); and (2) added tendon force due to the elongation of the strand when $\theta(t) \neq 0$ (F_{el}). For $\theta(t) \geq 0$ and small angular displacements for which the vector of the 2nd component is oriented along the centerline of the rocking block, F_{el} can be approximated to,

$$F_{el} = kb\theta \tag{A-1}$$

Where k is the axial stiffness of the prestressed strand.

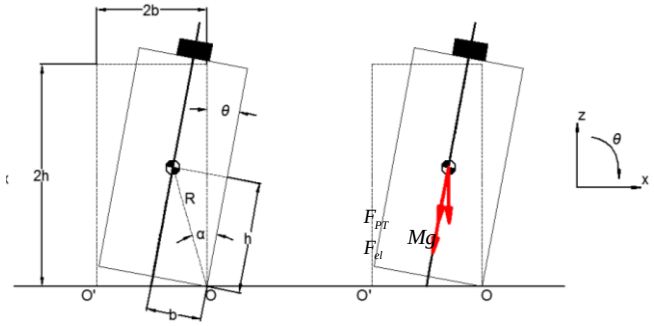

Figure A-1. Controlled rocking block

For $\theta(t) \geq 0$, the equation of motion of a rocking block is described by equation (A-2),

$$I_o\ddot{\theta} + MgR\sin(\alpha - \theta) + F_{PT}b + kb^2\sin(\theta) = 0 \quad \text{(A-2)}$$

Where $I_o = \frac{4}{3}MR^2$ and M are the moment of inertia with respect to the rotation centre (O or O') and total mass of the block, respectively.

For slender blocks with an aspect ratio less than 20^o, equation (A-2) is linearized as,

$$I_o\ddot{\theta} + MgR(\alpha - \theta) + F_{PT}b + kb^2\theta = 0 \quad \text{(A-3)}$$

Under the assumption of $kb^2 \geq MgR$ and the initial conditions of $\theta(0) = \theta_o$ and $\dot{\theta}(0) = 0$, the equation for $\theta(t)$ becomes,

$$\theta(t) = -\frac{\beta}{p_c^{\,2}} + (\theta_o + \frac{\beta}{p_c^{\,2}})\cos p_c t \quad \text{(A-4)}$$

Where

$$\beta = \frac{MgR\alpha + F_{PT}b}{I_o} \quad \text{(A-5)}$$

$$p_c = \sqrt{\frac{kb^2 - MgR}{I_o}} \tag{A-6}$$

Where p_c is the *dynamic parameter* of the block in its controlled rocking motion.

The quarter period of this motion and the associated COR which was originally defined by Housner are described by equations (A-7) and (A-8), respectively. As the original COR was estimated based on impact mechanics and by equating the moment of momentum just before an impact to the moment of momentum just after the impact about the point of rotation after the impact, the supplemental force components do not affect the estimation of this parameter for a controlled rocking response. Therefore, equation 8 expresses the COR as originally proposed by Housner.

$$\frac{T}{4} = \frac{1}{p_c}\cos^{-1}\left(\frac{\beta}{\beta + \theta_o {p_c}^2}\right) \tag{A-7}$$

$$r = \left[1 - \frac{MR^2}{I_o}(1 - \cos(2a))\right]^2 \tag{A-8}$$

A.5 Summary of Experimental Investigation

Figure A-2 shows a rocking reinforced column with a 14 x 14 square in cross-section, 66 in height, 1.22 kips weight and an aspect ratio (h/b) of 33/7 which was constructed in the structural laboratory at Iowa State University. A concrete reinforced mass with dimensions of 12 x 50x 50 (height x width x length) cubic in and 2.38 kips weight was attached at the top of the column (Fig. A-2). The concrete mass was kept in place using two threaded bars and two longitudinal bars passing through the middle of its cross-section which were properly tighten on its exterior faces (Fig. A-2).

An unbonded seven-wire strand (Grade 270) created the connection between the rocking system and the reinforced foundation. The strand was initially prestressed to 31.3 ksi (F_{PT} =6.8 kips). In order to ensure full contact between the rocking column and foundation as well as to prevent shear sliding, a 1 in height grout was placed between the foundation and the column while grout was also placed around the column sides and up to a height of 1 in (total grout height, 2 in). Steel angles-channels with dimensions of 4 x 3 x 3/8 cubic in were attached at the corners of the column to prevent crushing of concrete in this region when the impact takes place.

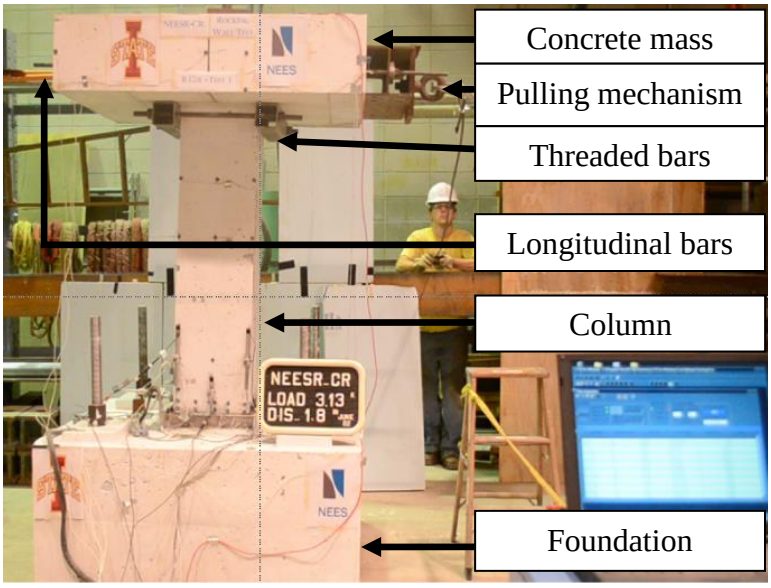

Figure A-2. Rocking System and Foundation-Base

Laboratory tests were undertaken to determine the material properties of the concrete and the grout so that they can be used in the FE model. The concrete elastic modulus used in the foundation, column and mass was 3,825 ksi whereas the same parameter for the grout

layer was 6,000 ksi. For the prestressed strand and the mild reinforcing steel bars used in the column, mass and foundation, the specified Young's modulus was 29,000 ksi.

A series of controlled rocking tests was conducted with 0.4%, 1% and 3% as initial top lateral drifts. The tests were repeated three times for each initial condition by pulling the top of the column horizontally to the desired initial lateral drift using an offset hook attached at the mid-height of the concrete mass. A hydraulic jack located at the same height was used to apply the horizontal pulling force. The instrumentation of the specimen used a series of light emitting diodes (LED) which were imposed along the length and height of the rocking system. The LED monitoring system used 120 Hz sampling frequency, adequate to capture the displacement response of this unit. Three direct-current differential transformers (DCDT) were attached along the bottom edge of the column and two string-pots were located at the mid-height of the column and the mid-height of the concrete mass to monitor the lateral displacement of the system.

A.6 Finite Element Modelling

Explicit direct integration, as used herein, constitutes a conditionally stable and damping dependent numerical method, and uses a very small time step (i.e., 1E-6 seconds). This method presents several advantages: (a) each time step is relatively inexpensive and proceeds fast; (b) geometric and material nonlinearity can be easily accommodated in the analysis solution; and (c) no convergence criteria as required for an implicit analysis are needed (Cook et al., 2003).

The use of this FE approach aims at: (a) producing a rocking dynamic displacement response for controlled rocking systems that will closely capture the measured response for

different levels of initial lateral displacements; (b) reducing the solution time; and (c) minimizing the analysis error expressed using 'Artificial Energy' (Abaqus Analysis User's Guide, Abaqus 6.13).

A.6.1 Material definitions

Since no visible damage was observed for the controlled rocking experimentally tested unit after a large number of free vibration tests, elastic material definitions were deemed adequate for all analyses. The grout and concrete material definitions were both supplemented with the Rayleigh damping model by using different values for each initial lateral drift analysis, as explained later. Only the mass component of Rayleigh damping (ALPHA) was used, while the stiffness component (BETA) was given a zero value as it was found that: (a) its use causes the model displacement response to further diverge from the experimental response; and (b) can dramatically reduce the analysis time step since a damping dependent numerical method is used by the FEA software (Abaqus Analysis User's Guide, Abaqus 6.13).

A.6.2 Geometric configuration

The model dimensions were the same as in the experimental unit that was previously described. However, in order to reduce the number of nodes used in the analyses, a smaller foundation size (i.e., 25 x 25 x 4 cubic in) was used, since modelling the foundation in full did not benefit the FEA analysis results. Smaller dimensions were also given to the concrete mass, while the mass density was modified to give the same weight, maintaining the same weight and centre of gravity as well as the aspect ratio for the rocking system. Moreover, a

hollow rectangular section was modelled and attached to the foundation bottom surface to accurately model the exact length and axial stiffness of the prestressed strand. The strand was firmly anchored using two 5 x 5 x 5 cubic in steel blocks located at the top of the column and at the bottom of the hollow rectangular section (Fig. A-3). Finally, the steel angles located at the bottom corners of the column were not specifically accommodated in the model, as it was found they have no significant influence on the rocking displacement response of the column.

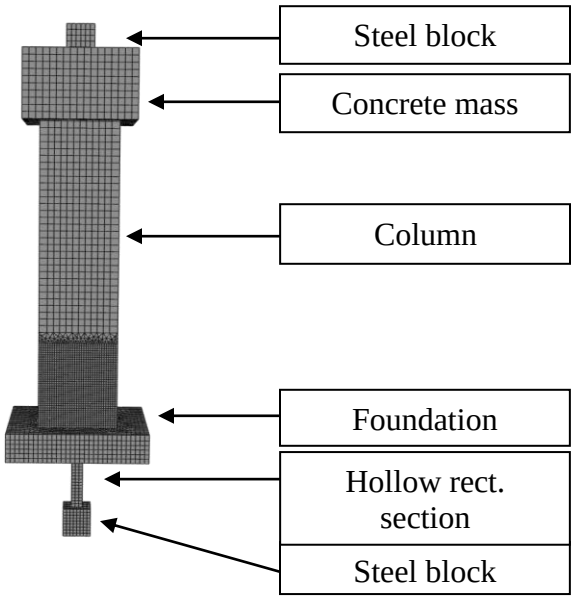

Figure A-3. Three-dimensional Finite Element Model of the Rocking System

A.6.3 Discretization

The FE model of the test unit was discretized, as follows:

(i) Column: The upper and lower parts were meshed using C3D8R – 8-node brick elements – while C3D10M – 10-node quadratic tetrahedron elements were used to form the transition layer as shown in Figure A-3. To reduce the solution time, the mesh options of reduced integration and orthogonal kinematic split were employed.

Hourglass control was also activated to minimize the "spurious/hourglass modes" effects that the reduced integration elements can initiate. A finer uniform mesh (0.4 in C3D8R typical element edge length) was used for the bottom 15 in height of the column which ensured no effect of the transition layer used to separate the upper and lower discretization patterns (Fig. A-3). The top part of the column was discretized using coarser mesh (1 to 1.2 in C3D8R typical element edge length). C3D10M elements of various sizes were used to create the aforementioned transition layer of 2 in. In general, the brick element edge size of the upper and lower parts of the column should not exceed a 3:1 ratio, in order to prevent the division of the transition layer into 'poor-shape-elements' of very large and small corner angles (Cook et. al., 2003).

(ii) Foundation: Meshed with C3D8R elements having a 0.8 in typical edge length and the same element properties as the Column part. This component was partitioned into two parts: a 25 x 25 x 1 cubic in grout layer at the top and a 25 x 25 x 3 cubic in concrete layer beneath.

(iii) Steel blocks and the two hollow rectangular sections: Meshed with C3D8R elements having a 0.6 in typical edge length and the same element properties as the Column part.

(iv) Concrete Mass: Meshed with C3D8R elements having a 1 in typical edge length and the same element properties as the Column part.

(v) Mild Reinforcing Steel & Prestressing Strand: The mild steel used to reinforce the Column part and the prestressing strand were discretized with T3D2 linear 3-D truss elements of 1 in typical length.

A.6.4 Contact definitions

The option of 'General Contact' was the contact algorithm used to simulate the contact interactions in the model. The 'Hard' contact option was used to define the normal behaviour of the contact interaction, while the tangential behaviour used 'Penalty Friction Formulation') with a friction coefficient of 0.6 which was sufficient to ensure no relative horizontal motion between the two contact surfaces.

A.6.5 Analysis steps

Three steps were performed during the dynamic analysis using the same sampling frequency as the experimental test runs and with the foundation being constrained from any displacement in all directions during all three steps. In the first step, the application of the initial prestressing force and initiation of the desired lateral drift were imposed on the rocking column which was free from any displacement constraint. In the second step, the rocking column was free to move in the vertical direction, while displacement constraints were applied in the other two directions. This step aimed at capturing the decay of kinetic energy, while eliminating any undesirable sliding motion and instability of the rocking column with respect to its foundation before the rocking response begins. In the last step, the constraints which were specifically applied in the second step were released to allow the rocking motion of the column.

A.6.6 Mass scaling

In order to reduce the solution time of the analyses, mass scaling with a 2E-6 seconds target time increment per 10 increments was used for all the three steps. Even though rocking

is an inertia dependent phenomenon, a careful use of this option is generally beneficial since it significantly reduces the solution time without compromising the outcomes of the FE rocking response analyses.

A.7 Model Reliability

After a displacement response convergence study with respect to different discretization patterns, the reliability of the output with respect to the artificial energy was examined. Artificial energy should be negligible when compared with the kinetic energy. This comparison is repeated in the same manner for all the FEA results and the 3% initial lateral drift case is presented in Figure A-4 as a typical output.

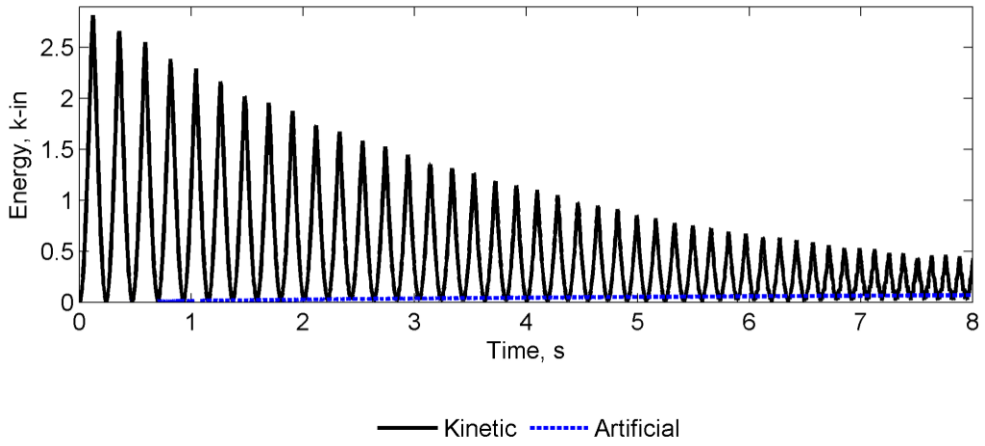

Figure A-4. Artificial vs. Kinetic Energy in the system for an analysis with 3% initial lateral drift

A.8 Comparison of Results

In this section, the experimental displacement responses for 0.4%, 1% and 3% are compared with the respective FEA results and those obtained with the modified SRM adjusted to account for the controlled rocking effect (designated as SRM-CR). In Figure A-5,

it can be seen that the proposed finite element model is able to produce a dynamic response which successfully fits the actual response of the controlled rocking system for the three initial lateral drift conditions. In contrast, SRM-CR significantly deviates from the actual response both in its damping and quarter period characteristics as it can be discerned from this figure.

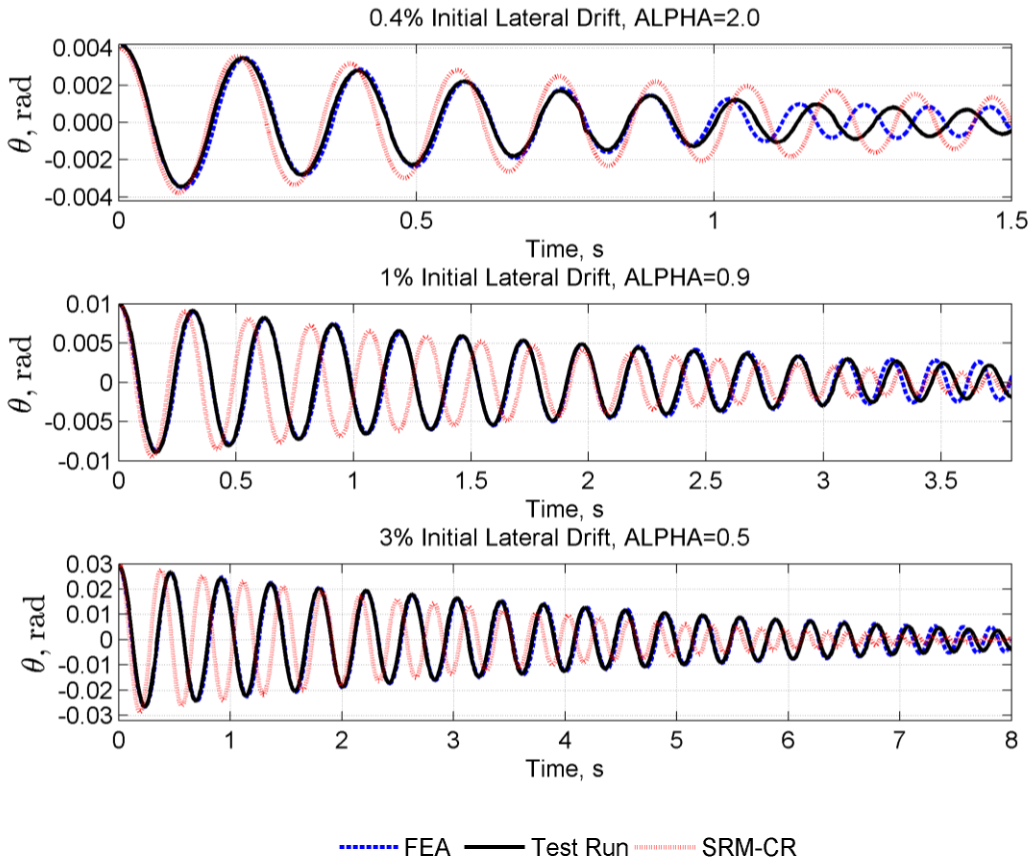

Figure A-5. Comparison of angular displacement time histories for 0.4%, 1% and 3% initial lateral drifts

The FEA model captures experimentally recorded angular displacement time histories accurately for all three cases. There is a small deviation seen at smaller angular displacements toward the end of the response. In particular, for 3% initial lateral drift, the

two responses fit well up to 0.7% angular displacement and for 37 quarter cycles, while for 1% initial lateral drift they start to diverge at 0.3% angular displacement and after the completion of 24 quarter cycles. Finally, for 0.4% initial lateral drift, the two responses closely follow each other up to 0.1% angular displacement and for 11 quarter cycles.

The comparison of the experimental displacement time histories with the SRM-CR simulation results strengthens the argument that the decay of motion is dependent on the level of lateral displacement peak. Consequently it follows that a single value of the COR estimated by Housner's model would be unable to express energy dissipation of this particular controlled rocking system for the different levels of angular displacement.

Looking at Figure A-5, the actual displacement response decays faster for the 0.4% initial lateral drift than the SRM-CR simulation, while it decays slower for the 1% and 3% initial lateral drifts compared to the SRM-CR simulation. Furthermore, the SRM-CR was shown to be inadequate to accurately estimate the quarter period of the actual response as seen for the 1% and 3% initial lateral drift cases of Figure A-5. This difference in the rocking quarter period is in agreement with observations made by previous researchers which is believed to be due to assuming the bottom corners as the rotation centres in SRM. In reality, the rotation centre of a rocking member connected with post-tensioning strands does not stay constant and it moves along this edge as a function of the angular displacement (Aaleti 2009; Ma 2009). As shown in Figure A-6, this movement of the rotation centre, which occurs due to the compression of the bottom edge, leads to a substantial decrease in the F_{el} force with respect to the angular displacement, increasing the quarter period of the rocking system compared to the idealized quarter period by the SRM-CR.

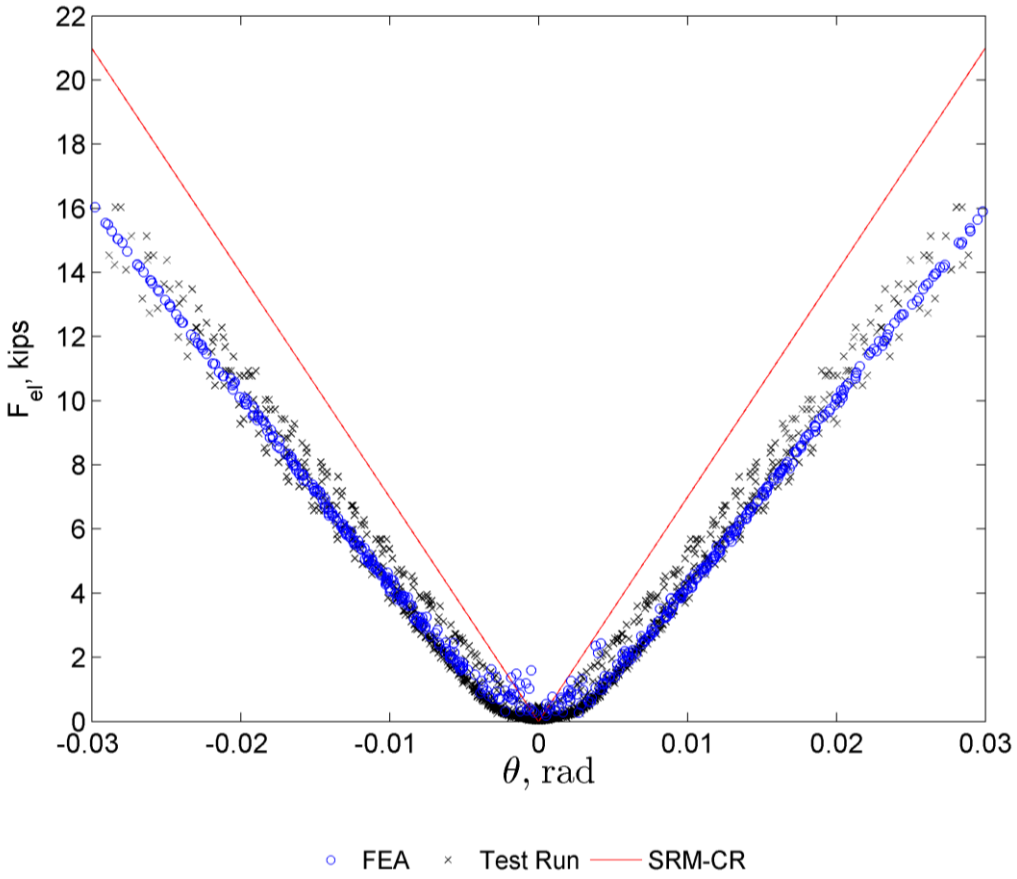

Figure A-6. Added tendon force due to elongation of the strand with respect to the angular displacement

Figure A-7 presents the part of the phase diagrams associated with positive angular velocities vs. angular displacements for the three different lateral drift cases used in Figure 5. It is seen that the FEA results closely follow the experimental response test run for the angular velocity versus angular displacement relationship. The two oscillations reach a maximum velocity value approximately at the point of zero angular displacement where a reduction in the angular velocity occurs due to the impact. In contrast, SRM-CR predicts higher impact velocities in all three initial lateral drifts, a behaviour that is tied up with the shorter quarter period predicted by the SRM-CR.

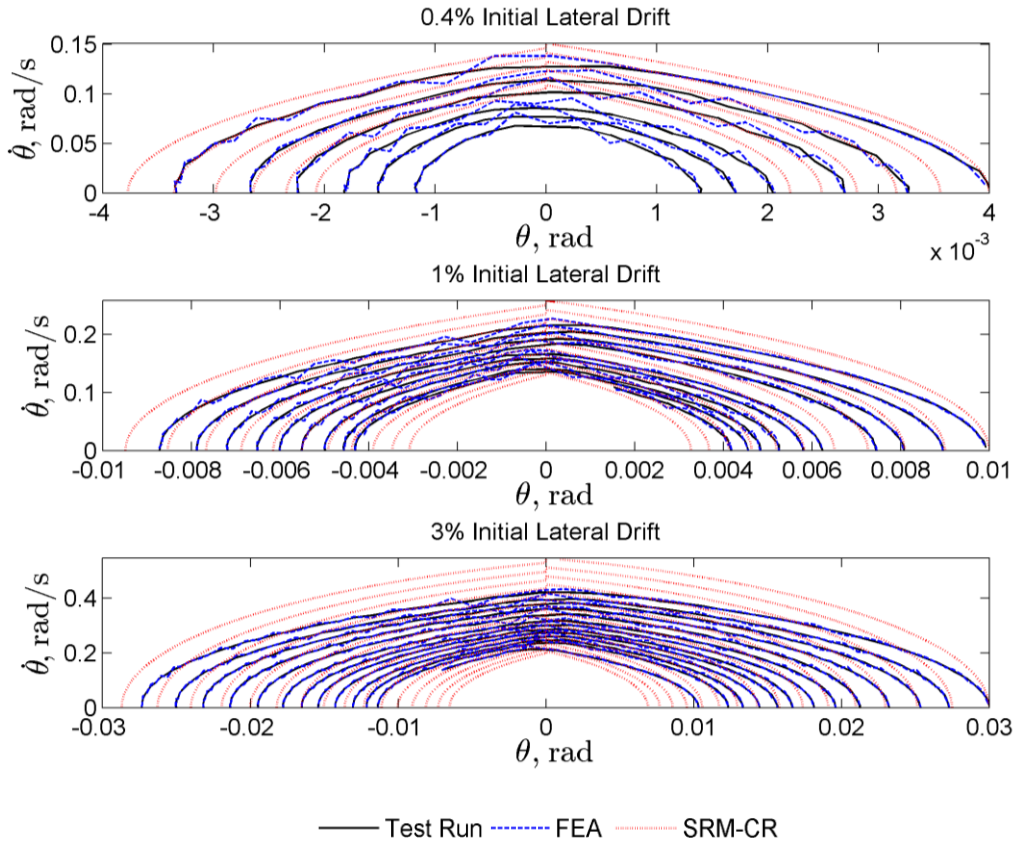

Figure A-7. Comparison of phase diagrams for 0.4%, 1% and 3% initial lateral drifts

A.9 Accumulated Energy Dissipation

Based on the SRM, energy dissipation should be expressed in the form of COR, while the motion is divided into two phases: (a) continuous and (b) impact phase. During the impact phase, there is a drop in the total energy of a rocking system, while the continuous phase is free of energy dissipation. As a result, decay of motion is theoretically expressed with an ideal step pattern which signifies instantaneous energy dissipation at every impact.

This section presents the decay of motion paths as estimated by the SRM-CR simulation and the FEA with the latter shown to be in good agreement with the experimental results according to Figures A-5, A-6 and A-7. Due to the low sampling frequency, accurate estimation of the experimental accumulated energy dissipation was not feasible; and

therefore this component was not included in this section, assuming that it can be effectively expressed by the FEA results.

In order to calculate the energy content of the controlled rocking system by the SRM-CR, the equation of motion of equation (A-2) is employed to estimate the energy components. Accordingly, the energy content is divided into 4 components: (a) Kinetic energy (K), (b) Gravitational potential energy (U_g), (c) Potential energy due to the initial prestressing force (U_{PT}) and (d) Potential energy due to elongation of the strand (U_{el}). As far as FEA is concerned, decay of motion was directly provided by the history outputs of the analyses.

$$K = \frac{1}{2} I_o \dot{\theta}^2 \tag{A-9}$$

$$U_g = MgR(\cos(\alpha - |\theta|) - \cos(\alpha)) \tag{A-10}$$

$$U_{PT} = F_{PT} b\theta \tag{A-11}$$

$$U_{el} = kb^2(1 - \cos(\theta)) \tag{A-12}$$

Typical decay of motion patterns of the rocking oscillation as calculated by the SRM-CR and FEA are plotted in Figure A-8 showing that the FEA predicts a step function as was initially suggested by the SRM. As expected, the two simulations predict a significantly different trend with the SRM-CR decaying faster. At the same time SRM-CR suggests an instantaneous and of zero time interval impact phenomenon that results in a steep-vertical drop in the energy content at every impact. However, FEA simulation follows a smoother pattern due to the real-time non-zero impact duration and the viscous type Rayleigh damping that was used to simulate energy dissipation.

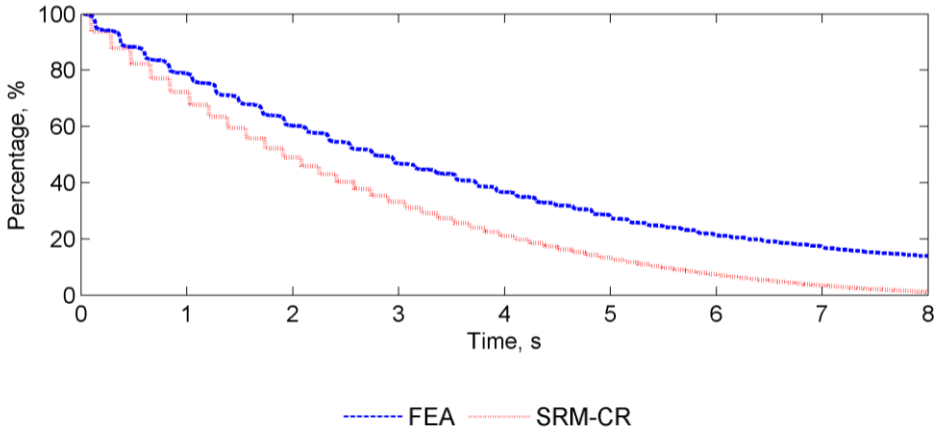

Figure A-8. Typical decay of motion expressed as the remaining energy in the rocking system as a function of time for the 3% initial lateral drift response

A.10 Conclusions

This paper has focused on proposing a suitable FE modelling technique for controlled rocking. A controlled rocking system consisting of a column and a mass was modelled by using a FEA software and the results were compared with the respective free vibration experimental test series for three different initial lateral drifts. Explicit time integration was shown to be an efficient method to model rocking behaviour as the proposed FE model was able to produce a rocking response that acceptably fits the real-time displacement time history and phase diagrams of the rocking specimen.

On the proposed FE technique, the meshing pattern was found to be a prominent parameter that controls decay of motion at the impact and the reliability of the FEA results by influencing the magnitude of the artificial energy output. In contrast to what might be expected, the option of a fine mesh only at the bottom corners of the column produced high artificial energy and an angular displacement response that grossly deviated from the actual response. In contrast, fine mesh along the total bottom edge of the column as shown in Figure

A-3 was necessary in the proposed modelling approach in order to reach reliable and accurate results.

As far as damping in controlled rocking is concerned, different Rayleigh damping values were necessary to achieve a good agreement with the experimental results signifying a change in damping characteristics for different angular displacement levels. This change was also evident by comparing the SRM-CR simulation which used a constant COR with experimental results for 0.4%, 1% and 3% initial lateral drifts, where the SRM-CR either underestimated (0.4%) or overestimated (1% and 3%) the decay of motion. This result was attributed to (a) a change in the damping features of the rocking system with respect to the level of angular displacement; and (b) the fact that SRM-CR estimated a higher value for the angular impact velocity leading to an increased amount of energy dissipation per impact for a given COR.

The comparison between the experimental and SRM-CR simulation results suggest that the latter would be improved by: (a) modelling of the moving rotation centre as a function of the angular displacement in order to accurately estimate the added tendon force due to the elongation of the strand and quarter period of the motion; and (b) modelling of a varying COR as a function of the angular displacement peak.

A.11 Acknowledgements

This work presented in the paper was undertaken as part of the "*NEES* Rocking Wall" project, with funding from the National Science Foundation under Grant No. 1041650 and Precast/ Prestressed Concrete Institute (PCI). Any opinions, findings, and conclusions or recommendations expressed in this material are those of the authors and do not necessarily reflect the views of the National Science Foundation or PCI. The authors would also like to

thank Sriram Aaleti, Assistant Professor of the University of Alabama, Maryam Nazari, Owen Steffens and Douglas Wood of Iowa State University laboratory for their help with completing the rocking system tests.

A.12 References

Aaleti, S., and Sritharan, S., 2009. A simplified analysis method for characterizing unbonded post-tensioned precast wall systems, *Engineering Structures*, **31**(12), 2966-2975.

Abaqus analysis user's guide version 6.13. *Dassault Systemes Simulia Corp.*

Ardila-Giraldo, O., 2013. Contact interface modeling in the dynamic response of rigid blocks subjected to base excitation, *4th ECCOMAS Them. Conf. on COMPDYN.*

Belleri, A., Torquati, M., Riva, P., 2013. Finite element modeling of 'Rocking walls', *4th ECCOMAS Them. Conf. on COMPDYN.*

Belytschko, T., Liu, W., Moran, B., 2000. Nonlinear Finite Elements for Continua and Structures, John Wiley & Sons, LTD.

Chatzis, M., and Smyth, A., 2012. Robust Modeling of the Rocking Problem, *J. Eng. Mech.*, ASCE, **138**(3), 247-262.

Chopra, A., and Yim, S., 1985. Simplified Earthquake Analysis of Structures with Foundation Uplift, *J. Struct. Eng.*, ASCE, **111**(4), 906-930.

Cook, R., Plesha, M., Malkus, D., 2003. Concepts and Applications of Finite Element Analysis, Fourth Edition, John Wiley & Sons (ASIA), PTE, LTD, SINGAPORE.

Housner, G., 1963. The behavior of inverted pendulum structures during earthquake excitations, *Bull. Seismol. Soc. Am.*, **53**(2), 403-417.

Ishiyama, Y., 1982. Motions of rigid bodies and criteria for overturning by earthquake excitations, *Earthquake Eng. Struct. Dyn.*, **10**(5), 635-650.

Lipscombe, P., and Pellegrino, S., 1993. Free rocking of prismatic blocks, *J. Eng. Mech.*, **119**(7), 1387-1410.

Ma, Q., 2009. The mechanics of rocking structures subjected to ground motion, *PhD Thesis, Department of CEE, The University of Auckland, New Zealand.*

Manos, G., Petalas, A., Demosthenous, M., 2013. Numerical and experimental study of the rocking response of unanchored body to horizontal base excitation, *4th ECCOMAS Them. Conf. on COMPDYN*.

O'Hagan, J., Twigden, K., Ma, Q., 2013. Sensitivity of post-tensioned concrete wall response to modeling of damping, *New Zealand Society for Earthquake Engineering Conference*.

Prieto, F., and Lourenco, P., 2005. On the rocking behavior of rigid objects, *Mechanica*, **40**(2), 121-133.

Psycharis, I., and Jennings, P., 1983. Rocking of slender rigid bodies allowed to uplift, *Earthquake Eng. Struct. Dyn.*, **11**(1), 57-76.

Shenton, H., 1996. Criteria for initiation of slide, rock, and slide-rock rigid-body modes, *J. Eng. Mech.*, ASCE, **122**(7), 690-693.